Advanced Science

ADVANCED SCIENCE Open Access

www.advancedscience.com

RESEARCH ARTICLE OPEN ACCESS

Repeated Disuse Atrophy Imprints a Molecular Memory in Skeletal Muscle: Transcriptional Resilience in Young Adults and Susceptibility in Aged Muscle

Daniel C. Turner[1,2] | Truls Raastad[1] | Max Ullrich[1] | Stian F. Christiansen[1] | Hazel Sutherland[3] | James Boot[4,5] | Eva Wozniak[4] | Charles Mein[4] | Emilie Dalbram[6] | Jonas T. Treebak[6] | Daniel J. Owens[3] | David C. Hughes[7] | Sue C. Bodine[7] | Jonathan C. Jarvis[3] | Adam P. Sharples[1]

[1]Department for Physical Performance, Norwegian School of Sport Sciences, Oslo, Norway | [2]Department of Molecular Medicine, University of Pavia, Italy | [3]Research Institute for Sport and Exercise Sciences, Liverpool John Moores University (LJMU), Liverpool, UK | [4]Genome Centre, Queen Mary University of London (QMUL), London, UK | [5]Francis Crick Institute, London, UK | [6]Novo Nordisk Foundation Center for Basic Metabolic Research, Faculty of Health and Medical Sciences, University of Copenhagen (UCPH), Copenhagen, Denmark | [7]Aging and Metabolism Research Program, Oklahoma Medical Research Foundation (OMRF), Oklahoma City, Oklahoma, USA

Correspondence: Daniel C. Turner (daniel.turner@unipv.it) | Adam P. Sharples (adams@nih.no)

Received: 10 November 2025 | **Revised:** 3 February 2026 | **Accepted:** 5 February 2026

Keywords: AChR (*CHRNA1, CHRND, CHRNG*) | aerobic metabolism | aging | disuse atrophy | DNA methylation | mtDNA | muscle memory | muscle stem cells | NAD^+ metabolism | nicotinamide riboside | *NMRK2* | *NR4A1* | *NR4A3* | skeletal muscle | transcriptome

ABSTRACT

Disuse-induced muscle atrophy commonly occurs following illness, injury, or falls and becomes increasingly frequent with ageing. Whether skeletal muscle retains a "memory" of repeated disuse remains unknown. We investigated repeated lower-limb immobilization in young adults and a refined aged rat model, integrating physiological, multi-omic, immunohistochemical, biochemical, and primary human muscle stem cell (MuSC) analyses. To enable robust age comparisons, we integrated previously published young rat data with newly generated aged rat data. In young human muscle, repeated disuse elicited attenuated transcriptional perturbations in oxidative and mitochondrial pathways, suggestive of a protective molecular memory, despite similar atrophy to initial disuse. In contrast, aged muscle exhibited a detrimental memory, characterized by greater atrophy, exaggerated suppression of aerobic metabolism genes despite recovery after initial disuse, NAD^+ and mitochondrial DNA depletion, and activation of proteasomal, extracellular-matrix, and DNA-damage pathways. Whereas young rats recovered muscle mass after initial disuse, aged rats failed to do so. Across species, repeated disuse induced DNA hypermethylation and downregulation of aerobic metabolism and mitochondrial gene networks. *NR4A1* and *NR4A3* were among the strongest disuse-suppressed genes; *NR4A1* acquired recovery-phase hypermethylation that maintained its transcriptional repression, while *NR4A3* was the most downregulated gene after initial atrophy and remained persistently suppressed into recovery. Acetylcholine receptor subunit genes (*CHRNA1*, *CHRND*) were epigenetically primed, demonstrating hypomethylation and strong upregulation after disuse, and further amplification after repeated atrophy, while *CHRNG* was selectively induced after repeated atrophy only. *NMRK2*, an NAD^+ biosynthesis gene, was the most downregulated gene across both atrophy periods, and supplementation with its substrate, nicotinamide riboside (NR), improved myotube size in MuSCs derived post-atrophy. Overall, repeated disuse atrophy imprints a molecular memory in skeletal muscle shaping transcriptional resilience in young adults and exaggerated susceptibility in aged muscle.

1 | Introduction

Age-related skeletal muscle loss (termed sarcopenia) is one of the main contributors to falling injury [1–3], often resulting in prolonged periods of disuse. Consequently, repeated falls in the elderly become increasingly common, leading to recurrent loss of skeletal muscle, and thus increased risk of frailty, morbidity, hospital admittance, reduced quality of life, and ultimately earlier mortality [2, 4–7]. Restoration of skeletal muscle following periods of disuse is also impaired in aged muscle [5, 8–12], further increasing the risk of repeated falls [2, 3]. Despite the well-characterized skeletal muscle wasting (atrophy) response to a single period of limb immobilization [8–10, 13–21], bed rest [22–26], and spaceflight [27–29], whether muscle atrophy is exacerbated following repeated disuse in both adult and aged muscle is currently unknown.

Skeletal muscle "memory" refers to the differential tissue response to repeated exposure to the same (or similar) environmental stimuli [30, 31]. While it is evident that skeletal muscle exhibits a 'positive' memory of anabolic stimuli, resistance [32–39] and endurance [34, 40] training in both humans and rodents, it is unknown whether skeletal muscle possesses a "negative" memory of disuse-induced muscle atrophy. Specifically, whether an earlier encounter of disuse renders the muscle more susceptible to further wasting if re-encountered in the future, such as following injury recurrence or repeated fall-related injury in the elderly.

Epigenetics is considered a key mechanism underpinning skeletal muscle memory, whereby retention of epigenetic modifications in skeletal muscle are either; (a) modified following exercise training and retained during detraining, leading to sustained elevations in gene transcription [33, 34, 36, 37, 39, 40] and protein abundance [38] and/or (b) enhanced upon later retraining, resulting in amplified changes in gene expression [33, 34, 36, 37, 39, 40]. Among the various epigenetic modifications, DNA methylation has emerged as one of the most prominent regulators of skeletal muscle memory. DNA methylation undergoes genome-wide alterations and modulates the transcriptional response to acute exercise and chronic training, affecting divergent pathways according to the mode of exercise performed [33, 36, 37, 39, 40–55]. Moreover, DNA methylation is dynamic and can both precede and modulate the time course of transient gene expression in skeletal muscle within minutes to hours following a single bout of exercise (reviewed in [56]). However, some DNA methylation changes are long-lasting, particularly those induced by chronic training, thereby providing a key mechanism mediating skeletal muscle memory of exercise [31, 33, 34, 36, 37, 39, 40].

Despite the epigenetic role in modulating gene transcription in response to positive stimuli, studies examining the DNA methylation response to negative stimuli, such as muscle disuse atrophy remain scarce. Nevertheless, there is clear evidence of a dysregulated methylome in skeletal muscle of aged [57–61] and diseased populations (e.g., type-II diabetes [42, 51, 62] and cancer [48]), in which greater aerobic fitness (higher $\dot{V}O_{2max}$) [57], higher physical activity, or exercise training can recalibrate both the nuclear [39, 48, 57, 58, 59] and mitochondrial methylome [63] toward epigenetic signatures resembling youthful muscle. Following disuse atrophy, hypermethylation and reduced expression of targeted genes such as *PPARGC1A* after nine days of bed rest in human muscle [64], and *Nos1* after acute immobilization in mice, have been reported [65]. Our group have also demonstrated hypomethylation and increased expression of E3 ligases (*Murf1* and *MAFbx/Fbxo32*), the acetylcholine receptor (AChR) subunit (*Chrna1*), and the histone deacetylase (*Hdac4*) following tetrodotoxin (TTX)-induced disuse atrophy in young adult rat muscle [66]. To date, however, most studies have predominantly focused on targeted gene methylation with limited data available on genome-wide methylation. A recent study integrating methylome and transcriptome analyses after 2 weeks of disuse atrophy in young adult humans (via lower limb casting), reported a predominance of global hypermethylation associated with a greater number of downregulated than upregulated genes [39]. However, leg casting-induced disuse was preceded by resistance training; and therefore, it is unknown whether such alterations occur following disuse atrophy without prior resistance training, which would be more representative of the general population [39]. A recent study analyzing genome-wide DNA methylation in purified muscle stem cells (MuSCs) following injury in adult mice demonstrated sustained differential methylation long after recovery [67], whereas myoblasts retain DNA methylation changes after repeated inflammatory exposure in vitro [68]. However, no studies have investigated combined methylome and transcriptome responses following repeated atrophy to determine whether skeletal muscle imprints a "negative" memory of disuse-induced atrophy in both young adult and aged muscle.

We aimed to determine whether skeletal muscle exhibits a "negative memory" of disuse atrophy. We hypothesized that prior disuse episodes would leave persistent molecular imprints that exacerbate subsequent atrophy, particularly in aged muscle. As repeated atrophy and consequent frailty in elderly humans raises ethical concerns, we combined physiological, multi-omic, immunohistochemical, biochemical, and primary muscle stem cell analyses in parallel young adult human and aged animal models of disuse atrophy, recovery and repeated atrophy. To reduce animal use and enable a direct age comparison, we also integrated our previously published young rat data [66] with newly generated aged rat data, confirming that young rats recover muscle mass after disuse, whereas aged rats do not. We demonstrate that skeletal muscle retains a molecular memory of disuse. In young adults, repeated immobilization elicited a resilient and "protective" transcriptional memory, characterized by attenuated alterations in aerobic metabolism and mitochondrial pathways after repeated disuse, despite full recovery of muscle mass and function. However, this transcriptional response did not mitigate muscle loss after repeated atrophy. In contrast, repeated disuse in aged muscle resulted in heightened susceptibility, with further suppression of aerobic metabolism and mitochondrial pathways, depletion of NAD^+ and mtDNA content, and greater muscle wasting despite recovery of gene expression after initial disuse. Proteasomal, extracellular matrix (ECM), and DNA-damage related pathways were uniquely elevated in aged muscle following repeated disuse. *NR4A3*, a nuclear receptor critical for muscle metabolism, was the most downregulated gene after initial disuse atrophy, and remained persistently suppressed into recovery in humans. Epigenomic profiling revealed conserved DNA hypermethylation in aerobic and mitochondrial gene networks across species after both

TABLE 1 | Young adult human baseline characteristics. Values presented as mean ± standard deviation (SD).

	Male ($n = 7$)	Female ($n = 3$)	All ($n = 10$)
Age (yrs)	27.1 ± 4.1	23.7 ± 3	26.5 ± 4.1
Height (cm)	181.7 ± 2.7	167.9 ± 7.5	177.5 ± 7.9
Weight (kg)	93.4 ± 16	62 ± 12.6	84 ± 20.9
Body mass index, BMI (kg/m^2)	28.4 ± 5.3	21.8 ± 2.6	26.4 ± 5.5
Total lean body mass, LBM (kg)	64.8 ± 4.4	41.5 ± 7.2	57.8 ± 12.3
Fat mass, FM (kg)	24.8 ± 13.1	18.3 ± 5.7	22.3 ± 11.4
Fat free mass, FFM (kg)	68.2 ± 4.5	43.9 ± 7.3	60.9 ± 12.8
Body fat, BF (%)	25.4 ± 9.4	29.1 ± 4.5	26.5 ± 8.2
Immobilized leg lean mass, LLM (kg)	11.4 ± 1.2	7.4 ± 1.5	10.2 ± 2.3
Non-immobilized LLM (kg)	11.5 ± 1.3	7.1 ± 1.6	8.9 ± 2.5

initial atrophy and repeated atrophy, alongside locus-specific memory genes, including *NR4A1* and AChR (*CHRNA1*, *CHRND and CHRNG*) subunit genes. Finally, NMRK2, a key NAD^+ biosynthesis gene, was the most downregulated gene across both periods of atrophy in young adult humans. Supplementation with its substrate, nicotinamide riboside (NR), increased myotube size in human MuSCs derived post-atrophy.

2 | Methods

2.1 | Human Ethics and Participant Information

Ethical approval was granted by the Regional Committees for Medical and Health Research Ethics (REK, Application ID 227924). The study was registered with the Norwegian Agency for Shared Services in Education and Research (Sikt) under reference number 627824. Participants were familiarized with the study intervention and the possible associated risks. Informed written consent and completion of an approved health and pre-biopsy medical questionnaire were obtained prior to participation. Ten young adults, males ($n = 7$) and females ($n = 3$) living in Oslo, Norway participated in the study. Participants were free from any known injury, illness, and disease and had no previous history or predisposition to deep vein thrombosis (DVT). Participant baseline characteristics are presented in Table 1. All human data collection was conducted at the Norwegian School of Sport Sciences.

2.2 | Assessment of Physical Activity Levels in Humans

The International Physical Activity Questionnaire Short Form (IPAQ-SF) was used to assess short-term physical activity levels prior to the study [68]. Participants also completed an additional non-validated questionnaire including questions related to the specific type of sport (e.g., team, endurance, speed/power) or activity (e.g., cardiorespiratory fitness, strength, concurrent), duration of participation, and competition level (i.e., recreational, national, international) to assess long-term physical activity levels.

2.3 | Human Study Design

In a repeated measures design, participants underwent 2 weeks (wks) (14 days) disuse atrophy (via unilateral limb immobilization) → ≈ 7 wks (49 ± 5 d) recovery, followed by → 2 wks repeated disuse atrophy (Figure 1A). During immobilization, participants were fitted with a knee brace (DonJoy X-Act ROM, Enovis/DJO LLC, USA) fixed at 30° knee flexion to prevent any weight bearing of the non-dominant leg. Crutches were provided to enable ambulation without weight bearing on the braced immobilized leg. Following immobilization, the knee brace and crutches were removed, and participants returned to their normal ambulatory activity to allow recovery. Finally, the same non-dominant leg underwent a second period of immobilization (repeated atrophy). Before immobilization, participants were trained using the crutches and knee brace and were instructed to only remove the knee brace only when showering and sleeping. Daily movements (e.g., ankle rotation/dorsiflexion/plantarflexion) were encouraged to reduce the risk of DVT [69]. There were no reported cases throughout the present study. Before and after each immobilization, muscle biopsies and measurements of SkM size and strength were conducted in the morning (± 1 h across timepoints) under fasted conditions following the same testing order (Figure 1A). Participants were also advised to refrain from strenuous exercise and alcohol consumption 24 h prior to muscle biopsy and testing procedures. Muscle biopsies and the testing protocol are detailed below. Upon completion of the study intervention, for ethical reasons and courtesy of participation, all participants were provided with the opportunity to undertake supervised resistance training programme (3 d/wk for 7 wks consisting of 2 lower body and 1 upper body sessions each wk) to restore any loss of SkM. Where, previously two to four weeks of strength training was sufficient for restoring SkM following a similar duration of atrophy in young adult humans [8, 11, 70].

2.4 | Human Skeletal Muscle Biopsy Procedures

Muscle biopsies were obtained from the immobilized leg according to our procedures described elsewhere [48, 49]. Briefly, local anaesthesia (Xylocaine with 10 mg/mL lidocaine + 5 μg/mL adrenaline, AstraZeneca, Södertälje, Sweden) was administered

to the biopsy area, and muscle tissue (133 ± 47 mg excluding muscle tissue for immunohistochemical analysis; see below) was obtained from the mid-belly (10% proximal of the mid-thigh) of the *m. vastus lateralis (VL)* muscle using a modified Bergström technique (6 mm Pelomi-needle, Albertslund, Denmark) with manual suction (i.e., a 50 mL syringe connected to the Bergström needle). All human muscle biopsies were obtained under fasted conditions at 09:30 ± 47 min across all timepoints and participants, following a standardized protocol to minimize circadian variability and ensure a narrow sampling window relative to diurnal regulation of skeletal muscle metabolism. For immunohistochemical (IHC) analysis, a proportion (≈ 50 mg) of muscle tissue was embedded in optimal cutting temperature (OCT) compound (CellPath, Chemi-Teknik AS, Oslo, Norway) ensuring myofibers were aligned in parallel before freezing in pre-cooled (above liquid nitrogen, LN_2) isopentane (Sigma–Aldrich, Oslo, Norway) placed on dry ice and stored at −80°C. Remaining tissue was rinsed in pre-cooled (4°C) saline containing 0.9% NaCl (Braun, Melsungen, Germany) and dissected to remove any trace of visible fat, connective tissue, and blood(vessels were discarded). Tissue intended for RNA, DNA, and protein isolation was immediately weighed, transferred to nuclease-free Eppendorf tubes (Invitrogen RNase-free Microfuge Tubes, Fisher Scientific, Oslo, Norway), snap-frozen in LN_2, and stored at −80°C. Remaining tissue used for in vitro experiments was submerged in pre-cooled (4°C) transfer media (Hams F-10 medium that includes 1 mM L-glutamine/LG, 0.2% heat inactivated fetal bovine serum/hiFBS, 100 U/mL penicillin, 100 µg/mL streptomycin/PS, and 2.5 µg/mL amphotericin-B/AB, Fisher Scientific) for subsequent primary cell isolations (detailed below).

2.5 | Assessment of Body Composition in Humans

Height (cm) and body weight (kg) were measured using a digital stadiometer and scale, respectively (Seca, Hamburg, Germany). Whole-body composition and leg lean mass (LLM) were assessed by dual-energy X-ray absorptiometry (DEXA; Lunar iDXA, enCORE software version 18; GE Healthcare, Chicago, USA). Total LLM was defined as all lean mass located distally from the collum femoris and inferior pubic ramus. A triangular segment depicting the pelvic area and a midline separating left and right legs were constructed as previously described [71]. Specifically, the horizontal line of the triangle segment transversed slightly above the two iliac crests, and the two angled lines crossed the collum femoris, meeting just below the genital area [71]. An additional line crossing the intercondylar eminence separated the upper and lower leg. All images were analyzed single-blinded by three experienced personnel, and the average values were reported. The coefficient of variation (CV) for test-retest reliability was 1%.

2.6 | Assessment of Muscle Cross-sectional Area (mCSA) in Humans

Anatomical muscle cross-sectional area (mCSA) of the *m. rectus femoris (RF)* and *VL* muscles were assessed using panoramic B-mode ultrasound scanning using a linear transducer (L18-5) fixed to an ultrasound system (MACH 30; Hologic SuperSonic Imagine, Aix-en-Provence, France). During scanning, participants lay supine (knee angle at 0°C) with their leg muscles relaxed and feet strapped to a stable box to prevent any hip rotation. Three measurements per muscle (*RF* and *VL*) were measured and analyzed by following a transverse trajectory line drawn across the mid-thigh (i.e., 50% of the distance between the greater trochanter and distal end of the muscle) using a marker pen, demonstrating a low (< 2.5%) CV across all timepoints (RF baseline 2.4 ± 1.1%, atrophy 1.6 ± 1%, recovery 2.1 ± 1.1%, repeated atrophy 1.8 ± 1.6%, VL baseline 1.7 ± 1.3%, atrophy 1.3 ± 0.7%, 1.8 ± 1% recovery, 1.6 ± 0.7% repeated atrophy). Only acquired images free from visible artifacts or stitching-related issues were considered acceptable for analysis. Participants were encouraged to redraw the trajectory line during the immobilization and recovery periods to ensure accurate probe repositioning during subsequent timepoints. A transparent plastic sheet was also used to mark the trajectory and other clear landmarks (e.g., scars and the patella) to provide additional accuracy during rescanning. Finally, previous images were displayed during rescanning to confirm image acquisition accuracy between timepoints. All images were analyzed single-blinded using ImageJ2 with Bio-Format plugin (version 2.14.0/1.54f, U. S. National Institutes of Health, Bethesda, Maryland, USA) [57, 58] at the end of the intervention. One participant was excluded from all mCSA analyses due to inaccurate repositioning or visible imaging artefacts.

2.7 | Assessment of Muscle Strength in Humans

Maximal voluntary isometric knee extension and flexion torque (Nm) were measured at 90°, 60°, and 30° knee flexion using a dynamometer (HUMAC NORM; Computer Sports Medicine Inc, Massachusetts, USA). Participants were first familiarized with the protocol one week prior to baseline testing. Prior to strength testing, participants performed a standardized warm-up consisting of 5 min low intensity cycling, 5 min stretching and 3 × submaximal efforts (50%–80%). Following the warm-up, participants performed 5 × maximal repetitions at each knee flexion angle (in order of 90°, 60°, and 30°). Verbal encouragement was provided during each repetition. The greatest torque produced was considered their maximum voluntary contraction (MVC). If the difference in torque between the first and second strongest repetition was > 5%, participants performed an additional repetition. MVC was acquired on Biopac MP150 system (Goleta, CA, USA) with a sampling frequency of 1000 Hz and analyzed using AcqKnowledge software (version 4.4.2, Biopac Systems, Inc., Knivsta, Sweden).

2.8 | Animals and Study Design

Repeated disuse in elderly humans is associated with frailty and increased risk of falls, raising ethical concerns. Therefore, we limited human experiments to young adults and used aged rats as a surrogate model for repeated atrophy in aged muscle. To minimize animal use and adhere to ethical refinement principles, we did not include a direct young rat control group; instead, we integrated previously published young rat data [66] with newly generated aged rat data, enabling robust age comparisons while reducing unnecessary duplication in young adult rats. Ethical

approval was obtained, and experimental procedures were conducted with the permissions within a project license granted (PA693D221) under the British Home Office Animals (Scientific Procedures) Act 1986. Aged (23 ± 1 months) male Fischer 344 rats (Charles River) weighing 354 ± 54 g were housed at 20°C and 45% relative humidity on an alternating 12 h light and 12 h dark cycle, with food and water available ad libitum. Only male Fischer 344 rats were used in this study. This decision was driven by welfare and practical considerations during the extended pre-experimental housing period, as male rats form stable social groups after import whereas female rats do not form reliable social pairings. Social housing was essential to minimize stress in very old animals. Sex specific comparisons were therefore not possible and are acknowledged as a limitation. Animals were assigned to 1 of 4 groups (n = 3 per group), including a control group (sham control) and 3 experimental groups (atrophy, recovery, and repeated atrophy). All experimental groups received tetrodotoxin (TTX) to the common peroneal nerve (CPN), preventing contraction of the ankle dorsiflexor muscles. TTX binds to the voltage-gated sodium channel in the nerve cell membranes and so prevents the conduction of action potentials. Therefore, muscles innervated by the blocked CPN cannot be activated to contract. This induces disuse atrophy of the hind limb dorsiflexor muscles, i.e., the tibialis anterior (TA) and extensor digitorum longus (EDL). TTX-induced nerve silencing of the TA and EDL muscles is advantageous compared to denervation or hindlimb unloading as it allows normal conduction in the tibial nerve to achieve plantarflexion, and therefore animals can undertake locomotion for daily living (Figure 2A) [59–61]. The atrophy and recovery groups received a single infusion of TTX (6–7 d) followed by 9 d of TTX abstinence (e.g., TTX → recovery), whereas the repeated atrophy group received a second TTX infusion (5–6 d) following recovery (e.g., TTX → recovery → and repeated TTX) (Figure 2A). The sham control group consisted of $n = 1$ for each timepoint (TTX/recovery/repeated TTX) that received the same surgical procedures (detailed below) as the experimental groups in the absence of TTX administration. Pre- and post-intervention animal weights for each group are presented in Table S1 and muscle weights are provided in Figure S3. Rats were socially housed in pairs throughout the experiment in accordance with best welfare practice, which precluded precise measurement of individual nutritional intake. Body weight was recorded at each timepoint, and wet food was provided when required. Body weight remained stable during the atrophy and recovery phases and decreased only after repeated atrophy (Table S1), indicating that alterations in recovery were not attributable to reduced nutritional intake. Objective assessment of dorsiflexion in very old, caged rats is challenging; therefore, intervention efficacy and specificity were verified using: (i) transcriptomic signatures that were highly responsive to both the application and withdrawal of TTX, (ii) paired comparisons between treated and contralateral control muscles within each animal, (iii) selective reductions in dorsiflexor muscle mass, with minimal changes in adjacent plantarflexors, and (iv) saline-infused sham controls that confirmed surgical procedures alone did not affect muscle mass or gene expression.

2.9 | Animal Experimental Procedures

Surgical and TTX-administration procedures are described elsewhere [66, 72]. Briefly, animals were first anaesthetized via inhalation of a gaseous mixture of 3% isoflurane in oxygen for induction and 1%–2% for maintenance prior to subcutaneous implantation of a mini osmotic pump (Mini Osmotic Pump 2002; Alzet, Cupertino, CA) in the scapular region. Silicone tubing attached to the mini osmotic pump was then passed under the skin to the site of the left CPN. A second incision was made laterally through the skin, just proximal to the knee joint, and through the biceps femoris muscle (posterior compartment of the thigh) to enable access to the CPN. A silicone cuff extending from the silicone tubing was placed around the nerve. All incisions were closed in layers. The mini osmotic pump (Mini Osmotic Pump 2002; Alzet, Cupertino, CA) delivered TTX to the CPN. The osmotic pump successfully delivered 0.5 µL/h of TTX (350 µg/mL in sterile 0.9% saline), continuously blocking ankle dorsiflexion for inital disuse-atrophy period after which the TTX was exhausted, while maintaining normal voluntary plantarflexion via the tibial nerve. The nature of the osmotic pump means that delivery of its contents starts as soon as the pump is implanted; therefore, silencing of the CPN was present immediately after surgery. TTX was not administered to the right limb, and it served as a contralateral control for each individual animal. For the repeated disuse-atrophy period, the rats were anaesthetized briefly after the recovery period, and the empty osmotic pump was removed through an interscapular incision and replaced with a new TTX-loaded pump. The welfare and mobility of the rats were checked daily by animal welfare staff. Rats were euthanized using a rising concentration of carbon dioxide in oxygen until cessation of breathing, followed by cervical dislocation. All rat tissue collections were performed at a consistent time of day between the hours of 08:00 and 13:00 across all experimental conditions, during the early inactive phase. The scheduling of operating days and subsequent harvesting days introduced no systematic bias for muscle from one group to be harvested consistently earlier or later than muscle from another group across all experimental conditions. Muscles were harvested immediately after euthanasia, weighed, and cut into transverse pieces approximately 2 mm thick. Pieces from the left and right limbs were mounted on the same piece of cork and frozen in pre-cooled isopentane to ensure simultaneous processing of experimental and contralateral control samples. Serial transverse sections from the same block were then used for all downstream analyses, including nucleic acids, protein, and for IHC.

2.10 | Human Muscle Derived Stem Cells (MuSCs) Experimental Procedures

Isolation of human muscle derived stem cells (MuSC) and subsequent cell culture procedures are previously described by our group [59, 72]. Briefly, pre- and post-atrophy muscle biopsies (n = 4 for both pre- and post-biopsies) were immediately transferred to a sterilized class II culture hood (MSC-advantage,Thermo Scientific) in low serum transfer media (components described above). Visible fat and connective tissue were removed, and remaining muscle tissue was washed 3 × PBS (1×) containing PS and AB), before undergoing repeated rounds of scissor mincing in trypsin (0.5%)-EDTA (0.2%) and centrifugation (340 × g for 5 min at 24°C) to promote cell migration. The supernatant, cell pellet, and remaining non-homogenized tissue were seeded into separate T25 pre-gelatinized

flasks containing 5 mL growth media (GM: Ham's F-10, 10% hiFBS, 10% heat inactivated new born calf serum/hiNBCS, 2 mM LG, PS, and AB) and left unagitated in a humidified incubator (37°C, 5%, VWR ILCO 180 Premium) for 5–7 d to promote cell growth. GM was changed every 2–3 d thereafter until sufficient cell attachment and growth (< 80% confluency within cell colonies) was achieved. MuSC were transferred and sub-cultured in T75 flasks to further increase cell yield and ensure sufficient MuSC numbers for subsequent experiments (described below).

Both pre- and post-atrophy MuSCs (7×10^4 cells/mL in 2 mL of GM) were seeded onto pre-gelatinized six-well plates and left until ≈ 80% confluency was attained (which occurred between 24 and 48 h). Cells were then washed 3 × PBS (1×), and media was switched to low serum media (DM: same components as GM with lower 2% hiFBS) to permit differentiation over 10 d. An additional 1 mL of DM was added at 72 h, and the media was switched to DM containing either 0.5 mM nicotinamide riboside (NR, ChromaDex Inc, USA), previously used by our group [73], or control (H_2O) for both pre- and post-atrophy conditions. Cell pellets derived from 4 × wells at 0 h, 7 d, and 10 d (± NR supplementation) were snap-frozen and stored at −80°C for later copurification of DNA ($2 \pm 0.19_{A260/A280}/0.14 \pm 0.14_{A260/A230}$) and RNA ($2.05 \pm 0.03_{A260/A280}/1.86 \pm 0.48_{A260/A230}$) using the AllPrep RNA/DNA Mini Kit (Qiagen). The remaining 2 × wells were treated for subsequent immunocytochemistry analysis (described below). There were no differences in the proportion of myoblasts (42 ± 22% vs. 45 ± 26%, $p = 0.62$) and fibroblast (58 ± 22% vs. 56 ± 26%, $p = 0.62$) in pre- and post-atrophy MuSC, respectively. All MuSC were between passage 3 and 6 to avoid issues of cellular senescence [74].

2.11 | Immuno-Histo/Cytochemistry, Imaging, and Analysis

Serial sections at either 8 µm (human VL muscle) or 10 µm (mid-belly of the rat TA muscle) thickness were made at −20°C (CM1860, Leica Biosystems GmbH, Heidelberger, Germany), mounted on microscope slides (Fisherbrand Superfrost Plus Microscope Slides, Fisher Scientific), air-dried for 30 min and stored at −80°C. When immuno-labeling muscle cross sections, samples were first air-dried for 30 min prior to blocking in 2% bovine serum albumin (BSA, Sigma–Aldrich) in 1× PBS (10 mM phosphate buffer, 3 mM KCl, pH 7.4, Merck, Oslo, Norway) with 0.05% added tween (PBS-T, Tween 20, VWR, Oslo, Norway) and 1% fat-free dry milk (Sigma–Aldrich) for 1 h at room temperature (RT). Muscle cross-sections were then counterstained for dystrophin (1:500; ab15277, Abcam, Cambridge, UK), myosin heavy chain (MyHC) type I (1:100; BA-F8, DSHB Supernatant, Schiaffino, S, Iowa, USA) and MyHC type IIA (1:100; SC-71, DSHB Supernatant, Schiaffino, S, Iowa, USA) diluted in 0.05% PBS-T and 1% milk overnight at 4°C (Table 2). After overnight incubation, samples were labeled with goat anti-rabbit (GaR) IgG H+L (1:200; Alexa Fluor 488, cat. #A-11008 or Alexa Fluor 633, cat. #A-21070, Thermo Fisher Scientific, Waltham, MA, USA), goat anti-mouse (GaM) IgG1 (1:200; Alexa Fluor 488, cat. #A-21121) and/or GaM IgG2b (1:200; Alexa Fluor 594, cat. #A-21145) diluted in 0.05% PBS-T and 1% milk for 1 h and RT (Table 2). Slides were washed 3 × 5 min in 0.05% PBS-T between each blocking and Ab labeling steps. Finally, coverslips were mounted using ProLong Gold Antifade Mountant with 4′,6-diamidino-2-phenylindole (DAPI, cat. #P36935, Thermo Fisher Scientific) and left to air-dry at RT overnight prior to imaging. For imaging, tile scan images (1024×1024 frame size) of whole cross-sections were acquired using a ZEISS LSM 800 (with Airyscan) confocal microscope (ZEISS, Oberkochen, Germany) equipped with a 10×/0.3 objective and subsequently processed using either ZEN 2 (blue edition, version 2.6) or ImageJ2 (version 2.14.0/1.54f, U. S. National Institutes of Health, Bethesda, Maryland, USA) software. Automated analysis of myofiber cross-sectional area (fCSA) and fiber type were conducted using MyoVision 2.0 software [59]. Issues surrounding human muscle tissue processing (e.g., biopsy size, freeze-damage) resulted in variable sample numbers for average (type I and II combined; $n = 8$ for baseline/atrophy, $n = 7$ for recovery, $n = 6$ for repeated atrophy) and type I/II ($n = 7$ baseline, $n = 8$ atrophy, $n = 6$ recovery, $n = 5$ repeated atrophy) fiber analysis. The number of fibers analyzed from human biopsies was 398 ± 331 (average), 149 ± 94 (type I), and 281 ± 77 (type II). The total number of fibers analyzed from whole rat muscle was 6297 ± 2067 (average), 280 ± 109 (type I), 1237 ± 546 (type IIA), 69 ± 48 (type I/IIA), and 4712 ± 1613 (type IIX/IIB).

For characterizing myogenic proportions (% myoblasts and fibroblasts) and myotube differentiation/maturation, MuSC were washed 3 × TBS (1×), fixed in 4% PFA for 15 min, incubated in blocking/permeabilization solution (5% goat serum/GS and 0.2% Triton X-100 in 1× TBS) for 1 h at room temperature (RT). MuSCs were then washed and incubated overnight (4°C on a rocker) in Ab solution (2% GS and 0.2% Triton X-100 in 1× TBS) containing anti-desmin (1:50; ab15200, Abcam) and TE-7 (1:100; CBL271, Merck) primary AB for counterstaining myoblasts and fibroblasts, respectively. After overnight incubation, cells were washed 3 × TBS and incubated at RT for 3 h (4°C on a rocker) in secondary Ab solution containing anti-rabbit IgG TRITC (1:75; T6778, Sigma–Aldrich) for myoblasts and GaM Alexa Fluor 488 (1:500; ab150117, Abcam) for fibroblasts. Finally, cells were washed 3 × TBS, prior to counterstaining nuclei using DAPI (300 nM; D1306, Thermo Fisher Scientific) for 30 min at RT. DAPI was removed, and stained cells were washed and stored in TBS for later image acquisition. The same microscope and image acquisition settings (described above) were used when imaging both muscle cross-sections and MuSCs (2 × duplicate wells per condition/timepoint, 3 × 3 tile scan images per well). The ImageJ2 cell counter was used to quantify the number of myoblasts and fibroblasts. The polygon tool was used to outline the sarcolemma of all myotubes (cells with ≥3 nuclei) for assessing myotube area (μm^2).

2.12 | RNA Extraction From Muscle Tissue

Skeletal muscle tissue derived from humans (33 ± 6 mg) and animals (27 ± 4 mg) was added to 2 mL homogenizing mix tubes (Fisherbrand, Fisher Scientific) containing 600 µL Buffer RLT (Qiagen) with added 1% β-Mercaptoethanol (β-ME) before transferring to a tissue homogenizing instrument (MagNA Lyser; Roche) for subsequent homogenization (3 × 45 s at 6000 rpm, placing samples on ice for 5 min between each disruption). Following homogenization, RNA was purified using a RNeasy Mini kit (Qiagen) and treated with DNase (RNAse-Free DNase Set, Qiagen) as per the manufacturer's instructions. RNA quantity

TABLE 2 | Primary (1°) and secondary (2°) antibodies (Ab) used for immunohistochemistry (IHC) and Western blot (WB) procedures.

Application	Antibody	Supplier (cat. #)	Concentration	Species
IHC (1°)	Anti-dystrophin	Abcam (ab15277)	1:500	Human/Rat
	BA-F8/anti-MyHCI	DSHB	1:100	Human/Rat
	SC-71/anti-MyHCIIA	DSHB	1:100	Rat
	Anti-Desmin	Abcam (ab15200)	1:50	Human
	TE-7 Anti-Fibroblasts	Merck (CBL271)	1:100	Human
	DAPI	Thermo Fisher (P36935)	in mountant	Human/Rat
	DAPI (*for MuSC*)	Thermo Fisher (D1306)	300 nM	Human
WB (1°)	OXPHOS	Abcam (ab110413)	1:500	Human/Rat
	CS	Abcam (ab96600)	1:4000	Human/Rat
IHC (2°)	GaR IgG (H+L) (Alexa Fluor 488)	Thermo Fisher (A-11008)	1:200	Human
	GaM IgG (H+L) (Alexa Fluor 488)	Abcam (ab150117)	1:500	Human
	GaR IgG (H+L) (Alexa Fluor 633)	Thermo Fisher (A-21070)	1:200	Rat
	GaM IgG1 (Alexa Fluor 488)	Thermo Fisher (A-21121)	1:200	Rat
	GaM IgG2b (Alexa Fluor 594)	Thermo Fisher (A-21145)	1:200	Human/Rat
	Anti-rabbit IgG TRITC	Sigma–Aldrich (T6778)	1:75	Human
WB (2°)	GaM IgG (H+L) HRP	Thermo Fisher (31430)	1:30 000	Human/Rat
	GaR IgG (H+L) HRP	CST (7074)	1:3000	Human/Rat

DSHB = Developmental Studies Hybridoma Bank, CST = Cell Signaling Technology.

and purity for both human (128 ± 175 ng/mg tissue, 1.94 ± $0.06_{A260/A280}$/2.18 ± $0.16_{A260/A230}$) and rat (406 ± 215 ng/mg tissue, 2.06 ± $0.02_{A260/A280}$/2.15 ± $0.17_{A260/A230}$) samples were quantified via spectrophotometry (QIAxpert, software version 2.4, Qiagen) and concentrations confirmed via fluorometry (Qubit, Qiagen). RNA integrity prior to sequencing was confirmed via Agilent Bioanalyser 2100 with RIN scores 7.22 ± 0.36 for human and 8.29 ± 0.62 for rat samples (detailed below).

2.13 | RT-qPCR for Targeted mRNA Analysis of Aged Rat Muscle Tissue and Human MuSCs

Methods for targeted mRNA expression analysis via real-time-quantitative polymerase chain reaction (RT-qPCR) by our group have been explained elsewhere [40, 48, 49, 59]. Briefly, a one-step QuantiFast SYBR Green kit (Qiagen) was used for preparation of PCR reactions. Each 10 µL reaction contained 4.75 µL experimental sample (7.36 ng/µL totaling 35 ng per reaction), 0.075 µL of both forward and reverse primer (100 µM stock, final concentration 0.75 µM) of the genes of interest (primer details are provided in Table 3), 0.1 µL of reverse transcriptase, and 5 µL of SYBR Green Master Mix (totaling a final reaction volume of 10 µL). A thermocycler (Rotorgene 3000Q, Qiagen) was used to amplify target transcripts. Reverse transcription was initiated with a hold at 50°C for 10 min (cDNA synthesis) and 5 min at 95°C (transcriptase inactivation and initial denaturation), before 40 cycles of; 95°C for 10 s (denaturation) followed by 60°C for 30 s (annealing and extension). Only intended targets (via Basic Local Alignment Search Tool/BLAST search; https://blast.ncbi.nlm.nih.gov/) were identified, thus yielding a single peak after melt curve analysis. All relative gene expression was quantified using the comparative Ct ($^{\Delta\Delta}$Ct) method [75]. For *Nmrk2* expression analysis in aged animal muscle tissue, C_T values (mean of technical duplicates) for each condition (atrophy/recovery/repeated atrophy) were relativized to pooled C_T values from the control limb (n = 9) and reference gene, *Polr2a* (19.27 ± 0.41, 2.12% CV). For temporal mRNA analysis of *MRF* and *NMRK* genes in human MuSCs, C_T values (mean of technical duplicates) from pre- and post-atrophy MuSCs at 7 and 10 d (± NR) were relativized to their own 0 h C_T value and pooled reference gene, *RPL13A* (14.90 ± 0.43, 2.87% CV). To determine the effects of NR supplementation, C_T values from 10 d +NR were relativized to 10 d -NR and pooled *RPL13A* values for both pre- and post-atrophy timepoints. Primers were designed using (BLAST http://blast.ncbi.nlm.nih.gov/) and Clustal Omega (https://www.ebi.ac.uk/Tools/msa/clustalo/) and purchased from Sigma.

2.14 | RNA-seq and Associated Bioinformatic Analysis

Total RNA (100 ng) from each sample was used to prepare mRNA libraries using the NEBNext mRNA isolation kit in conjunction with the NEBNext Ultra II Directional RNA Library preparation kit (New England Biolabs, Massachusetts, USA), and samples were randomized before preparation. Fragmentation of isolated mRNA prior to first strand cDNA synthesis was carried out using incubation conditions recommended by the manufacturer for an insert size of 300 bp (94°C for 10 min). Thirteen cycles of PCR were performed for final library amplification. Resulting libraries were quantified using the Qubit 4.0 spectrophotometer (Life Technologies, California, USA) and average fragment size assessed using the Agilent 4200 Tapestation with D1000 screentape (Agilent Technologies, Waldbronn, Germany). A final sequencing pool was created using equimolar quantities of each

TABLE 3 | qPCR primers.

Species	Gene	Primer sequence (5' – 3')	Length (bp)	Reference
Human	***RPL13A***	F: GGCTAAACAGGTACTGCTGGG	105	Turner et al., [59]
		R: AGGAAAGCCAGGTACTTCAACTT		
	MYOD	F: GCCACAACGGACGACTTCTA	117	Turner et al., [59]
		R: GTGCTCTTCGGGTTTCAGGA		
	MYOG	F: TCCCAGATGAAACCATGCCC	103	Turner et al., [59]
		R: AGGCCCCTGCTACAGAAGTA		
	NMRK1	F: AAATGTTGCTCCATACCATCCC	70	newly designed
		R: CTGCAGCTCCTAGTAATGCT		
	NMRK2	F: AGCTCTTCCGTGAAGTCCTG	62	newly designed
		R: TGATTCCTGGGAGCGGTTCA		
Rat	***Polr2a***	F: GCTGGACCTACTGGCATGTT	102	Seaborne et al., [72]
		R: ACCATAGGCTGGAGTTGCAC		
	Nmrk2	F: GCCGTATGAGGAATGCAAGC	90	newly designed
		R: ATGGGCCATACGTGACCATC		

sample with compatible indexes. Fifty-nine bp paired-end reads were generated for each library using the Illumina NextSeq 2000 in conjunction with the NextSeq 2000 P3 100 cycle kit (Illumina Inc., Cambridge, UK). Resulting FastQ files were imported and processed in Partek Flow software (version 12.4.0; Partek, Inc. Missouri, USA) to filter contaminants (rDNA/tRNA/mtrDNA) using bowtie2 (v2.2.5) and align reads to the hg38 *Homo sapiens* (release 39) and rn7 *Rattus norvegicus* genome assemblies using Spliced Transcripts Alignment to a Reference (STAR) alignment tool (v2.7.3a). Total number of pre/post-aligned reads was 35/34 million and 49/49 million for human (65 bp average read length) and rat (59 bp average read length) samples, respectively. Phred scores were >33 for both human and rat RNA samples, thus trimming and filtering of reads was not required. Normalized differential gene expression analysis was performed using *DESeq2* median of ratios within the Partek Flow software. Principal component analysis (PCA), cluster heatmaps, and volcano plots were created in R studio. Venn diagrams were redrawn from the open-source DeepVenn web application. Pathway (KEGG and REACTOME) and gene ontology (GO; cellular component/CC, molecular function/MF, and biological process/BP) performed via the Database for Annotation, Visualization, and Integrated Discovery (DAVID) knowledgebase and associated figures created in R studio. Custom background gene lists of detected genes following *DESeq2* normalization were used for functional annotation analysis. For human analysis, normalized reads for each timepoint (atrophy/recovery/repeated atrophy) were relativized to baseline. For rat samples, all experimental conditions in the left limb (atrophy/recovery/repeated atrophy) were relativized to pooled right contralateral non-surgical limb. Given there were no DEGs detected between sham and pooled contralateral control limb samples, we excluded sham samples from further analysis and used the pooled contralateral non-surgical limb samples for the control group. Genes with a $\geq$ 20% fold change (FC) and false discovery rate (FDR) of $\leq$ 5% were considered differentially expressed genes (DEGs). Data were presented as either $\log_2$ or FC $\pm$ confidence intervals (CI). Genes with negative changes presented as signed FC (-1/ratio). To perform temporal clustering of the identified DEGs and DMRs (described below), self-organizing map (SOM) profiling was conducted using Partek Genomics suite, as previously described [38, 40, 46, 59]. SOM analysis plots a standardized mean (z-score normalization), shifting the mean to a value of 0 and scaling to a standard deviation of 1. By subtracting the mean of the group this centers the data around zero. Subsequently, dividing by the standard deviation, scales the data so the spread is consistent. This allows removal of the absolute differences, focusing on relative changes, to enable comparison of gene transcripts and DMRs on a common scale. The SOM profiling then clusters DEGs and DMRs based on similar temporal profiles, allowing visualization of signatures across time relative to the group mean. This also allows the temporal signature of the DEGs and DMRs on the same genes to be compared on the same scale across t the time-course of the intervention. All package links and references are available in Table S2.

2.15 | DNA Extraction From Muscle Tissue

Skeletal muscle tissue derived from humans (21 $\pm$ 3 mg) and animals (12 $\pm$ 2 mg) was added to 2 mL homogenizing mix tubes (Fisherbrand, Fisher Scientific) containing 180 µL Buffer ATL (Qiagen, Hilden, Germany) before transferring to a tissue homogenizing instrument (MagNA Lyser; Roche, Basel, Switzerland) for subsequent homogenization (3 × 45 s at 6000 rpm, placing samples on ice for 5 min between each disruption). Following homogenization, 20 µL proteinase K (Qiagen) was added, and samples were incubated at 56°C until complete lysis ($\approx$ 30–60 min) before continuing with DNA purification using a DNeasy Blood & Tissue kit (Qiagen) as per the manufacturer's instructions. DNA quantity and quality for both human (251 $\pm$ 47 ng/mg tissue, 2 $\pm$ $0.01_{A260/A280}$/2.14 $\pm$ $0.08_{A260/A230}$) and rat (1427 $\pm$ 426 ng/mg tissue, 2.02 $\pm$ $0.02_{A260/A280}$/2.02 $\pm$ $0.09_{A260/A230}$) samples were quantified using spectrophotometry (NanoDrop 2000; Thermo Fisher Scientific) and concentrations confirmed

via fluorometry (Qubit, Qiagen). DNA integrity was confirmed prior to sequencing via Agilent Bioanalyser 2100 with DIN scores 7.11 ± 0.17 for human and 7.22 ± 0.23 for rat samples.

2.16 | Reduced Representation Bisulfite/ Enzymatic Methyl Sequencing (RRBS/ RREM): Library Preparation and Sequencing

Reduced representation bisulfite sequencing (RRBS) libraries were prepared from 100 ng of genomic DNA using the Diagenode Premium RRBS v2 library preparation kit, as per the manufacturer's protocol. For human samples, two groups of ei samples, and three groups of 7 samples were prepared after qPCR quantification of adapter-ligated sample and prior to bisulfite conversion. Fourteen cycles of final library amplification were performed after assessment of the bisulfite converted library pool by qPCR. For rat samples, reduced-representation enzymatic methyl-seq (RREM) libraries were prepared using 100 ng of genomic DNA in conjunction with the NEBNext Enzymatic Methyl-Seq kit (New England Biolabs, Massachusetts, USA). Briefly, DNA samples were digested using MspI restriction enzyme followed by end-repair and adapter ligation. A two-step enzymatic conversion was then performed by Oxidation of 5mC and 5hmC using TET2 and glucosylation of 5hmC using T4-BGT. Deamination of unmodified cytosines was subsequently performed using APOBEC. Converted samples were then uniquely barcoded and amplified by PCR prior to sequencing. Libraries were sequenced using the Illumina NextSeq 2000 with P3 SBS 100-cycle sequencing kit for human, and with P4 XLEAP 100-cycle sequencing kit for rat, both generating 50 bp paired-end reads.

2.17 | RRBS/RREM: Quality Control, Trimming, Alignment, and Methylation Calling

Libraries were processed using a standard workflow. Raw basecall files were demultiplexed using Illumina bcl2fastq /2.19.1, and unique molecular identifiers (UMIs) were extracted using umi_tools. Reads were adapter and quality-trimmed (minimum phred score 30) with trim_galore (in RRBS mode; reads less than 15 bp after trimming were discarded). Trimmed reads were aligned to the human reference genome (hg38) or rat genome Rn6 using bismark/0.22.1 with bowtie2, with the PBAT option enabled. PCR duplicates were removed with deduplicate_bismark in a UMI-aware manner. CpG methylation calls were obtained using bismark_methylation_extractor. All package links and references are available in Table S2.

2.18 | RRBS/RREM: Identification of Differentially Methylated Positions (DMPs) and Regions (DMRs)

Downstream DMP and DMR analysis was performed in R. Per-CpG coverage files were imported into methylKit with sites of low (< 10 reads) or extreme coverage (top 0.1%) removed and outlier samples excluded. For humans, data from each sample was then merged based on only CpGs present in at least 6 samples in each group. Each of our groups contained n = 7–8 samples after outlier removal, making this threshold a minimum of 75% of samples and giving a total of ≈ 1.8 million total CpGs analyzed. For rats, there were 9 samples (n = 3 per experimental condition of atrophy, recovery, and repeated atrophy) and n = 9 samples for the contralateral control limbs. Therefore data from each sample were merged based on CpGs present in all samples (100%), giving a total of 29K CpGs analyzed. Differential methylation was identified at individual CpGs (DMPs) and then 1-kb tiled regions (DMRs) using calculateDiffMeth. The percentage methylation of each CpG was calculated using the percMethylation function in methylKit and during differential analysis the mean percentage methylation of each CpG was calculated for each group. For DMRs, mean percentage methylation for each experimental group was calculated by averaging the percentage methylation of all CpGs within a given DMR across all samples from the given group. For human analysis, we performed 6 pairwise comparisons of: (1) Atrophy vs. Baseline, (2) Recovery vs. Baseline, (3) Repeated Atrophy vs. Baseline, (4) Recovery vs. Atrophy, (5) Repeated Atrophy vs. Recovery, (6) Repeated Atrophy vs. Atrophy. For rat analysis we also performed: (1) Atrophy vs. Control, (2) Recovery vs. Control, (3) Repeated Atrophy vs. Control, (4) Recovery vs. Atrophy, (5) Repeated Atrophy vs. Recovery, (6) Repeated Atrophy vs. Atrophy. As with the rat RNA-seq analysis, the pooled right/non-surgical limb (contralateral control limb n = 9) served as the control condition. Differentially methylated CpGs and regions were annotated to genes and regulatory features for humans using TxDb.Hsapiens.UCSC.hg38.knownGene, org.Hs.eg.db and annotatr, and for rats using TxDb.Rnorvegicus.UCSC.rn6.refGene, org.Rn.eg.db and annotatr. Default settings were used unless otherwise specified. Only DMRs with FDR ≤ 0.05 were considered significant. SOM clustering (described above) was performed on significant DMRs using percentage methylation, which allows baseline (human) and control (rat) values to enable temporal profiling. All package links and references are available in Table S2.

2.19 | Mitochondrial DNA Content

Mitochondrial DNA (mtDNA) content was assessed via RT-qPCR. Primers encoding for nuclear DNA (nDNA) markers; β_2 microglobulin (*B2M*), hemoglobin subunit beta *(HBB)*, tubulin-specific chaperone A (*Tbca*), glyceraldehyde 3-phosphate dehydrogenase (*Gapdh*), and mtDNA markers; mitochondrial 16S rRNA (*MT-RNR2*), D-loop region (*DLOOP*), cytochrome B (*CYTB*), mitochondrially encoded 16S rRNA (*mt-Rnr2*) and 12S ribosomal RNA (*mt-Rnr1)*, were used to determine nuclear DNA (nDNA) and mtDNA copy number, respectively. Primer information is presented in Table 4. For qPCR, 20 ng DNA (9.6 µL at 2.08 ng/µL in nuclease-free H_2O) was added to 10 µL SYBR Green Mastermix (Qiagen) and 0.2 µL of both forward and reverseprimers (100 µM stock, 1 µM final concentration) to ensure 20 µL reaction volume. DNA was then amplified using a Rotor-Gene Q 5-Plex HRM thermocycler (Qiagen) with supporting software (version 2.3.1). Thermal cycler settings consisted of 3 min at 95°C (initial denaturation), followed by 40 cycles of: 10 s at 95°C, 30 s at 62°C (annealing), and final extension for 10 s at 95°C. Melt curve analysis was performed at 0.5°C increments from 65°C to 95°C. Mitochondrial DNA content was reported as the ratio of mtDNA (*MT-RNR2, CYTB*, and/or *DLOOP* for human; *mt-Rnr2*

TABLE 4 | Primers used for nuclear DNA (nDNA) and mitochondrial DNA (mtDNA) markers for assessment of mtDNA content.

Species	Gene	Primer sequence (5' – 3')	Length (bp)	Reference
Human	***B2M***	F: TGCTGTCTCCATGTTTGATGTATCT	86	Lapatto et al., [77]
	(nDNA)	R: TCTCTGCTCCCCACCTCTAAGT		
	HBB	F: CAGGTACGGCTGTCATCAGTTAG	185	Lapatto et al., [77]
	(nDNA)	R: CATGGTGTCTGTTTGAGGTTGCT		
	DLOOP	F: CATCTGGTTCCTACTTCAGGG	106	Lapatto et al., [77]
	(mtDNA)	R: CCGTGAGTGGTTAATAGGGTG		
	CYTB	F: GCCTGCCTGATCCTCCAAAT	132	Lapatto et al., [77]
	(mtDNA)	R: AAGGTAGCGGATGATTCAGCC		
	MT-RNR2	F: GGGGCGACCTCGGAGCAGAA	213	Lapatto et al., [77]
	(mtDNA)	R: ATAGCGGCTGCACCATCGGGA		
Rat	***Tbca***	F: TGTCCCACCTGTTTGTTCTCT	50	Kemper et al., [78]
	(nDNA)	R: GGTCCTTGGACACCTAGACG		Arduini et al., [79]
	Gapdh	F: GGAAAGACAGGTGTTTTGCA	129	Stevanovic-Silva et al., [80]
	(nDNA)	R: AGGTCAGAGTGAGCAGGACA		
	mt-Rnr1	F: CTCAAGACGCCTTGCCTAGC	131	Kemper et al., [78]
	(mtDNA)	R: TCGTATGACCGCGGTGGCT		Arduini et al., [79]
	mt-Rnr2	F: AGCTATTAATGGTTCGTTTGT	132	Stevanovic-Silva et al., [80]
	(mtDNA)	R: AGGAGGCTCCATTTCTCTTGT		

and/or *mt-Rnr1* for rat) to pooled nDNA (*B2M/HBB* for human; *Tbca/Gapdh* for rat) determined using the $^{\Delta\Delta}$Ct method [75, 76].

2.20 | Protein Extraction and Western Blot

Skeletal muscle tissue derived from humans (21 ± 6 mg) and rats (38 ± 14 mg) was added to 2 mL homogenizing mix tubes (Fisherbrand, Fisher Scientific) containing either 1 mL RIPA buffer (Thermo Fisher Scientific) with added protease and phosphatase inhibitors (Halt inhibitor cocktail, Thermo Fisher Scientific) for human samples or sucrose lysis buffer (250 mM sucrose, 50 mM Tris pH 7.5, 1 mM EDTA, 1 mM EGTA, 1% Triton X-100, Sigma–Aldrich) with added inhibitors (Thermo Scientific Pierce Mini Tablets, Thermo Fisher Scientific) for rat samples. Tubes were then transferred to a MagNA Lyser instrument (Roche) for subsequent homogenization (3 × 45 s at 6000 rpm, placing samples on ice for 5 min between each disruption). Following homogenization, protein concentration was quantified for both human (73 ± 13 μg/mg) and rat (84 ± 18 μg/mg) tissue via the bicinchoninic acid (BCA) method (Pierce BCA protein assay kit, Thermo Fisher Scientific) and a FLUOstar Omega microplate reader (BMG LABTECH, Ortenberg, Germany) with supporting software (Omega version 1.3). For Western blotting, protein aliquots were first diluted in 4× Laemmli Sample Buffer (Bio-Rad) with 20 mM Dithiothreitol (DTT, Bio-Rad) and heated at either 45°C (oxidative phosphorylation, OXPHOS) or 70°C (citrate synthase, CS) for 10 min. Following denaturation, 20 or 25 μg for all protein samples (in 15 μL for human and 20 μL for rat) and 5 μL protein marker (10–250 kDa, Precision Plus Protein All Blue Prestained Protein Standards, Bio-Rad) were loaded into pre-cast gels (12 or 15 well, 4%–20% Mini-PROTEAN TGX Stain-Free, Bio-Rad) before undergoing protein separation via electrophoresis (200 volts/V for 30 min). The current was monitored pre- and post-electrophoresis. Following electrophoresis, gels were activated under UV light ChemiDoc MP Imaging System (Bio-Rad), and proteins transferred to PVDF nitrocellulose membranes (0.2 μm, Bio-Rad) using transfer stacks (Bio-Rad) and a Trans-Blot Turbo Transfer System (Bio-Rad). Following protein transfer, membranes were blocked (5% milk in 1% PBS-T for 1 h at RT) and subsequently labeled with primary antibodies against mitochondrial OXPHOS complexes (CI-NDUFB8, CII-SDHB, CIII-UQCRC2, CIV-MTCO1, CV-ATP5A) (1:500, cat. #ab110413, Abcam) and CS (1:4000, cat. #ab96600, Abcam). Primary antibodies were diluted in 1% milk in 1% PBS-T and incubated on a roller overnight at 4°C. After overnight incubation, OXPHOS and CS proteins were labeled with secondary antibodies, GaM IgG (H+L) HRP (1:30000, cat. #31430, Thermo Fisher Scientific) and GaR IgG (H+L) HRP (1:3000, cat. #7074, Cell Signaling Technology), respectively. Membranes were washed (3 × 5 min in 1% PBS-T) between blocking and antibody labeling steps. Finally, membranes were incubated in enhanced chemiluminescence (ECL) HRP substrate (SuperSignal West Dura Extended Duration Substrate, Thermo Scientific) for 5 min at RT to enable visualization of membrane-bound proteins via chemiluminescence using a ChemiDoc MP system (Bio-Rad) and analysis of band intensities using supporting software (Image Lab 6.1, Bio-Rad). For human samples, all timepoints for each participant were loaded on the same gel and repeated to ensure duplicate samples across two separate gels. Band intensities were relativized to their own baseline sample for subsequent timepoints (atrophy/recovery/repeated atrophy), and the average across the 2 gels was reported. Total protein normalization was performed using Bio-Rad stain-free technology. Lane-specific

normalization factors were derived from UV-activated stain-free images and applied uniformly to all target proteins. Loading consistency was then assessed by expressing relative total protein as the percentage difference from each human participant's baseline sample and, for animals, from each rat's right contralateral control limb. Mean percentage differences across samples were 19% for OXPHOS and 20% for citrate synthase in humans, and 11% for OXPHOS and 18% for citrate synthase in rats. Representative total protein gel images are provided in the relevant figures. One human recovery condition sample was excluded from all analysis due to low detection of protein. Thus, there was $n = 8$ (rather than $n = 9$) samples for the human recovery timepoint. Similarly for aged animal samples, the left/surgical and right/non-surgical limbs for each animal and condition (excluding repeated atrophy as the protein lysates were low quality and quantity) were loaded on the same gel across two separate gels. Band intensities of left/surgical limb were relativized to thier own right/non-surgical limb for each condition (sham/atrophy/recovery). Control samples consisting of a mixture of all human or rat samples were loaded in duplicate within each gel to ensure consistent sample loading. There was no CII-SDHB band detected in 1 out of the 2 gels for both human and rat samples. Therefore, data was derived from only one gel for this protein.

2.21 | NAD^+ Measurements

NAD^+ levels were measured using an enzymatic cycling assay [81]. Briefly, 11 ± 1 mg (human) and 8 ± 2 mg (rat) muscle were lysed in 400 µL 0.6 M perchloric acid ($HClO_4$) and homogenized using steel beads and a TissueLyser II (Qiagen). Following homogenization, samples were centrifuged for 5 min at 13 000 g. The supernatant was transferred to new tubes and neutralized in 100 mM Na_2HPO_4 (1:300 for human, 1:800 for rat). For the assay, 100 µL of diluted extract was pipetted into a white 96-well plate after which 100 µL of reaction mix was added. The reaction mix contained: 100 mM Na_2HPO_4, 10 µM flavinmononucleotide, 2% ethanol, 90 U/mL alcohol dehydrogenase, 130 mU/mL diaphorase, 2.5 µg/mL resazurin, and 10 mM nicotinamide. A Hidex Sense Microplate Reader (Hidex, Finland) was used to measure the fluorescence of accumulated resorufin (Ex 544 nm/Em 580 nm) for 30 mins immediately after the reaction mix was added. Samples were run in duplicate, and NAD^+ content was calculated from the increase in fluorescence of a dilution series of NAD^+. Values were normalized to protein concentration by dissolving the resultant pellets from the previous centrifugation step in 0.2 M NaOH via heating to 95°C. Protein concentrations were determined using the BCA assay (Pierce BCA protein assay kit, Thermo Fisher Scientific).

2.22 | Statistical Analysis

A Shapiro-Wilk's test of normality was first performed for all physiological (e.g., body weight, SkM mass, strength, mCSA, and fCSA), protein abundance, mtDNA content, and NAD^+ measurements. A repeated (for human) or between (for aged animals) measures one-way analysis of variance (ANOVA) with Tukey's HSD post hoc detected significant ($p \leq 0.05$) differences whenever data were normally distributed. Whenever data were non-normally distributed, a Friedman (for human) or Kruskal-Wallis (for aged animals) test with follow-up Dunn's post hoc was carried out. For human myofiber (fCSA and fiber type) analysis, a mixed-effects model was used to account for missing subjects at some timepoints and for clustering of multiple fiber-level observations within each subject (unequal fibre counts per timepoint). For animal fCSA frequency distributions were compared between left and right limbs using the Kolmogorov–Smirnov test on raw fiber-level data. Tests were performed per animal and fiber type, and *p*-values were combined across animals using Fisher's method. For animal body weight (individual conditions), myofiber, mtDNA, and NAD^+ content analyses, a two-way ANOVA (within subject factor: limb, between subject factor: condition/timepoint) with Tukey's HSD post hoc was performed. For mean animal body weight across all conditions, an unpaired t-test was performed. All statistical analysis was conducted in GraphPad Prism software for macOS (version 10.4.1, Massachusetts, USA), and associated figures were created using GraphPad or R studio for macOS (version 4.4.3). All data were presented as mean ± standard deviation (SD) unless otherwise stated in the figure legends. RNA-seq and RRBS/RREM data statistical analyses are described above. For integration of RNA-seq and RRBS data, differentially expressed genes (DEGs) and differentially methylated regions (DMRs) were first identified using the approaches detailed in the RNA-seq analysis section and RRBS/RREManalysis section. These datasets were then integrated using self-organizing map (SOM) profiling. This approach enabled temporal clustering of DEGs and DMRs on a common scale, allowing visualization of coordinated inversely related transcriptional and epigenetic signatures across atrophy, recovery, and repeated atrophy.

3 | Results

3.1 | Physiological Characterization of Muscle Size, Strength and Quality, Myofiber Structure, Fiber-Type, and Myosin Isoform Expression in Response to Atrophy, Recovery, and Repeated Atrophy in Young Adult Humans

To characterize the physiological changes to muscle size, muscle strength, muscle quality, myofiber structural characteristics, fiber-type composition, and myosin isoform expression changes across atrophy, recovery, and repeated atrophy in young adult skeletal muscle (Figure 1A), we first assessed leg lean mass (LLM), quadriceps anatomical cross-sectional area (mCSA), knee extension and flexion strength (isometric MVC), muscle quality (strength normalized to mCSA), fiber cross-sectional area and fiber-type distribution, as well as transcript expression of key myosin light chain (MYL) and myosin heavy chain (MYH) genes. The first period of disuse-induced atrophy (hereafter referred to as "atrophy") resulted in a significant -3.6% reduction in total LLM of the immobilized limb ($p = 0.005$, Figure 1B). Upon returning to normal habitual activity (i.e., "recovery"), mass was fully restored to pre-atrophy baseline levels ($p = N.S.$, recovery vs. baseline). The second period of disuse (i.e., "repeated atrophy") led to a similar, significant −3.2% loss compared to recovery ($p = 0.004$, Figure 1B). Further, assessment of *vastus lateralis (VL)* and *rectus femoris (RF)* mCSA in the immobilized limb revealed a -9% reduction in *VL* mCSA after initial atrophy ($p = 0.0003$), which was fully restored during recovery (recovery vs. baseline,

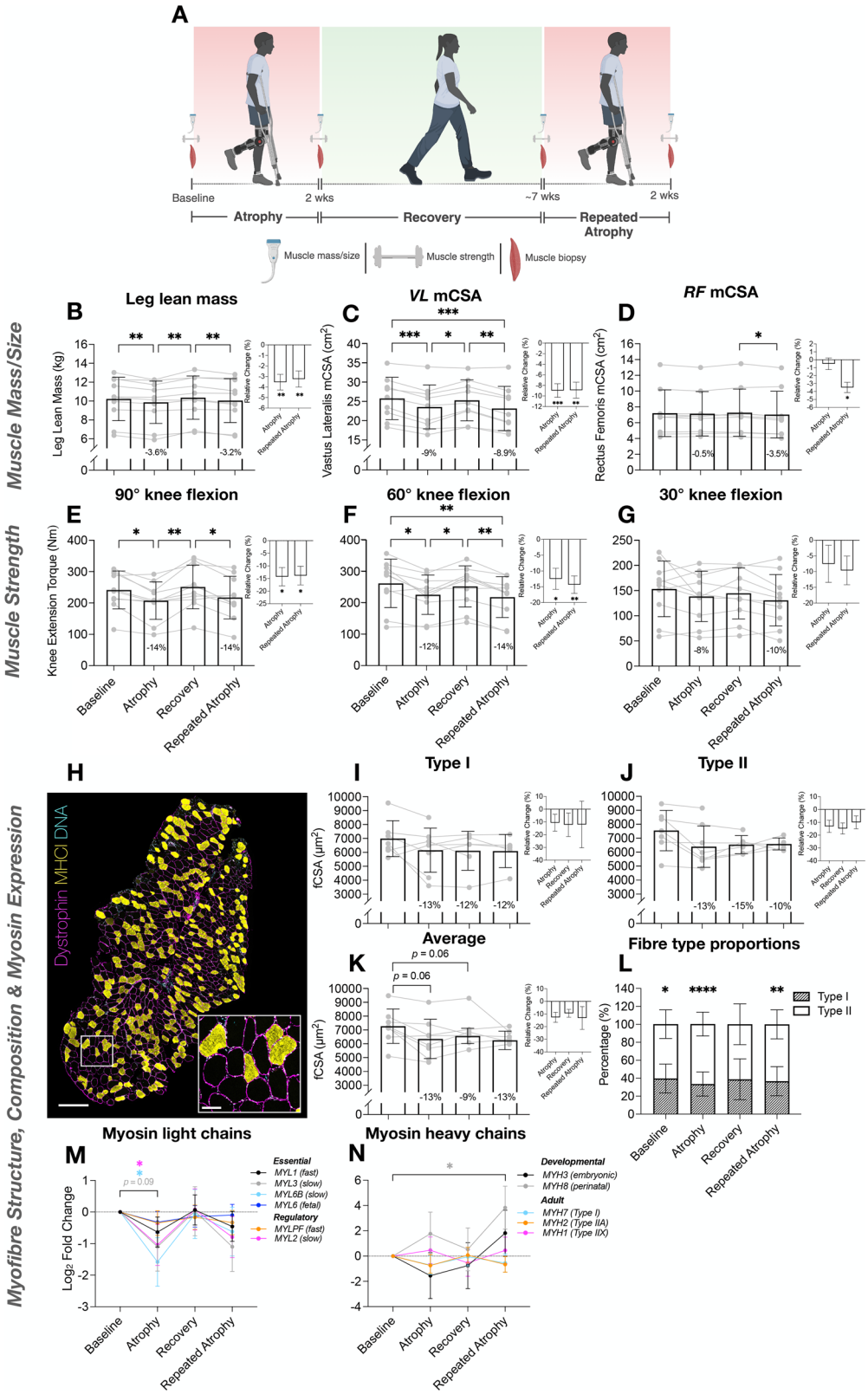

FIGURE 1 | Young adult human intervention study design (created using BioRender.com) (A). Changes in leg lean mass (LLM) (B), *Vastus Lateralis* (*VL*) mCSA (C), *Rectus Femoris* (*RF*) mCSA (D), and muscle strength/MVC torque at 90°, 60°, and 30° knee flexion angles (E–G respectively) after disuse (atrophy), recovery, and repeated disuse (repeated atrophy). Significant reductions in muscle size and strength were observed after disuse atrophy, restored during recovery, and reduced to a similar extent after repeated atrophy. A reduction in *RF* mCSA only occurred after repeated disuse (D). Bar graphs depict relative change (%) from the previous timepoint (i.e., atrophy vs. baseline, repeated atrophy vs. recovery). $N = 10$ for LLM (B) and MVC torque (E–G); $n = 9$ for mCSA (C-D). Myofiber analyses (H–L) revealed reduced fCSA after disuse yet this was not-statistically significant (H–K). $N = 8$ baseline and atrophy, $n = 6$ recovery, $n = 5$ repeated atrophy. (H) Representative fluorescence microscopic image (10× magnification; magenta =

p = *N.S*, Figure 1C). *VL* mCSA was also significantly reduced after repeated atrophy relative to both baseline (−10.6%, p = 0.0003) and previous recovery (−8.9%, p = 0.002, Figure 1C). *RF* mCSA was only significantly reduced after repeated atrophy relative to recovery (−3.5%, p = 0.02, Figure 1D). There were no significant changes in the non-immobilized limb for total LLM (Figure S1A–F) or *VL* and *RF* mCSA (p = *N.S.*, Figure S1G–J). There was, a significant increase in lower leg lean mass of the non-immobilized limb during both periods of disuse, possibly due to a greater reliance on plantarflexor and dorsiflexor muscles to support balance and locomotion during immobilization of the opposite limb (Figure S1F).

Concomitant with the loss of LLM and quadriceps mCSA was a significant reduction in knee extension strength (assessed via MVC) at 90° (−14.3%, p = 0.02) and 60° (−12.5%, p = 0.02) knee flexion following initial atrophy that was also fully restored during recovery (p = *N.S.*) (Figure 1E,F). Repeated atrophy induced a similar loss of strength at 90° (−13.8%, p = 0.02) and 60° (−14.3%, p = 0.002) following recovery (Figure 1E,F). Despite this loss of MVC at 60° and 90°, there were no significant changes in knee extension MVC at 30° knee flexion (p = *N.S.*, Figure 1G). Concurrent reductions in size and strength also resulted in impaired muscle quality (Figure S2A–I). Specifically, MVC at 90° knee flexion when normalized to *RF* mCSA was significantly reduced after atrophy (−12.8%, p = 0.05, Figure S2D), where repeated atrophy led to the greatest loss of specific force at 60° when normalized to *VL* (−7.1%, p = 0.03), *RF* (−12.2%, p = 0.04) and *VL*+*RF* mCSA combined (−8.2%, p = 0.02, Figure S2B,E,H respectively). Finally, repeated atrophy led to significantly reduced knee flexion isometric MVC at 90° (p = 0.03, Figure S2J). Mean MVC at 60° and 30° knee flexion also demonstrated the same trend but did not reach statistical significance (p = *N.S.*, Figure S2K,L).

At the myofiber level, IHC analysis revealed an average reduction in fiber type-specific cross-sectional area (fCSA) after atrophy, which approached significance when pooling fast and slow fibers (Figure 1H–K). Due to limited fiber number in the cross-sections from fewer samples at specific timepoints, we used the open-source "FibeRtypeR" [82] web application to predict fiber type proportions using RNA-seq data. FibeRtypeR analysis revealed a significantly greater proportion of type II fibers at baseline (60% type II vs. 40% type I, p = 0.01), atrophy (67% type II vs. 33% type I, p < 0.001) and repeated atrophy (63% type II vs. 37% type I, p = 0.003) with no significant difference after recovery (61% type II vs. 39% type I, p = 0.05) (Figure 1L). Overall, demonstrating a slow to fast fiber type shift following both periods of disuse that normalised after recovery (Figure 1L). To complement these data, we next interrogated all essential and regulatory fast (*MYL1, MYLPF*), slow (*MYL2, MYL3, MYL6B*), and fetal myosin light chains (*MYL6*) as well as adult (*MYH7, MYH2, MYH1*) and developmental (*MYH3*, *MYH8*) myosin heavy chains (Figure 1M,N) derived from the RNA-seq gene lists. On average, all 6 MYL genes decreased after atrophy, were fully restored after recovery, and then reduced again after repeated atrophy. The slow *MYL2* and *MYL6B* genes were significantly downregulated after atrophy (Figure 1M). A similar temporal profile was observed for slow(er) adult *MYH7* (type I) and *MYH2* (type IIA) genes that both decreased after atrophy and repeated atrophy whereas fast *MYH1* (type IIX) increased after both periods of atrophy (Figure 1N). Overall, suggesting a predominant downregulation of slow MYL and MYHC genes after repeated atrophy and an increase in type IIX myosin. Thus complimenting the IHC analysis demonstrating a shift toward a faster phenotype in response to disuse. Finally, expression of embryonic *MYH3* and perinatal *MYH8* both significantly increased after repeated atrophy (Figure 1N). Having established coordinated changes in muscle size, muscle strength, muscle quality, myofiber structural characteristics, fiber-type composition, and MYH and MYL gene expression across atrophy, recovery, and repeated atrophy in young adult humans, we next sought to determine whether similar or divergent patterns emerge in aged muscle. Due to ethical considerations described in the methods section above, aged animals (rather than aged humans) were used as a surrogate model to examine how ageing influences recovery capacity and susceptibility to repeated atrophy.

3.2 | Muscle Mass, Myofiber Structure, Fiber-type and Myosin Isoform Expression Responses to Atrophy, Recovery, and Repeated Atrophy in Aged Rats

To determine how ageing alters susceptibility to atrophy and repeated atrophy, and whether it impairs the recovery of muscle mass, myofiber structural characteristics, fiber-type composition, and myosin isoform expression, we evaluated muscle weights, histological fiber cross-sectional area and fiber-type distribution, and *Myh* and *Myl* gene expression across atrophy, recovery, and repeated atrophy in aged rats. There was no significant reduction in body weight in control animals after atrophy or recovery (p = *N.S.*) (Table S1), yet a significant reduction in body weight after repeated atrophy (−18.1%, p = 0.02, Table S1). Therefore, muscle weights were normalized to respective body weights for each condition throughout. TTX administration to the common peroneal nerve (CPN) (Figure 2A) resulted in an average reduction of TA muscle weight after initial atrophy (−4.4%, p = 0.6) that was not significant, and a significant loss after repeated TTX-induced atrophy (−29.8%, p = 0.002, Figure 2B). There was also a significantly larger reduction in EDL muscle weight following repeated atrophy (−31.1%, p = 0.01, Figure S3). Our previous study demonstrated that young adult rats recovered muscle mass and fiber CSA following TTX-induced atrophy [66]. A physiological and transcriptomic comparison between aged rats and previously published young rats is presented below to enable robust age-related insights while adhering to ethical refinement principles.

dystrophin/myofiber membrane, yellow = MyHCI/type I myofibers, cyan = DNA, non-staining = putative type II myofibers; Scale bar within tile scan image = 500 µm, scale bar within magnified inset image = 100 µm). FibeRtypeR [82] analysis suggested a larger proportion of fast/type II vs. slow/type I fibers at baseline, atrophy and repeated atrophy with no significant differences after recovery (L). Transcription of slow isoform *MYL* and *MYH* genes decreased after atrophy and repeated atrophy coupled with an increase in fast type IIX (*MYH1*) and developmental *MYH* gene expression after repeated atrophy (M,N). N = 9 for each timepoint derived from RNA-seq data. $^{*}p \leq 0.05$, $^{**}p \leq 0.01$, $^{**}p \leq 0.001$, $^{****}p \leq 0.0001$.

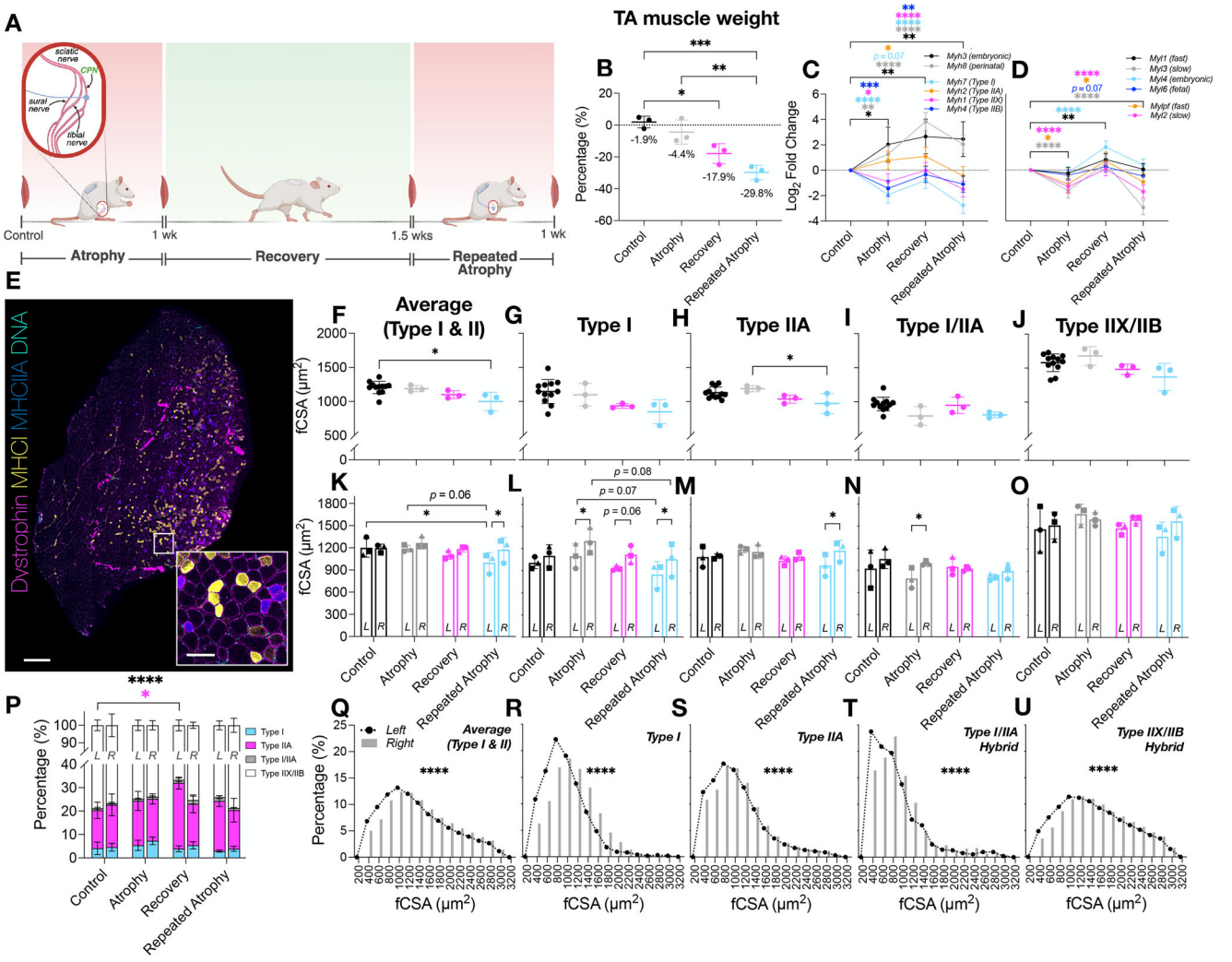

FIGURE 2 | (A) Schematic representation of the repeated disuse model in aged animals (created with BioRender.com). CPN = common peroneal nerve. (B) Reduction in TA muscle weight during atrophy and repeated atrophy with lack of recovery (presented as % change of the left TTX vs. right control limb normalized to body weight). (C) Myosin heavy chain transcriptional analysis revealed significant changes in developmental (*Myh3/8*) and adult (*Myh7/2/1/4*) isoforms after atrophy and repeated atrophy. (D) Essential (*Myl1/3/4/6*) and regulatory (*Mylpf/2*) myosin light chains were also differentially expressed after atrophy, recovery and/or repeated atrophy yet most were restored during recovery, despite continued muscle loss (E) Representative fluorescence microscopic image of a whole TA muscle section labeled with dystrophin (magenta), MyHCI (yellow), MyHCIIA (blue), DNA (cyan). Non-staining represents putative type IIX/IIB myofibers. Tile scan images acquired at 10× magnification (scale bar within whole-scan image = 500 μm, scale bar within magnified inset image = 100 μm). (F–O) There were significant reductions in fCSA in predominantly slow fibers after atrophy (type I and I/IIA hybrid fibers), and after repeated atrophy in average, type I and type IIA fibres. Symbol shapes represent individual animals. (P) Proportional fiber type analysis revealed greater contribution of type IIA and reduced number of IIX/IIB after recovery vs. control in the left surgical limb. (Q–U) Fiber size distribution analysis demonstrates a leftward shift and larger frequency of smaller (< 1000 μm^2) fibers in the left TTX vs. right control limb. *$p \leq 0.05$, **$p \leq 0.01$, ***$p \leq 0.001$, ****$p \leq 0.0001$. fCSA = myofiber cross-sectional area.

Despite TTX-cessation and a return to normal dorsiflexion in aged rats during the recovery period, TA muscle loss continued to occur after recovery (−17.9%, $p = 0.01$, Figure 2B), despite shorter TTX exposure and longer active recovery than young adult rats [66]. There was no significant reduction in plantarflexor (soleus, plantaris, and gastrocnemius) muscle weights, thus emphasizing precise selective silencing of the dorsiflexor muscles using TTX (p = *N.S.*, Figure S3A–D). At the transcript level, there was increased expression of developmental myosin heavy chain (*Myh3/8)* genes across all conditions (Figure 2C), whereas adult fast (*Myh1/4*), slow (*Myh7*) myosin heavy chains, as well as essential (*Myl3*) and regulatory (*Mylpf/2*) myosin light chains significantly decreased after both periods of disuse (Figure 2D). Interestingly, these genes returned to control levels upon recovery despite continued muscle loss during TTX cessation (Figure 2C,D) suggesting that *Myh1/4/7* and *Myl2/3/pf* genes were sensitive to the TTX-disuse stimulus. Conversely, *Myh2*, *Myl1*, and *Myl4* gene expression significantly increased following TTX cessation only. Overall, persistent elevation of developmental *Myh3* and *Myh8* mRNA expression coupled with significant reductions in adult fast and slow *Myh* and *Myl* isoforms occurred after both periods of atrophy. Coinciding with reductions in muscle weight and *Myh* and *Myl* expression, IHC analysis (Figure 2E) demonstrated a significant loss in average (type I & II combined, Figure 2F,K),

type I (Figure 2G,L), and type IIA (Figure 2H,M) fCSA after repeated atrophy. There was also a significant reduction in pure type I (Figure 2G,L) and hybrid I/IIA (Figure 2I,N) fCSA after initial TTX-induced atrophy, thus supporting the transcriptional expression data that suggests predominantly slow fibers were sensitive to TTX stimulus. When relativizing the left TTX to right control limb, there were no significant changes in fCSA across all fiber types (Figure S3F–J). Finally, there was a greater contribution of type IIA and a reduced proportion of IIX/IIB fibers after recovery (Figure 2P), where fCSA distributions were significantly left-shifted in the left limb, indicating a higher frequency of smaller fibers following TTX-exposure for each fiber type ($p < 0.0001$) (Figure 2Q–U).

Having established that aged muscle exhibits impaired recovery capacity, persistent myofiber atrophy, marked reductions in slow and fast myosin isoform expression, and altered fiber-type composition across atrophy, recovery, and repeated atrophy, we also observed that the majority of *Myh* and *Myl* genes returned toward control levels during the recovery period, despite continued loss of muscle mass. This dissociation between physiological outcomes and transcriptional normalization suggested that aged muscle retains sensitivity to TTX-induced disuse but is unable to translate transcriptional recovery *Myh* and *Myl* genes into restoration of muscle mass. To define the molecular basis of this divergent physiological–transcriptional relationship, and to establish a reference molecular profile for subsequent age comparisons, we next examined genome-wide transcriptomic responses following atrophy, recovery, and repeated atrophy in young adult human skeletal muscle, enabling direct comparison with the aged-rat transcriptome profiles that follow.

3.3 | Transcriptomic Responses to Atrophy, Recovery, and Repeated Atrophy in Young Adult Human Skeletal Muscle

To determine whether the physiological and structural responses observed in young adults are underpinned by coordinated alterations in gene expression, and to establish a molecular reference for comparison with the aged-rat transcriptome, we next performed transcriptomic analysis in young human skeletal muscle across atrophy, recovery, and repeated atrophy. In young adult humans, the largest changes in gene expression occurred after initial atrophy, where most genes were downregulated after both atrophy and repeated atrophy (Figure 3A–F). PCA analysis revealed a larger overlap between baseline and recovery as well as between atrophy and repeated atrophy timepoints, suggesting a closer transcriptomic profile between both periods of physical activity (baseline and recovery) and inactivity (atrophy and repeated atrophy) (Figure 3B). Among the 15,087 genes detected, there were 4-5-fold more DEGs after initial atrophy (381 DEGs) than after repeated atrophy (103 DEGs vs. baseline, 82 DEGs vs. recovery) with predominant downregulation of genes after both atrophy (63%) and repeated atrophy (77% vs. baseline, 85% vs. recovery) (Figure 3C–F). Following recovery from initial atrophy, more genes were upregulated (58%) (Figure 3E). Venn diagram analysis demonstrated a large proportion of overlapping downregulated (45% of total repeated atrophy DEGs vs. baseline and recovery) or upregulated (53%) genes after both periods of atrophy (Figure 3G). During recovery, there were no detected DEGs relative to baseline, with 536 DEGs following recovery from initial atrophy, which were all unique from atrophy and repeated atrophy comparisons (Figure 3E,G).

Interrogation of the most differentially expressed genes across comparisons revealed that *NMRK2*, an NAD^+ biosynthesis gene, was among the top-most downregulated DEGs after atrophy (-8.4 FC), ranked second to the nuclear receptor, *NR4A3* (-11.5 FC, Figure 3C,H). *NMRK2* was also the most downregulated gene after repeated atrophy vs. baseline (-5.0 FC) and when compared with recovery (-5.6 FC), as well as the most upregulated DEG after recovery vs. atrophy (9.2 FC, Figure 3C,H). Interestingly, after repeated atrophy only, the most upregulated genes were developmental myosin heavy chain *MYH8* (14.2 FC vs. baseline, 9.8 FC vs. recovery), tropomyosin-binding subunit *TNNT2* (8.3 FC vs. recovery) and NMJ nicotinic acetylcholine receptor (nAChR) subunit genes, *CHRNA1* (5.4 FC vs. baseline) and *CHRND* (4.0 FC vs. baseline) (Figure 3D,F). Another AChR subunit gene, *CHRNG* (2.86 FC vs. baseline), was one of the most upregulated after repeated atrophy only (Figure 3H).

Such transcriptional perturbations across the transcriptome corresponded to significant downregulation of enriched pathway and gene ontology (GO) terms related to aerobic metabolism, respiration (e.g., NAD^+ / NADH metabolism, TCA cycle, ETC, ATP synthesis) and mitochondrial structure, function and turnover after both periods of disuse, with these genes returning to baseline levels after recovery (Figure 3I–K, cluster 1). Furthermore, enrichment of upregulated genes (including AChR subunits and *MYH8 and TNNT2* highlighted above) were associated with muscle-specific terms, including acetylcholine receptor signaling, synaptic transmission, membrane depolarization, and skeletal muscle contraction (Figure 3I,J). Processed human RNA-seq data and whole DEG lists are available in Data S1.

3.4 | Temporal Profiling of Transcriptional Responses (SOM analysis) in Young Adult Human Skeletal Muscle

To build upon the global transcriptional alterations identified above, and to determine whether repeated disuse modifies the temporal coordination of gene expression rather than merely its magnitude, we next applied Self-Organizing Map (SOM) profiling to cluster transcripts according to their trajectories across atrophy, recovery, and repeated atrophy. This approach enabled us to distinguish genes that exhibited transcriptional protection during repeated disuse from those that retained or amplified their responses after atrophy into recovery or after repeated atrophy, respectively. Temporal SOM gene clustering analysis revealed most genes decreased (57%, cluster 1) and increased (41%, cluster 2) after atrophy, returned to baseline levels after recovery, and were less susceptible to changes after repeated disuse (Figure 3K). This represented a transcriptional attenuation, resulting in a smaller magnitude of change to repeated atrophy stimuli for both downregulated (cluster 1) and upregulated (cluster 2) genes. Based on SOM standardized means, there was a 40% smaller magnitude in downregulation of genes in cluster 1 and an 72% smaller magnitude in upregulation of genes in cluster 2 after repeated atrophy compared with

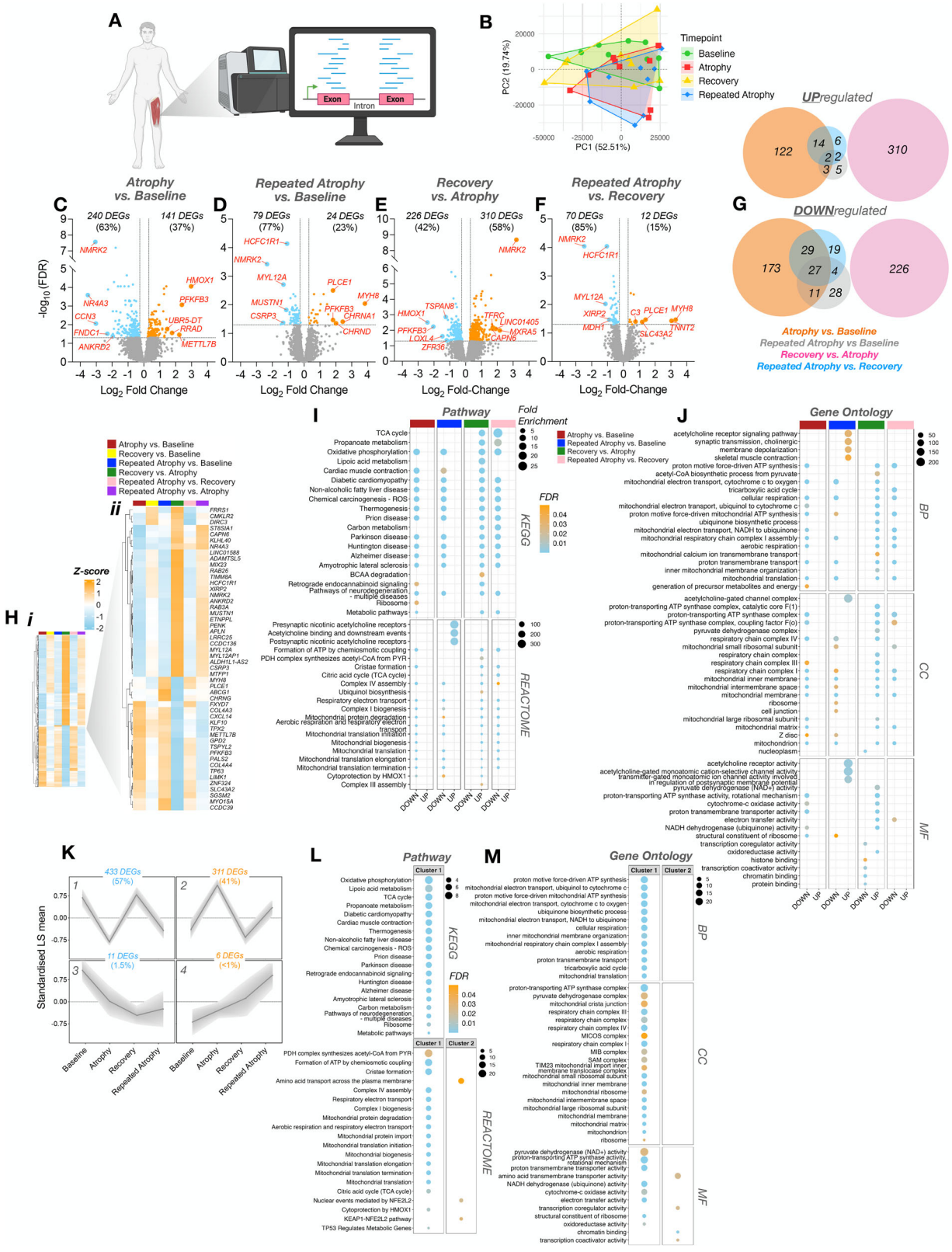

FIGURE 3 | (A) Schematic depicting the transcriptomic response to repeated disuse atrophy in young adult human skeletal muscle (created with BioRender.com). (B) Principal component analysis (PCA) by time point. (C–F) Volcano plots depicting the number of differentially expressed genes (DEGs) that were either DOWN-regulated (blue) or UP-regulated (orange) for each pairwise comparison. No genes met the FDR ≤ 0.05 and ±1.2-fold change (FC) thresholds for the repeated atrophy vs. atrophy and recovery vs baseline comparison. Twelve and ten genes met an unadjusted p value ≤ 0.001 for these comparisons respectively, and the full list is provided in Data S1. Labeled genes within volcano plots represent the top 5 DEGs according to greatest FC in either direction of change (FDR ≤ 0.05). (G) Venn diagrams depict the number of unique and common DEGs across all timepoints for both DOWN-regulated (bottom) and UP-regulated (top) DEGs. (H) Heatmap of all DEGs in at least one comparison (Hi). Magnified heatmap displaying the top 25 DOWN-regulated (blue) or UP-regulated (orange) genes according to average FC across all timepoints (Hii). Over-representation analysis (ORA)

initial atrophy in young adult human muscle. Pathway and GO terms associated with enrichment of downregulated genes after both periods of disuse (cluster 1) were present in the same aerobic metabolism, respiration and mitochondrial-related terms identified across global downregulated genes described above (i.e. NAD^+/NADH dehydrogenase activity, TCA cycle, ETC, ATP synthesis and mitochondrial structure, assembly and protein turnover pathway genes, Figure 3L,M). Genes that were upregulated after atrophy and increased to a lesser extent after repeated atrophy (cluster 2, Figure 3K), were enriched in terms related to amino acid transport, transcription coregulator/coactivator activity and chromatin binding (Figure 3L,M). In contrast, these terms/pathways were then enriched among downregulated genes after recovery from atrophy (Figure 3J). Therefore, the fewer number of total DEGs coupled with less susceptible alterations to repeated vs. initial atrophy suggests a transcriptionally protective memory of earlier atrophy. SOM cluster temporal analysis also identified 11 downregulated genes (*NR4A1, NR4A3, PRKAG2, RP9, CIITA, CORO2B, ENSG00000242299, RPL35, SNRPA1, UBE3D, RPL29P11*) after atrophy that remained downregulated during recovery, despite restoration of muscle mass (cluster 3, Figure 3K). This included nuclear receptor gene, *NR4A1* and *NR4A3*, as well as *PRKAG2* (AMPK gamma-2 subunit), where *NR4A3* was the top ranked downregulated genes within enriched metabolic processes. Ribosomal genes (*RPL35*, *RPL29P11*) also exhibited downregulated enrichment at the pathway level after atrophy (Figure 3J), indicating a transcriptional 'memory' of the initial disuse episode through the retention of suppressed expression even after the recovery period. Finally, 6 genes (*TNNT2, MYH3, DCLK1, ZBED6CL, CDC73, WDR44*) were upregulated after atrophy, remained elevated during recovery, with even larger increases in expression after repeated atrophy (cluster 4, Figure 3K). This included *TNNT2* (top ranked upregulated gene as discussed above), embryonic myosin heavy chain (*MYH3*), *DLK1* associated with regeneration of muscle following injury, and *ZBED6CL* also linked with muscle development. Therefore, whilst most genes demonstrated transcriptional protection after repeated atrophy, a small number of genes related to muscle development and regeneration (together with the AChR subunit genes (*CHRNA1*, *CHRND* and *CHRNG* discussed above) demonstrated amplified responses to repeated atrophy in adult human muscle. The retained upregulation and larger increases after repeated disuse also suggests a transcriptional memory of earlier atrophy in these genes.

Taken together, the global transcriptomic analysis and SOM temporal profiling demonstrate that young adult skeletal muscle predominantly exhibits a coordinated transcriptional protection against repeated disuse, characterized by attenuated suppression of NAD^+ and oxidative metabolism, mitochondrial, and structural gene networks, with only a small subset of developmental and neuromuscular genes retaining or amplifying their transcriptional response after a repeated atrophic episode. To determine whether ageing disrupts this protective molecular programme, and to identify transcriptional signatures underlying the impaired physiological recovery observed in aged muscle, we next examined transcriptomic profiles in aged rat muscle across atrophy, recovery, and repeated atrophy.

3.5 | Transcriptomic Responses to Atrophy, Recovery, and Repeated Atrophy in Aged Rat Skeletal Muscle

Transcriptomic and associated SOM profiling in young adult muscle revealed a coordinated transcriptional protection to repeated disuse, characterized by attenuated suppression of NAD^+ and oxidative metabolism, mitochondrial, and structural gene networks. To determine whether ageing alters this transcriptional resilience, and to identify molecular signatures underpinning the impaired physiological recovery observed in aged muscle, we next performed transcriptomic analysis in aged rat muscle across atrophy, recovery, and repeated atrophy. Alongside the loss of TA muscle mass during atrophy, recovery and repeated atrophy in aged animals, there were considerably large transcriptomic perturbations after atrophy and recovery with the greatest changes detected after repeated atrophy (Figure 4A–I). PCA analysis showed similar clustering of TTX-induced atrophy and repeated atrophy, and distinct clustering after TTX cessation-induced recovery (Figure 4B,C). There was also considerable overlap of the sham surgical and pooled non-surgical controls (Figure 4B). Given there were no DEGs detected between sham and pooled contralateral control limb samples, suggesting the surgery had no significant impact on gene transcription, we excluded sham samples from further analysis and pooled contralateral (right) non-surgical limb samples for the control group. Among the 11,284 genes detected post-normalization, there were 2106 DEGs in response to atrophy and 2008 after recovery, with approximately 2-fold more DEGs detected after repeated atrophy (3937 DEGs) vs. controls. The proportion of downregulated DEGs was 56% after atrophy (Figure 4D), 53% after recovery and 56% (vs. control) or 58% (vs. recovery) after repeated atrophy (Figure 4F–H). However, despite a similar number of total DEGs after atrophy and recovery, the majority of downregulated (90%) and upregulated (74%) DEGs were unique after TTX cessation (Figure 4J), as evidenced by the distinct PCA clustering of recovery samples (Figure 4C). Also, while the 2-fold greater number of DEGs after

of the top 20 enriched (J) pathway (KEGG, top 4 panels; REACTOME, bottom 4 panels) and (K) gene ontology (GO) terms for both DOWN-regulated and UP-regulated DEGs across all comparisons ("Atrophy vs. Baseline", "Repeated Atrophy vs. Baseline", "Recovery vs. Atrophy", "Repeated Atrophy vs. Recovery"). (K) Self-Organizing Maps (SOM) composed of 761 genes that were significantly differentially expressed in at least one comparison, revealing four cluster temporal profiles across the time-course of atrophy, recovery and repeated atrophy. Cluster 1 & 3 (blue) represent genes that were DOWN-regulated following atrophy. Cluster 2 & 4 (orange) depict UP-regulated genes atrophy. (L) Pathway and (M) GO analysis revealed enriched terms for clusters 1 and 2 only, in which most genes were either DOWN-regulated (Cluster 1, shown in panel K) or UP-regulated (Cluster 2, shown in panel K) after atrophy, recovered upon reloading and were less susceptible to changes after repeated atrophy. Cluster 3, shown in panel K represents genes that were downregulated after atrophy, with retained reductions in transcription during recovery and repeated atrophy. Cluster 4, shown in panel K, represents genes upregulated after atrophy, retained during recovery, followed by greater increases in expression after repeated atrophy. BP = biological process, CC = cellular component, MF = molecular function.

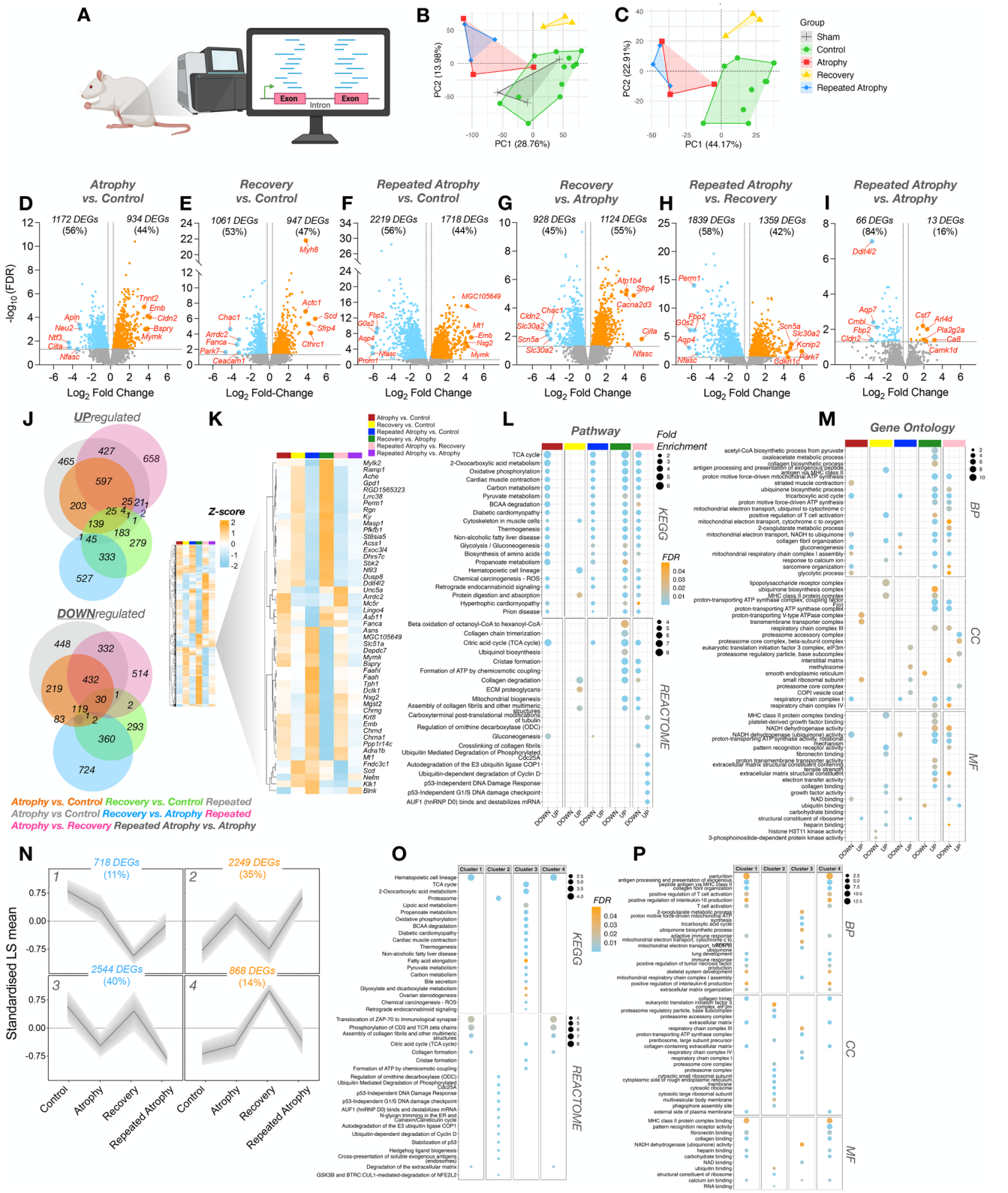

FIGURE 4 | (A) Schematic depicting transcriptomic (via RNA-seq) analysis of repeated TTX-induced disuse atrophy in aged animals (created using BioRender.com). Principal component analysis (PCA) including (B) and excluding (C) sham surgery group. (D–I) Volcano plots depicting the number of differentially expressed genes (DEGs) that were either DOWN-regulated (blue) or UP-regulated (orange) for each pairwise comparison. Labeled genes within volcano plots represent the top 5 DEGs according to greatest fold-change with FDR ≤ 0.05. There were no DEGs detected in sham vs. pooled contralateral control limb, suggesting the surgery had no significant impact on gene transcription. The sham group was therefore excluded for all downstream analyses and pooled contralateral limb was used as the control. (K) Heatmap of all DEGs in at least one comparison. Magnified heatmap displaying the top 50 DOWN- (blue) and top 50 UP-regulated (orange) genes (by gene symbol) by average fold-change across all pairwise

repeated atrophy vs. initial atrophy may be partially explained by the lack of recovery during the no TTX period, when relativized to previous recovery, the number of DEGs after repeated atrophy (3198 DEGs) was still 1.5-fold more than initial atrophy (2052 DEGs) (Figure 4H), that corresponded to a -11.9% reduction in muscle mass after repeated atrophy vs. recovery (Figure 2B). There were 79 DEGs after repeated vs. initial atrophy in aged animals with a larger number of downregulated (84%) versus upregulated (16%) genes (Figure 4I). Most of these were shared across both periods of atrophy (2461 DEGs/75% downregulated, 3935 DEGs/61% upregulated), but there were a smaller proportion of DEGs unique to repeated atrophy that were downregulated (1294 DEGs/25%) and upregulated (1550 DEGs/39%) (Figure 4J).

Regarding gene-specific alterations, the top downregulated DEGs included genes associated with NMJ function and stability (*Ache, Unc5a, Ntf3, Nfasc*), mitochondria and metabolism (*Park7, Perm1, Nfil3, Gpd1, Acss1, Mc5r, Dhrs7c, G0s2, Fbp2*), muscle structure and contraction (*Lrrc38, Ky, Mylk2, Rgn*) as well as DNA damage (*Fanca, Ddit4l2*) (Figure 4K). Interestingly, the myokine, *Apln*, important for angiogenesis, muscle regeneration, and ATP synthesis was among the top 5 downregulated genes after initial TTX-induced atrophy (-9.7 FC, Figure 4D) (that also decreased after repeated atrophy) and was also within the top 25 downregulated genes in young adult humans after atrophy (identified above,Figure 3H). Concerning the top upregulated genes, the muscle specific fusogenic gene, *Mymk* significantly increased after both atrophy (12.8 FC, Figure 4D) and repeated atrophy (18.6 FC, Figure 4F). Also, among the top-ranked upregulated genes after initial atrophy was tropomyosin-binding, *Tnnt2* (11.8 FC, Figure 4D). Embryonic *Myh8* was one of the most upregulated DEGs after recovery (14.3 FC, Figure 4E) and was among the top-ranked upregulated DEGs in young adult human muscle after repeated atrophy (Figure 3D,F). Further, NMJ AChR subunit genes, *Chrnd*, and *Chrna1* were both ranked among the top upregulated genes in aged rat muscle after both atrophy (*Chrnd* = 5.8 FC*, Chrna1* = 7 FC) and to an even greater extent after repeated atrophy (*Chrnd* = 12.5 FC*; Chrna1* = 16 FC) whilst *Chrng* significantly increased after repeated atrophy only (Figure 4K). Such AChR genes were also similarly upregulated in young adult human muscle following disuse (Figure 3D,H). Collectively, genes *Tnnt2, Myh8, Chrna1, Chrnd* and *Chrng*, increased in response to disuse-induced muscle wasting, irrespective of age, species and atrophy model utilized.

Enrichment analysis of downregulated genes revealed similar pathways and GO terms in aged rat muscle after both atrophy and repeated atrophy as also demonstrated in young human muscle (described above). Specifically, terms related to metabolic processes and aerobic respiration (e.g., NAD binding / NADH dehydrogenase activity, TCA cycle, ETC, and ATP synthesis) as well as muscle-specific terms (e.g., muscle contraction, cytoskeleton in muscle cells, and sarcomere organization) demonstrated enrichment in downregulated genes (Figure 4L,M). Further, most of these terms were enriched in upregulated genes after TTX cessation in the recovery period following initial atrophy, suggesting the genes in these pathways returned to control levels after the recovery period following initial disuse, despite continued muscle wasting after TTX cessation. This also suggests that these genes and pathways were responsive to TTX during disuse and normalised after reloading during the recovery period. This was also observed in young adult human muscle, where downregulated expression of genes within these pathways returned to baseline levels after reloading of the muscle during recovery. In aged rat muscle, enrichment analysis of upregulated genes that occurred after both atrophy and repeated atrophy was evident within ribosomal structure and subunit terms (Figure 4L). Interestingly, up-regulated genes enriched for pathways related to proteasomal core and accessory complex, ECM turnover, ubiquitin-mediated proteolysis and DNA damage pathways were evident after repeated atrophy only (Figure 4L,M). Processed aged rat RNA-seq and whole DEG lists are available in file Data S2. While DEG-level analyses in aged muscle revealed extensive transcriptional perturbations, including exaggerated suppression of oxidative metabolism, NAD^+/NADH, and structural gene networks after repeated atrophy, these comparisons do not capture the temporal transcriptional responses across the time-course of atrophy, recovery and repeated atrophy. Given that SOM profiling in young adult muscle identified clear predominant temporal signatures of transcriptional protection after repeated disuse, we next applied SOM clustering analysis in aged rat muscle to determine whether ageing disrupts this pattern of coordinated temporal regulation. This analysis enabled us to identify gene clusters that define the impaired recovery and heightened susceptibility of aged muscle across atrophy, recovery, and repeated atrophy.

3.6 | Temporal Profiling of Transcriptional Responses (SOM analysis) in Aged Rat Skeletal Muscle

To determine whether the temporal protection observed in young adult muscle is lost with ageing, and to establish how gene-expression trajectories relate to the impaired physiological recovery in aged rats, we next applied SOM temporal clustering to the aged-rat transcriptome across atrophy, recovery, and repeated atrophy. Temporal clustering analysis by SOM profiling revealed

comparisons. (J) Venn diagrams depicting the number of unique and common DEGs across all conditions for both UP-regulated (top) and DOWN-regulated (bottom) DEGs. Over-representation analysis (ORA) of the top 20 enriched (L) pathway (KEGG, top 4 panels; REACTOME, bottom 4 panels) and (M) gene ontology (GO) terms for both DOWN- and UP-regulated DEGs across all comparisons ("Atrophy vs. Control", "Recovery vs. Control", "Repeated Atrophy vs. Control", "Recovery vs. Atrophy", "Repeated Atrophy vs. Recovery"). (N) Self-Organizing Maps (SOM) composed of a total 6,379 genes that were DEGs in at least one comparison, illustrating gene cluster temporal profiles across the time-course of repeated disuse atrophy. Profiles 1 & 3 represent genes that were DOWN-regulated following the first period of atrophy whereas profiles 2 & 4 depict UP-regulated genes after initial atrophy. (L) Pathway and (M) GO analysis revealed enriched terms across all cluster profiles where most genes were either UP-regulated (cluster 2) or DOWN-regulated (cluster 3) after atrophy, recovered upon TTX cessation, followed by larger changes (in the same direction of initial atrophy) after repeated disuse atrophy. BP = biological process, CC = cellular component, MF = molecular function.

that 75% of genes (40% downregulated, cluster 3; 35% upregulated, cluster 2) after atrophy, were largely restored to control levels after TTX cessation during recovery, followed by larger magnitude changes after repeated disuse (Figure 4N). This indicates that most genes recovered after initial atrophy despite continued muscle loss in aged muscle, yet showed exaggerated responses after repeated atrophy. Specifically in cluster 3, downregulated genes after atrophy that returned to control levels during recovery (despite continued loss of muscle mass), followed by greater reductions during repeated atrophy, were enriched in: aerobic metabolism, TCA cycle, NAD binding/NADH dehydrogenase activity, ETC and ATP synthesis in the mitochondria as well as in muscle structure and function (cluster 3) (Figure 4O,P). Based on these SOM standardized means, on average there was a 95% larger magnitude of decreased expression of genes within cluster 3 after repeated atrophy compared with initial atrophy. Therefore, genes associated with these metabolic pathways demonstrated, on average, a 95% greater magnitude of downregulation in transcripts after repeated atrophy, whereas young adult human muscle demonstrated a less susceptible, attenuated transcriptional response in genes within the same pathways following repeated atrophy. This suggests a negative, detrimental and exaggerated transcriptional response to repeated atrophy in aged muscle. Importantly, these genes still recovered to control levels during recovery, despite continued muscle wasting in aged animals. Therefore, the amplified response to repeated atrophy in aged muscle was not simply due to the lack of recovery but rather an exaggerated response to repeated atrophy having experienced earlier TTX-induced disuse atrophy. Genes within cluster 2 (Figure 4N) that were upregulated after atrophy, returned to control levels during recovery and were upregulated to a greater extent during repeated atrophy, were enriched in proteasome, ECM turnover, and DNA damage pathways in aged muscle (Figure 4O,P). Based on SOM standardized means, there was an average 141% larger magnitude in upregulation of genes in cluster 2 after repeated atrophy compared to the initial atrophy. These genes and terms were unique to aged muscle, also demonstrating recovery of gene expression despite continued muscle wasting during the recovery period, followed by exaggerated transcriptional and physiological responses to repeated atrophy. A small proportion of genes also decreased (11%, cluster 1) or increased (14%, cluster 4) to a lesser extent during atrophy with the largest change occurring during recovery, followed by a return to atrophy levels during repeated atrophy (Figure 4N). Genes in both clusters 1 and 4 were enriched in inflammatory pathways, ECM turnover, collagen assembly and matrix organization (Figure 4O,P), suggestive that changes in inflammatory and ECM genes were associated with continued muscle wasting in aged muscle, despite TTX cessation.

Together, these DEG-level and temporal transcriptional analyses demonstrate that aged skeletal muscle exhibits a marked susceptibility to repeated disuse, characterized by greater suppression of oxidative metabolism, mitochondrial, NAD^+/NADH, and structural gene networks, despite the recovery of these pathways during the TTX cessation period. These findings, coupled with the continued physiological decline observed in aged rats during the recovery period, suggest that ageing disrupts the capacity to translate transcriptomic restoration into physiological recovery. To contextualize this age-related susceptibility within species, and to determine whether these exaggerated molecular responses diverge from those observed in younger muscle exposed to the same disuse paradigm, we next compared the aged-rat physiological and transcriptomic responses with previously published young adult rat data generated using the same TTX-induced atrophy and recovery model.

3.7 | Physiological and Transcriptomic Responses to TTX-Induced Atrophy and Recovery in Young Adult Rat Skeletal Muscle

In both young adult human and aged rat muscle, initial and repeated atrophy were characterized by marked downregulation of genes associated with aerobic respiration and mitochondrial function, with these pathways recovering upon return to habitual activity in both species despite divergent physiological outcomes. Given the full physiological recovery observed in young adults and the persistent muscle loss in aged rats, we next examined previously published data from young adult rats exposed to the same TTX-induced atrophy and recovery model to contextualize the age-related susceptibility observed herein. This within-species comparison enables robust interpretation of age effects while adhering to ethical refinement principles, as it avoids unnecessary duplication of animal experiments. Notably, our earlier work demonstrated that young adult rats recovered muscle mass and fCSA following a slightly longer period of TTX exposure and a shorter active recovery interval than that used in the present aged cohort [66]. Specifically, young adult rats received 2-weeks of TTX exposure vs. 1-week in aged rats in the present study, resulting in an average −51% and −69% loss of TA muscle mass and fCSA, respectively (Figure 5A–C). Interestingly, a shorter 1-week recovery period in young adult rats (vs. 1.5 wks in aged animals) resulted in recovered TA mass and fCSA by 53% and 63%, respectively compared to the prior 2-week atrophy period (Figure 5A,C). This physiological response contrasts with aged animals herein, where TA muscle weight and fCSA continued to decrease during a longer active recovery, despite less atrophy observed following shorter TTX exposure (Figure 5B,C). Together with similar recovery of genes within the same pathways in young adult human muscle and aged rat muscle, this suggests that the lack of recovery in aged animals is dependent on age and not insufficient time to recover. In support of this, overlapping transcriptome datasets from young and aged animals revealed a considerable degree of overlap of DEGs after atrophy (77% upregulated and 72% downregulated DEGs) with a much smaller overlap after recovery (34% upregulated and 26% downregulated) (Figure 5D–H).

3.8 | Integrative Methylome-Transcriptome Analysis Identifies Epigenetic Regulation of Metabolic, Mitochondrial, and Neuromuscular Gene Networks After Repeated Atrophy

To determine whether the transcriptional signatures identified above in both young adult humans and aged rat were accompanied by coordinated epigenetic alterations, we next integrated RNA-seq and RRBS datasets by mapping DEGs and differentially methylated regions (DMRs) onto shared temporal trajectories using SOM profiling. This approach enabled us to identify genes that exhibited inverse SOM profiles of DNA methylation and

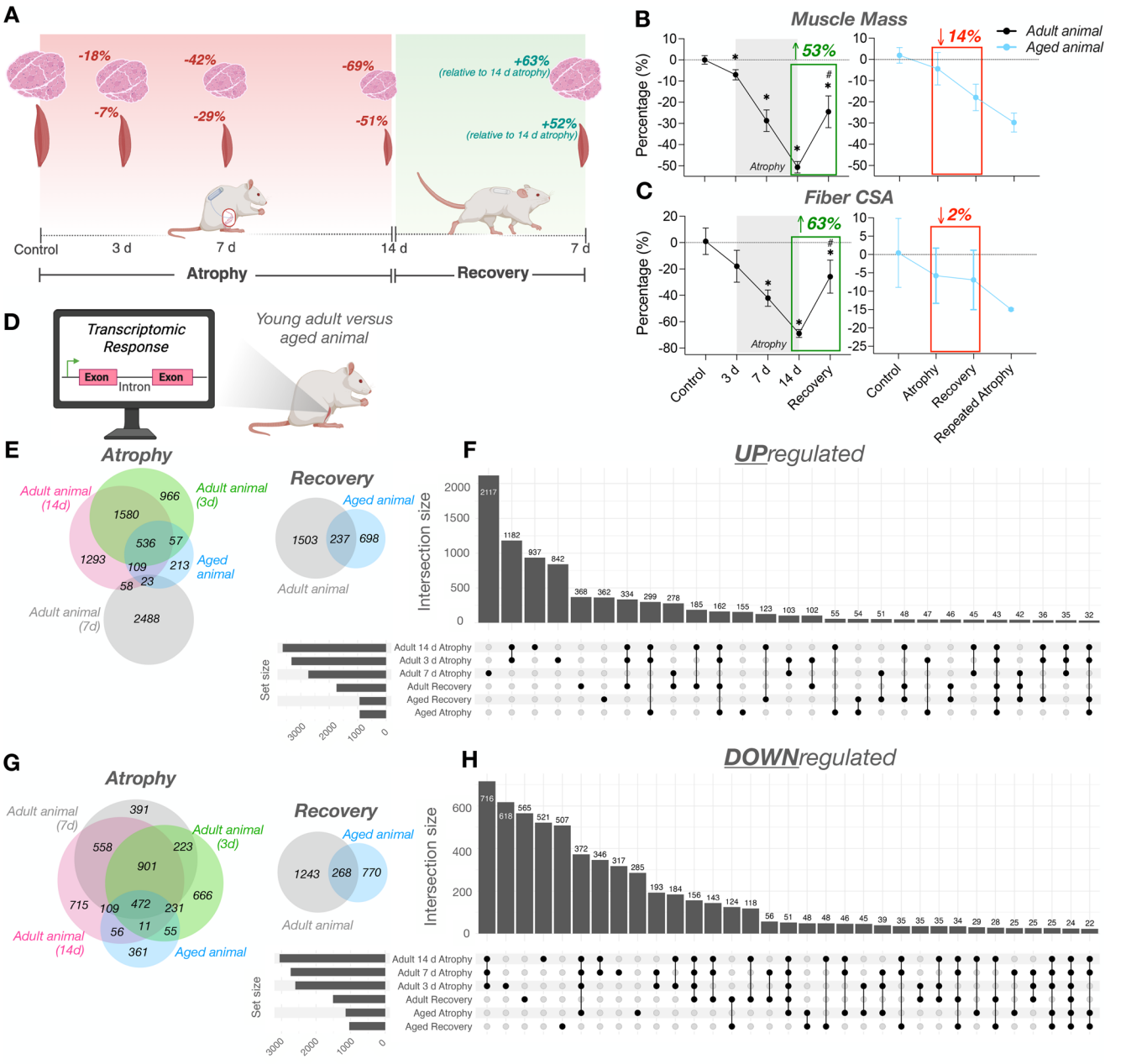

FIGURE 5 | (A) Schematic of study design (created using BioRender.com) of TTX-induced atrophy (3, 7, and 14 days/d) and subsequent recovery (7 d) in young adult rats (Fisher et al.,) [66]. There was a loss of TA muscle mass (B) and fCSA (C) at 3, 7, and 14 d atrophy (−7% to −18%, −29% to −42%, and −51% to −69%, respectively). In contrast to aged animals, muscle mass and fCSA was restored by 53 and 63%, respectively following 7 d recovery in young adult animals (B,C redrawn from Fisher et al., [66]). (D) Overlap of transcriptome in young adult and aged rat muscle revealed many common UP-regulated (E,F) and DOWN-regulated (G,H) DEGs after atrophy and a larger proportion of unique genes after recovery.

gene expression across atrophy, recovery, and repeated atrophy, thereby defining the Differentially Methylated, Differentially Expressed Genes (DmDEGs) regulated by repeated disuse and recovery. Repeated periods of disuse atrophy and recovery led to DMRs that were inversely associated with the DEGs identified in both young (Figure 6A–D) and aged (Figure 6E–H) skeletal muscle. In young adult humans, 71 DMRs on 57 genes (from cluster 1 above, Figure 3K) were identified as DmDEGs with an inverse relationship of hypermethylation and decreased expression (Figure 6Bi, Ci). These DmDEGs were hypermethylated and downregulated after atrophy and repeated atrophy, with both DNA methylation and gene expression returning to baseline levels after recovery where skeletal muscle size was restored (cluster 1, Figure 6Bi, Ci).

ORA analysis identified these DmDEGs as enriched in NAD^+ metabolism, the electron transport chain (ETC), ATP synthesis, mitochondrial structural pathways, and mitochondrial ribosome components (Figure 6D), demonstrating that the pathway terms enriched within cluster 1 of the transcriptomic analysis (down-regulated after atrophy, returning to baseline during recovery, and showing reduced susceptibility during repeated atrophy; depicted earlier, Figure 3K) were also subject to epigenetic regulation in response to both disuse atrophy and repeated atrophy.

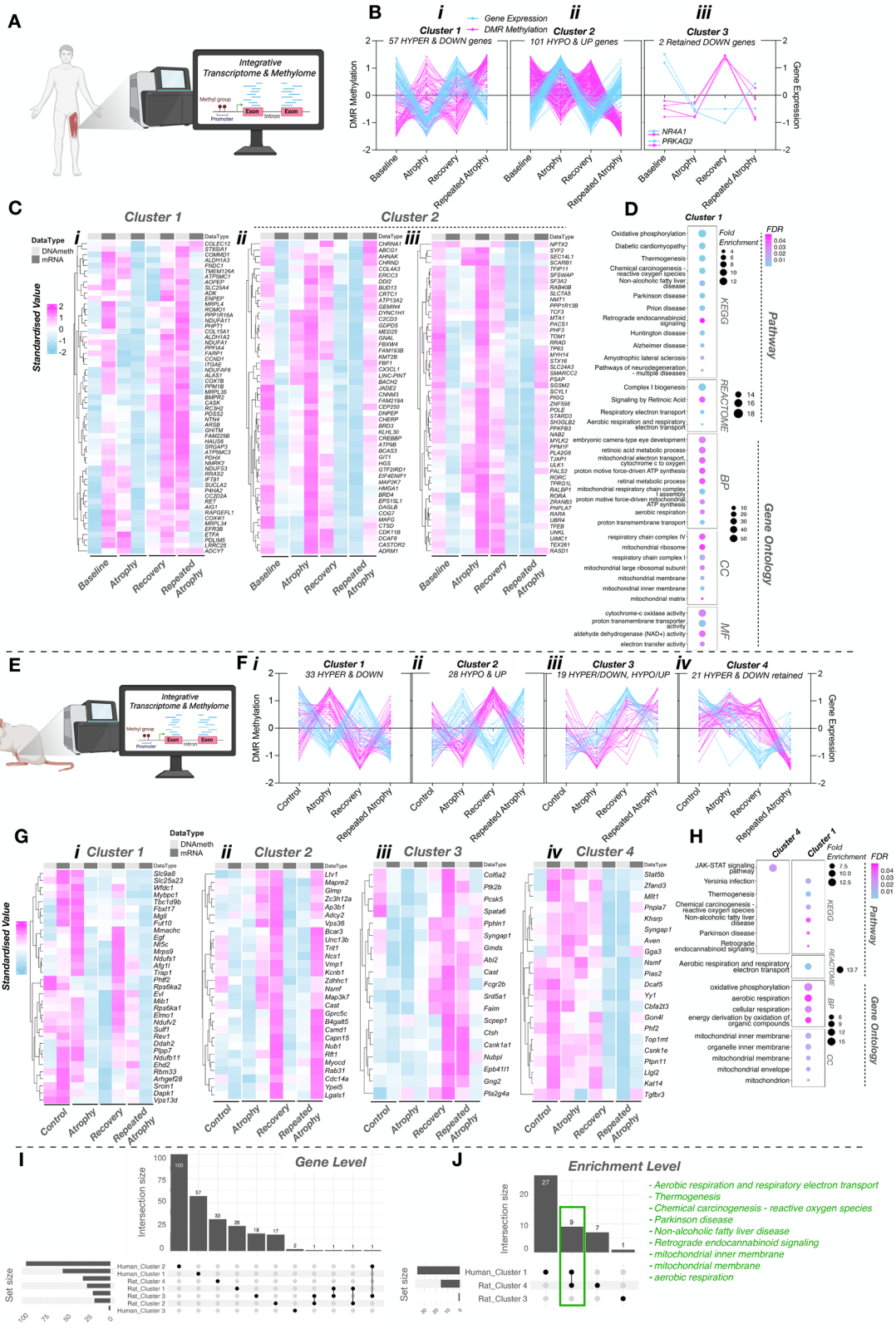

FIGURE 6 | Integrative DNA methylome and transcriptome analyses in young adult human (A–D) identified 57 hypermethylated and downregulated genes after both periods of disuse that were returned to baseline levels after recovery (cluster 1, Bi, Ci); 101 hypomethylated and upregulated genes after both periods of disuse that also returned to baseline levels after recovery (cluster 2, Bii, Cii and Ciii); 2 downregulated/hypermethylated genes after initial atrophy that were retained during recovery (cluster 3, Biii). There were significant pathway and GO terms for cluster 1 in young human muscle of hypermethylated/downregulated genes after atrophy, restored during recovery, and hypermethylated/downregulated after repeated atrophy enriched in aerobic metabolism/respiration, NAD^+ activity, ETC, ATP synthesis, mitochondrial and ribosome terms (D). Integrative analyses in aged rat muscle (E–G) revealed 33 genes (Fi, Gi, cluster 1) hypermethylated/downregulated after atrophy, hypomethylated/upregulated upon TTX cessation during recovery, and hypermethylated/downregulated after repeated atrophy; 28 unique genes (Fii, Gii, cluster 2) were hypomethylated/upregulated after

Notably, *NMRK2*, a key gene involved in NAD^+ biosynthesis and most downregulated genes after both periods of disuse in young adult humans, was among these epigenetically regulated loci. *NMRK2* exhibited hypermethylation and reduced expression during both atrophy periods, followed by hypomethylation and increased transcription toward baseline levels during recovery. In addition to these hypermethylated and downregulated genes, there were 189 DMRs on 101 genes that were hypomethylated and upregulated after both atrophy and repeated atrophy (cluster 2, Figure 6Bii, Cii, Ciii). There was no significantly enriched pathway or GO terms for this cluster, thus suggestive that most of these genes likely have divergent molecular, cellular and biological roles. However, several interesting hypomethylated and upregulated genes emerged from this cluster. Specifically, the AChR genes, *CHRND* and *CHRNA1* (that were upregulated after atrophy and/or repeated atrophy across both human and rat muscle transcriptomes, Figure 3D–H), demonstrated the largest hypomethylation and increased expression after repeated atrophy (Figure 6Bii, Cii). These genes were among the few DmDEGs in young human muscle that demonstrated increased susceptibility and exaggerated responses to repeated atrophy. Finally, *NR4A1* and *PRKAG2* (AMPK gamma-2) were downregulated after atrophy, and despite no detectable change in DNA methylation after atrophy, this was followed by hypermethylation and sustained suppression of transcription during the recovery and repeated atrophy periods (cluster 3, Figure 6Biii). This pattern suggests that the retained reduction in expression during recovery is likely driven by the emergence of hypermethylation at these loci, even though skeletal muscle size and function were restored upon returning to habitual activity. The full DNA methylome analysis for atrophy, recovery and repeated atrophy in young adult human muscle is depicted in Figure S4. The corresponding processed DMR data set is provided in Data S3.

In aged rat muscle, integrative analysis of DNA methylome and transcriptome (Figure 6E) revealed 41 DMRs on 33 unique genes that were hypermethylated and downregulated after atrophy (cluster 1, Figure 6Fi, Gi), hypomethylated and upregulated upon TTX cessation during the recovery period, and finally hypermethylated and downregulated after repeated atrophy. As with the young human muscle, these genes were associated with aerobic metabolism/respiration, electron transport and mitochondrial components (Figure 6H). Integrative analysis also revealed 40 DMRs on 28 unique genes (cluster 2, Figure 6Fii, Gii) that were hypomethylated and upregulated after atrophy, hypermethylated after recovery, and hypomethylated and upregulated again after repeated atrophy. ORA analysis revealed no significantly enriched pathways or GO terms for this cluster. There were also 26 DMRs on 19 unique genes (cluster 3, Figure 6Fiii, Giii) that were hypermethylated and downregulated after atrophy, hypermethylated yet upregulated during recovery, and hypomethylated and upregulated after repeated atrophy, with no significantly enriched pathways or GO terms. Interestingly, 43 DMRs on 21 unique genes (cluster 4, Figure 6Fiv, Giv) demonstrated hypermethylation and downregulation after atrophy, with retained hypermethylation and a continued decrease in gene expression during recovery, followed by subsequent hypomethylation and increased gene expression after repeated atrophy. These genes were enriched for JAK–STAT signaling pathways (cluster 4, Figure 6H) and exhibited retained epigenetic and transcriptional signatures following the initial atrophy period that persisted into recovery, yet became oppositely hypomethylated and upregulated after repeated atrophy. The full DNA methylome analysis in response to atrophy, recovery and repeated atrophy in aged rat muscle is depicted in Figure S6. The corresponding processed DMR data set is provided in Data S4.

Despite the differential physiological response to repeated atrophy and recovery, both young adult humans (cluster 1, Figure 6Bi, Ci, D) and aged animals (cluster 1, Figure 6Fi, Gi, H) demonstrated associated DNA methylation and gene transcription of genes enriched within the same pathway and GO terms related to aerobic metabolism/respiration, electron transport and mitochondria (Figure 6D,H). However, the majority of these DmDEGs were specific to young human or aged rat muscle (Figure 6I), despite enrichment of the same metabolic pathways across species and models of atrophy (Figure 6J). Further cross-species comparison of the shared transcriptomic and epigenetic responses to repeated disuse in young adult human and age animal muscle via UpSet plots (Figure S5), identified several common up (Figure S5A) and downregulated DEGs (Figure S5B) as well as hypo-methylated (Figure S5C) and hyper-methylated DMRs (Figure S5D). It was also apparent that out of the 761 DEGs used for the SOM temporal profiling in human muscle, 54% (414 out of 761) of the genes were also differentially expressed in the aged rat muscle (Figure S5E). Pathway (Figure S5F) and GO (Figure S5G) analyses suggested these shared genes were also related to oxidative metabolism, NAD^+, TCA cycle, ETC, ATP synthesis and mitochondrial function. Among these shared DEGs, there were 406 DMRs on 189 shared DEGs in young adult human muscle (Figure S5H) that were associated with oxidative metabolism, ETC, ATP synthesis and mitochondria (Figure S5I,J). In aged animals, there were 56 DMRs on 16 shared DEGs (Figure S5K) that were related to mitochondria and RNA splicing (Figure

atrophy, hypermethylated/restored after recovery, and hypomethylated/upregulated again after repeated atrophy (Fiii, Giii, cluster 2); 19 unique genes (cluster 3) that were hypermethylated/downregulated after atrophy, hypermethylated yet upregulated during recovery, and hypomethylated/upregulated after repeated atrophy; 21 unique genes (Fiv, Giv, cluster 4) were hypermethylated/downregulated after atrophy, with retained hypermethylation and a continued decrease in gene expression during recovery followed by subsequent hypomethylation and increased gene expression after repeated atrophy. Significant enriched pathway and GO terms (H) for cluster 1 were related to aerobic metabolism/respiration, electron transport and specifically mitochondrial structure (cluster 1) and JAK-STAT enrichment (cluster 4). Average DMR methylation is depicted in aged animal heatmaps whenever there is >1 DMR for a given gene (G). Average mRNA expression is also presented where there were multiple transcript variants (G). UpSet plot analysis of young adult human and aged rat muscle gene revealed only a few epigenetically regulated genes symbols that overlapped between both models (I). However, there were 9 overlapping enriched pathway / GO terms between human and animal muscle (J). Note that 'DMR Methylation' is standardized percentage DMR methylation derived from SOM profiling analysis and 'Gene Expression' is representative of standardized LS means from SOM profiling analysis (B,F). BP = biological process, CC = cellular component, MF = molecular function.

S5L). Overall, these data demonstrate epigenetic regulation of shared genes associated with oxidative metabolism across species and age in response to atrophy, recovery and repeated atrophy.

Collectively, these integrative analyses demonstrate that repeated atrophy imprints coordinated epigenetic and transcriptional alterations across metabolic, mitochondrial, and neuromuscular pathways, with several DmDEGs in these pathways showing inverse SOM profiles across atrophy, recovery, and repeated atrophy. Given NAD^+ metabolism genes featured prominently among these epigenetically regulated clusters, we next examined whether repeated disuse disrupts NAD^+ biosynthesis and salvage pathways in young adult humans and aged rats.

3.9 | Regulation of NAD^+ Biosynthesis Pathways Following Repeated Atrophy

Genes involved in NAD^+/NADH metabolism were strongly represented among the DmDEGs identified through the integrative SOM analysis, showing downregulation and hypermethylation after atrophy and repeated atrophy in both young adult human (Figure 7A–D) and aged rat muscle (Figure 7E–I). Moreover, the NAD^+ biosynthetic gene, *NMRK2*, was the most downregulated genes after both periods of atrophy, with inversely associated DNA methylation across the time course of atrophy, recovery, and repeated atrophy. Genes enriched in these pathways were also restored during the recovery period. Targeted mRNA analysis (via RT-qPCR) of *Nmrk2* in aged rat muscle revealed a non-significant reduction in *Nmrk2* expression after atrophy, followed by a significant increase during recovery and a larger significant reduction after repeated atrophy (Figure 7E,G). Given the predominant role of *NMRK2/Nmrk2* in synthesizing NAD^+, coupled with over-representation of NAD/NADH metabolism related enrichment terms for downregulated genes during both periods of atrophy, we next interrogated gene expression of other NAD^+ biosynthesis genes and whether such alterations corresponded with a reduction in NAD^+ content in both young adult (Figure 7A–D) and aged muscle (Figure 7E–I). In young adult humans, while most of these NAD^+ genes were downregulated after both periods of atrophy, *NMRK2* was the only significantly downregulated DEG out of the 18 genes analyzed (Figure 7A–C). Furthermore, *NMRK2* was the most upregulated gene across all DEGs after recovery from atrophy in humans (Figure 3E), was among the identified DmDEGs, and was downregulated to a lesser extent after repeated vs. initial atrophy. Given *NMRK2* was the only significantly downregulated NAD^+ gene, this was also associated with no significant changes in NAD^+ content (Figure 7D). In contrast, half of the 14 NAD^+ genes assessed in aged animals were significantly differentially expressed, where most genes were downregulated after atrophy, either unchanged/restored or increased after recovery, followed by greater downregulation after repeated atrophy (Figure 7E–G), with corresponding significant reductions in absolute NAD^+ content in the left (L) TTX vs. right (R) control limb after repeated atrophy (Figure 7H,I). Collectively, these findings identify *NMRK2*/*Nmrk2* as a consistently downregulated gene across both species following repeated atrophy and that aged muscle is prone to greater disuse-induced pertubations in NAD^+ metabolism genes, resulting in reduced NAD^+ availability. Given that NMRK2 activity contributes directly to NAD^+ regeneration and that its suppression occurred across atrophic episodes, we next sought to determine whether NMRK2-related deficits extend to human MuSC function, and whether supplementation with its substrate, nicotinamide riboside (NR), could modulate NMRK1/2 expression and myogenic capacity in MuSCs derived before and after atrophy.

3.10 | Nicotinamide Riboside (NR) Enhances Myogenic Responses in Human Post-Atrophy MuSCs

Given NMRK2 was the most strongly downregulated genes after both periods of atrophy in humans, and catalyzes NAD^+ synthesis via its substrate, nicotinamide riboside (NR), we next examined whether NR supplementation could modulate NMRK1/2 expression and myogenic potential in MuSCs isolated from pre- and post-atrophy human biopsies (Figure 7J–M). Although Nmrk2 expression and NAD^+ content were significantly reduced after repeated disuse in aged animals, these omics-driven discoveries were made after tissue allocation in the animal experiments, and muscle stem cells were therefore not available for parallel studies in aged rat muscle. Similar proportions of myoblast (desmin+) to fibroblasts (TE-7+) were observed between pre- and post-atrophy MuSC, thus negating possible effects of differential cell populations (Figure 7L). Despite limited myotube formation in the MuSC, likely due to a higher proportion of fibroblasts (≈ 60%) vs. myoblasts (≈ 60%) (Figure 7K,L), post-atrophy MuSCs were more responsive to NR supplementation, where myotube size significantly increased in NR treated post-atrophy MuSCs at 10 days when compared to 7 d differentiation ($p = 0.03$, Figure 7M). This was supported by significantly lower *MYOD (early differentiation)* and greater (non-significant) *MYOG (fusion/later differentiation)* gene expression in NR-supplemented MuSCs, coupled with greater (albeit non-significant *NMRK1* and *NMRK2* expression (Figure 7N–Q). Interestingly, mtDNA content demonstrated lower mean (non-significant) mtDNA in post- vs. pre-atrophy MuSCs (Figure 7R–U). Collectively, post-atrophy MuSCs were more responsive to NR supplementation that induced myotube growth.

Together, these findings indicate that post-atrophy MuSCs were more responsive to NR, in part through modulation of *the MRFs* and *NMRK1/2* expression and myotube size, suggesting that NAD^+ salvage influences myotube growth following disuse. To determine whether these cellular effects correspond to broader alterations in mitochondrial pathways in vivo, and given the strong enrichment of mitochondrial and aerobic metabolism genes within the DmDEG clusters identified above, we next examined mitochondrial gene expression, protein abundance, and mtDNA content across atrophy, recovery, and repeated atrophy in both young adult human and aged rat skeletal muscle.

3.11 | Mitochondrial Gene Expression, Protein Abundance, and mt DNA Content across Atrophy, Recovery, and Repeated Atrophy in Young Adult Human and Aged Rat Muscle

In addition to the NAD^+ metabolism pathways described above, genes involved in mitochondrial structure, function, assembly, and turnover were strongly represented among the DmDEG clus-

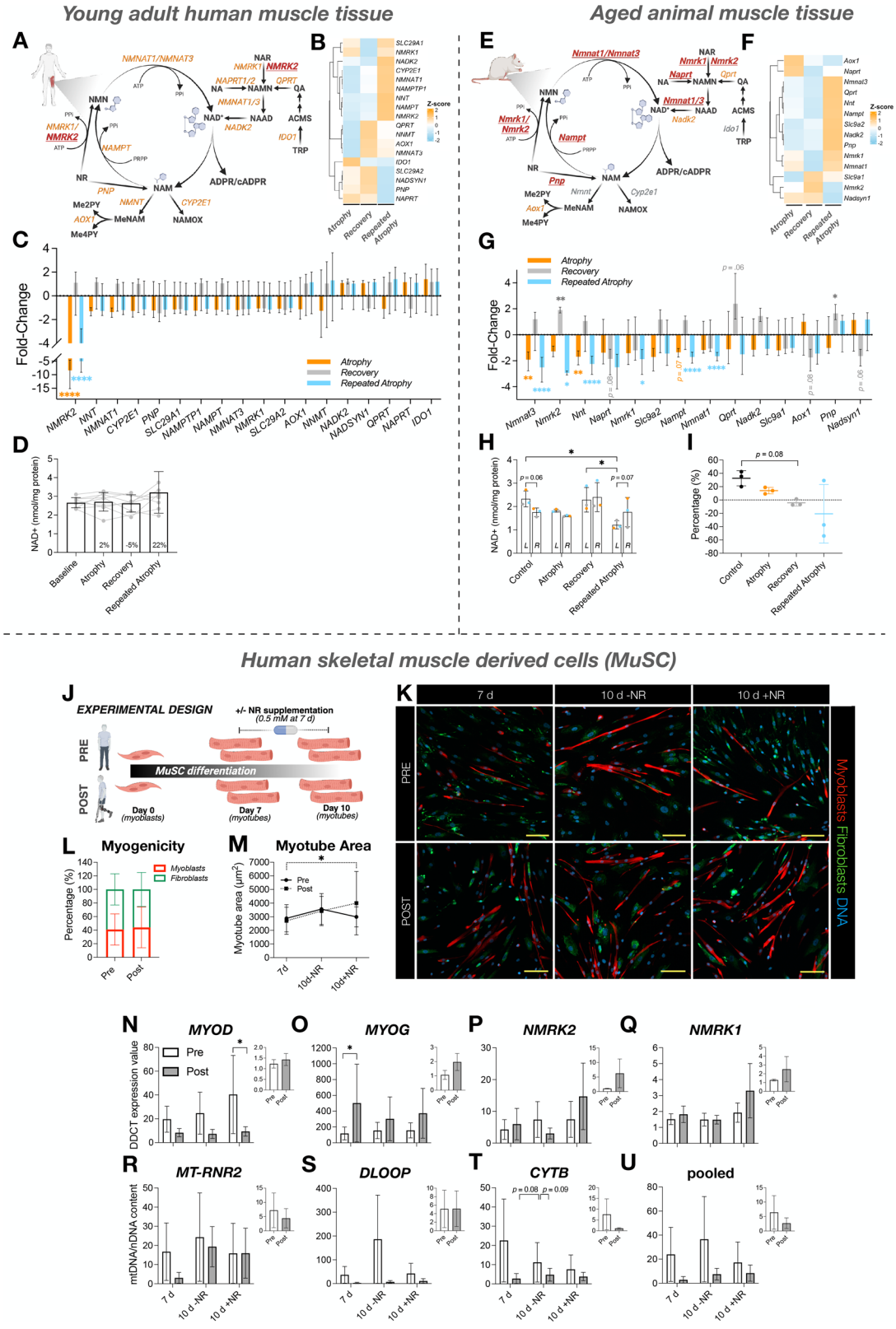

FIGURE 7 | mRNA expression of NAD^+ biosynthesis genes and corresponding NAD^+ content in young adult human (A–D) and aged rat (E–I) skeletal muscle. (A,E) Schematic representation of Preiss-Handler and salvage NAD^+ biosynthetic pathways (redrawn from Damgaard & Treebak, 2023 [83] using BioRender.com). Key metabolites are depicted as black text. Genes encoding NAD^+ biosynthesis enzymes are shown in either orange (if non significantly expressed) or red text (significantly downregulated after atrophy or repeated atrophy). In young adult humans, *NMRK2* was the only significantly downregulated DEG out of the 18 NAD^+ genes (B,C), which did not lead to significant alterations in NAD^+ content (D). In aged animals, most of the 14 NAD+ genes assessed were significantly downregulated after atrophy and repeated atrophy and were restored upon recovery (F,G), resulting in significantly reduced absolute (H) NAD^+ content in the left TTX vs. right control limb after repeated atrophy. Relative NAD^+ content (I). Nicotinamide riboside (NR) supplementation (0.5 mM) in human pre- and post-atrophy MuSCs from 7 d to 10 d of myotube formation ($n = 4$) (J,K).

ters in both species. Specifically, genes involved in aerobic respiration (e.g., ETC and oxidative phosphorylation) and mitochondrial structural components were hypermethylated and downregulated after both periods of atrophy, with the majority of these genes returning to baseline/control levels in both human and rat muscle despite restoration of muscle size in humans and continued wasting in aged rats. Furthermore, these genes demonstrated larger reductions in transcription in aged rat muscle after repeated disuse, whereas these genes were less susceptible to reductions in young adult human muscle following repeated disuse. Given these data, we next assessed the expression of mitochondrial fission, fusion, transport, and biogenesis-related genes, together with mRNA and protein abundance of ETC complexes I–V. We also quantified mtDNA copy number and citrate synthase protein abundance as markers of mitochondrial content. In young adult human muscle (Figure 8A), the majority of the 66 genes profiled across ETC complexes I-V were significantly suppressed after both periods of atrophy, where most genes either returned to baseline levels or increased after recovery (Figure 8B). This resulted in significant changes occurring after both atrophy and repeated atrophy in 24 (out of 66) ETC genes; within complex I (7 out of 32 genes), III (3 out of 8 genes), IV (8 out of 13 genes), and V (6 out of 9 genes) with non-significant changes for genes in CII (Figure 8B). Concerning genes related to mitochondrial fission and mitophagy (*FIS1, DRP1*), fusion (*MFN1/2, OPA1*), transport (*SLC25A51, SLC25A4)*, and biogenesis (*PPARGC1A, TFAM*), 8 out of 9 of these genes non-significantly decreased after atrophy and repeated atrophy, all of which returned to baseline levels or non-significantly increased after recovery (Figure 8C). There was a significant reduction in *PPIF* after atrophy, a mitochondrial membrane gene controlling calcium overload and fatigue resistance in muscle (Figure 8C). Given the large transcriptional perturbations in ETC-specific genes across all 5 complexes in both atrophy periods, we next assessed ETC (I-V) protein abundance. The reductions in gene expression did not correspond to significant changes in ETC protein complex abundance (Figure 8D). Interestingly, however, mtDNA content (Figure 8E) and citrate synthase protein abundance (Figure 8F) significantly decreased after repeated atrophy only in young adult humans. Collectively, in young adult muscle, these data suggest that the large transcriptional perturbations of genes enriched in mitochondrial-specific pathways and GO terms culminated in impaired mitochondrial content following repeated disuse only, despite restoration of these parameters and skeletal mass muscle during recovery.

In aged animals, most genes across all ETC complexes were differentially expressed (Figure 9A,B). Specifically, 57% (38 out of 67) of genes encoding complex's I (13 out of 30), II (4 out of 4), III (7 out of 9), IV (6 out of 14) and V (8 out of 10 genes) were significantly downregulated after atrophy and/or repeated atrophy (Figure 9A,B). Similarly to young adult humans, the majority of these genes recovered during TTX cessation despite continued muscle wasting after a return to habitual physical activity. Furthermore, *Sdhb, Cox6a1, Cox8a, and Atp5pf* were significantly upregulated during recovery (Figure 9B). In contrast to young adult humans, aged rat muscle demonstrated a greater average reduction across all 67 genes following repeated atrophy (-1.72 FC) vs. the initial atrophy period (-1.52 FC), despite a similar average FC between recovery and control (0.1 FC). Mitochondrial fusion (*Mfn1/2*), transport (*Slc25a4)* and biogenesis (*Ppargc1a*) genes also significantly decreased after atrophy and/or repeated atrophy whereas *Tfam* significantly increased after repeated atrophy (Figure 9C). Most genes recovered during TTX cessation, and *Opa1* and *Ppif* genes both significantly increased during recovery (Figure 9C). As with the ETC genes described above, there was a greater average reduction across all mitochondrial-related genes (excluding *Tfam* which increased) after repeated atrophy (-2.23 FC) compared to previous atrophy (-1.56 FC) relating to a 43% larger reduction in expression after repeated atrophy compared to initial atrophy, where most genes recovered upon returning to habitual physical activity (average 0.72 FC) (Figure 9B,C). At the protein level, there were no significant changes in protein abundance of ETC complexes I-V (Figure 9D) nor citrate synthase across the conditions analyzed (e.g., sham, atrophy, and recovery, Figure 9E). Finally, there was a reduction in mtDNA content during atrophy (−18% albeit not significant), recovery (−41%), and the greatest reduction after repeated atrophy (−50%) when *Mt-Rnr1* and *Mt-Rnr2* genes were combined (Figure 9F).

Overall, these data demonstrate that repeated atrophy imposes substantial and age-dependent disruption of mitochondrial gene expression, and mtDNA content, with aged muscle, in particular, exhibiting exaggerated transcriptional susceptibility. These data compliment the multi-layered and thorough assessment of physiological, transcriptional, epigenetic, metabolic, and mitochondrial responses to repeated disuse. An overview of all results are depicted in a summary illustration (Figure 10).

4 | Discussion

4.1 | Summary of Main Findings

Skeletal muscle exhibits a molecular memory of repeated disuse-induced atrophy. In young adult humans, repeated immobilization induced a comparable loss of skeletal muscle interspersed with full recovery. Consistent with this, young adult rats also

(K) Fluorescence microscopic tile scan (3 × 3) images of MuSCs labeled for myoblasts (desmin, red), fibroblasts (TE-7, green) and DNA (DAPI, blue), acquired at 10× magnification (scale bar = 200 μm). (L) Myoblasts (≈ 40%) and fibroblast (≈ 60%) proportions were similar between pre- and post-atrophy MuSCs. NR supplementation resulted in significantly increased myotube area at 10 vs. 7 d ($p = 0.03$) in post-atrophy MuSCs only (M). qPCR analysis revealed lower *MYOD* expression in post-atrophy 10 d NR treated MuSCs (N) coupled with greater *MYOG* expression at 7 d post-atrophy with greater average increases in *MYOG* (albeit non-significant) in post-atrophy 10 d NR treated MuSCs (O). Despite greater average *NMRK2* (P) and *NMRK1* (Q) expression in 10 d NR supplemented post-atrophy MuSCs, this was not significantly different from pre-atrophy or non-treated MuSCs. (R–U) There was a trend toward lower mtDNA content in post- vs. pre-atrophy MuSCs at each timepoint/condition, as well as lower mtDNA in NR treated pre-atrophy MuSCs only, albeit not statistically significant. Larger main figures relativized to 0 h, small inset figures represent 10 d NR treated relativized to 10 d non-treated MuSCs. *$p \leq 0.05$, **$p \leq 0.01$, ***$p \leq 0.001$, ****$p \leq 0.0001$. Myogenicity (L) and myotube area (M) data presented as mean ± SD. Gene expression (N–Q) and mtDNA (R–U) data presented as mean ± standard error of the mean (SEM).

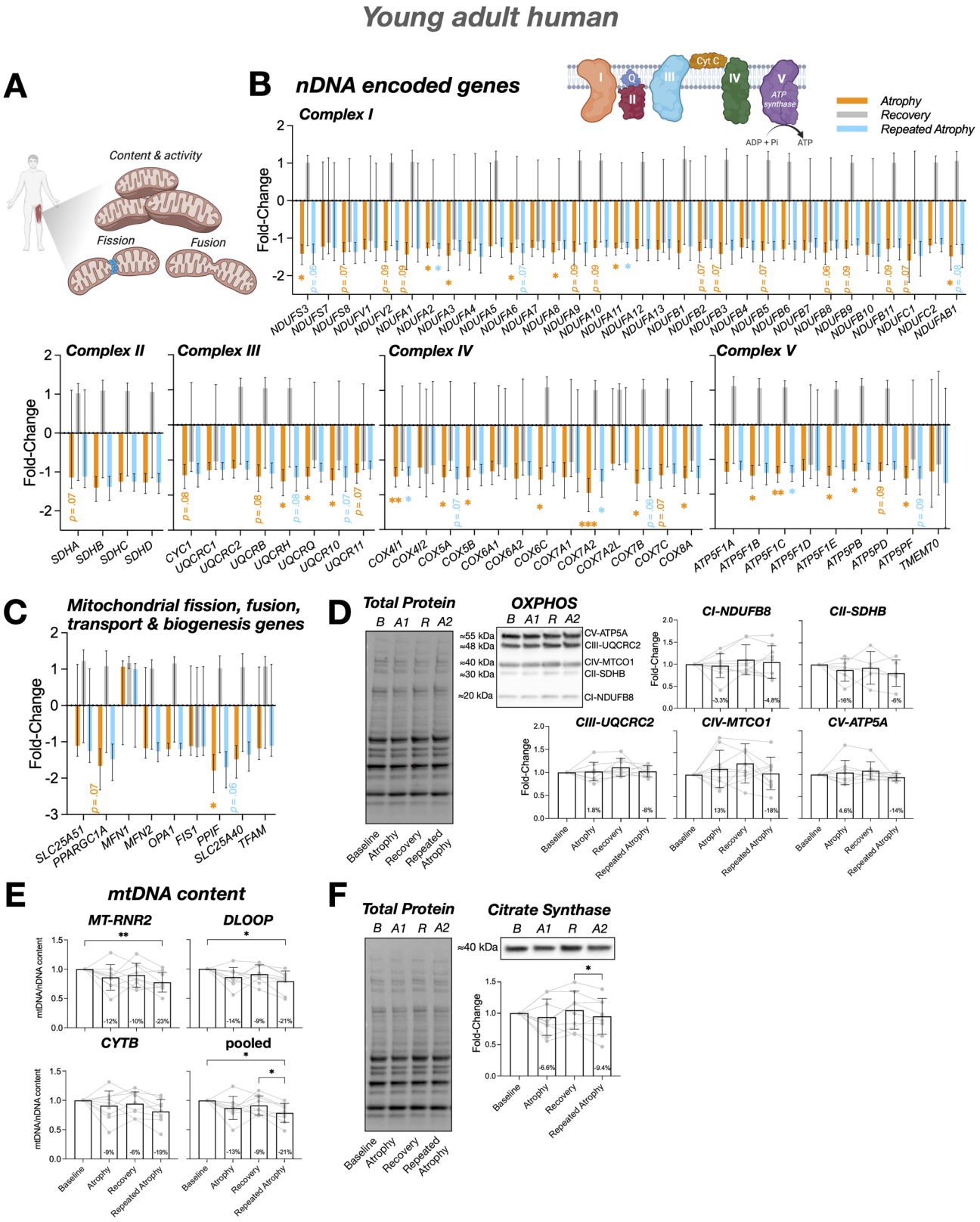

FIGURE 8 | Mitochondrial response to repeated periods of disuse in young adult human skeletal muscle (A–F). (A) Schematic illustrating key components of mitochondrial content, activity, fusion, and fission processes (created using BioRender.com). (B) Temporal transcriptional response of ETC complex I–V genes, showing that most genes significantly decreased after atrophy and repeated atrophy, and recovered upon return to normal activity. (C) Transcriptional response of mitochondrial fission, fusion, transport, and biogenesis-related genes across atrophy, recovery, and repeated atrophy. (D) ETC complex (I–V) protein abundance, which did not demonstrate significant changes across conditions. (E,F) mtDNA content and citrate synthase protein abundance, both of which significantly decreased after repeated atrophy. Gene expression data presented as mean (signed) fold change ± absolute 95% confidence intervals. *$p \leq 0.05$, **$p \leq 0.01$, ***$p \leq 0.001$, ****$p \leq 0.0001$.

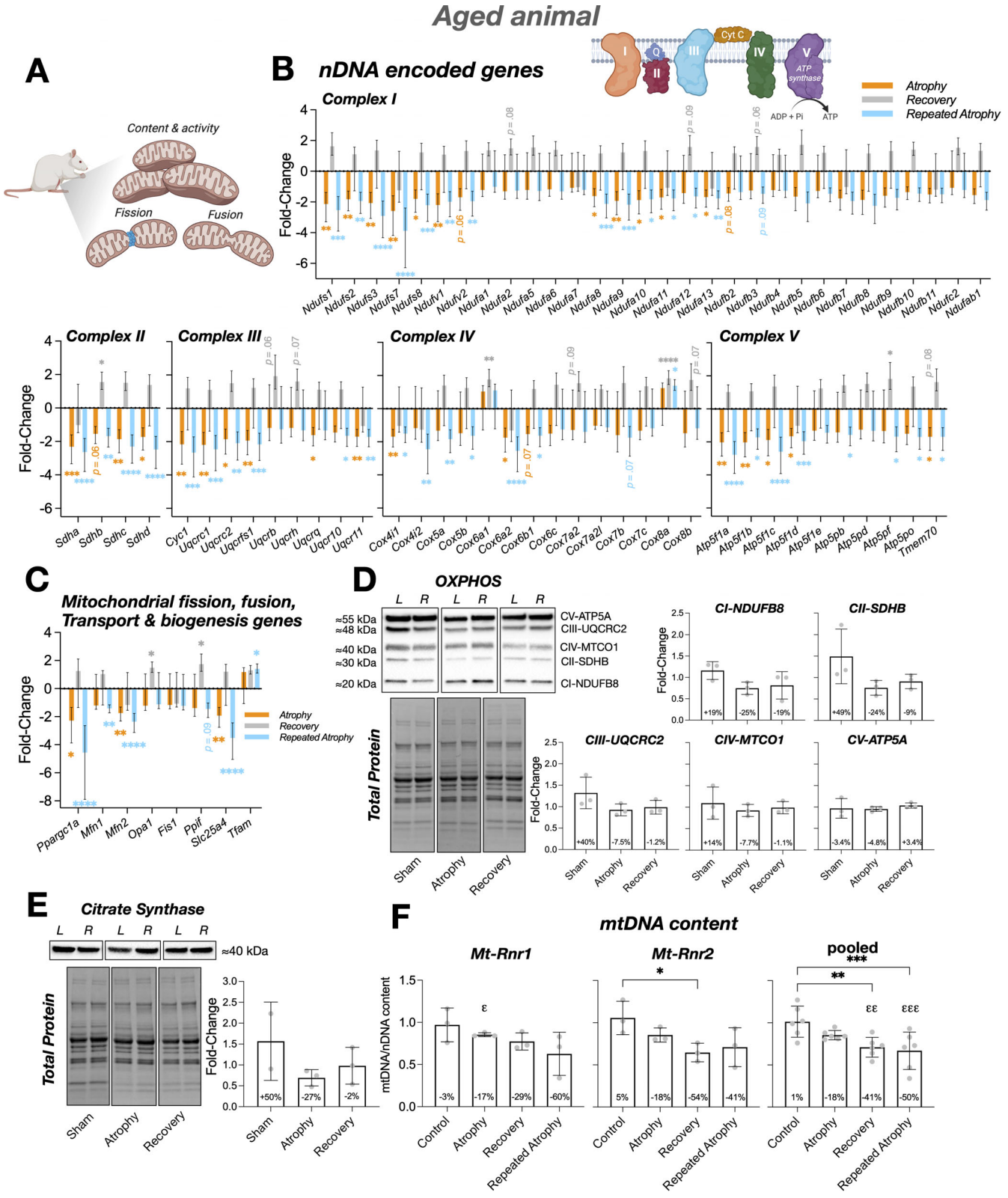

FIGURE 9 | Mitochondrial response to repeated periods of disuse in aged rat skeletal muscle (A–F). (A) Schematic illustrating key components of mitochondrial content, activity, fusion, and fission processes (created using BioRender.com). (B) Temporal transcriptional response of ETC complex I–V genes, demonstrating significant decreases after atrophy and repeated atrophy, with recovery upon TTX cessation. (C) Transcriptional response of mitochondrial fission, fusion, transport, and biogenesis-related genes across atrophy, recovery, and repeated atrophy in aged muscle. (D) ETC complex (I–V) protein abundance, which did not show significant changes across sham, atrophy or recovery conditions. (E) Citrate synthase protein abundance across conditions, which did not show significant changes. (F) mtDNA content significantly decreased after recovery, and repeated atrophy, with the largest reduction of 50 percent after repeated atrophy. Gene expression data presented as mean (signed) fold change ± absolute 95 % confidence intervals. $^{*}p \leq 0.05$, $^{**}p \leq 0.01$, $^{***}p \leq 0.001$, $^{****}p \leq 0.0001$.

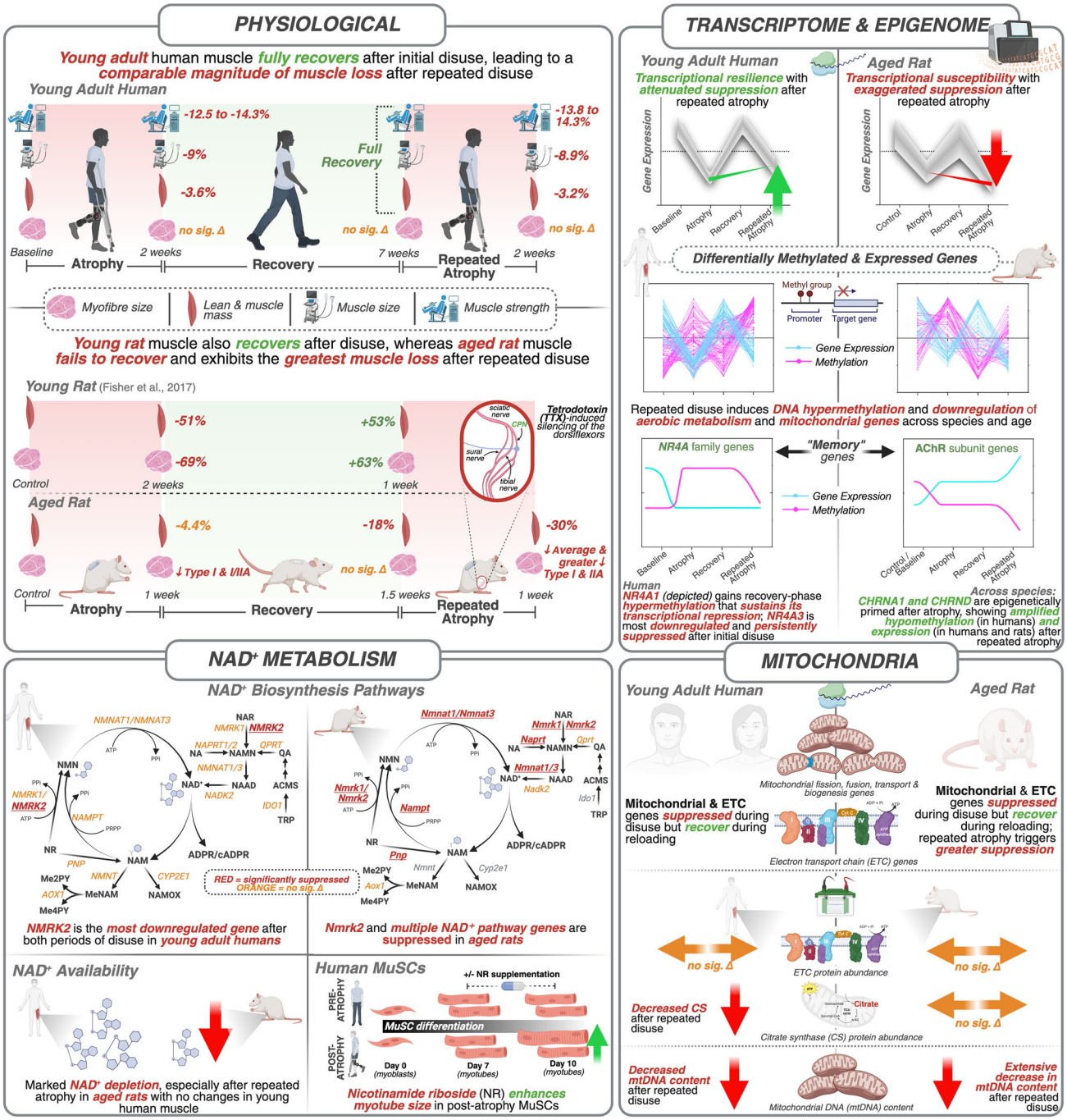

FIGURE 10 | Summary of the physiological, transcriptional, epigenetic, metabolic and mitochondrial responses to repeated disuse muscle atrophy.

recovered muscle mass and fiber CSA after initial disuse, whereas aged rats did not, reinforcing the age-dependent divergence in recovery capacity. In young adult human muscle, repeated disuse triggered a predominantly protective molecular resilience where transcriptional perturbations of genes associated with oxidative metabolism and mitochondria (structure and function) were attenuated after repeated disuse-atrophy. In contrast, aged muscle displayed a detrimental molecular susceptibility, characterized by further suppression of genes within similar pathways following repeated disuse, despite transcriptional recovery and continued muscle wasting upon returning to normal habitual activity. Proteasomal, ECM, and DNA damage associated gene pathways were uniquely elevated following repeated atrophy in aged muscle. Integrated methylome and transcriptome analyses revealed conserved epigenetic regulation of aerobic metabolism and mitochondrial genes across species, along with locus-specific memory genes including *NR4A1* and nicotinic acetylcholine receptor (AChR) subunit genes. *NMRK2* was the most downregulated gene across both periods of atrophy that also demonstrated inversely associated DNA methylation. Notably, supplementation of human MuSCs with *NMRK2* substrate, nicotinamide riboside (NR), improved myotube size in MuSCs derived post-atrophy. Importantly, repeated disuse in elderly humans is associated with frailty and increased fall risk, raising ethical concerns. Therefore, our design limited human experiments to young adults and employed aged rats as a surrogate model for repeated

atrophy with age. In addition, to comply with the 3Rs (Reduction, Refinement, Replacement), we avoided unnecessary duplication by not including a direct young rat control group; rather, we integrated previously published young rat data [66] with newly generated aged rat data, enabling robust age comparisons while minimizing animal use.

4.2 | Molecular Memory of Repeated Disuse-induced Skeletal Muscle Atrophy

Skeletal muscle retains an epigenetic 'memory' of prior growth, as demonstrated by persistent hypomethylation during detraining in humans and mice [33, 36, 37], and amplified gene expression upon retraining [33, 34, 36, 37]. Our findings now extend this concept to a clinically relevant negative stimulus. Specifically, disuse-induced atrophy, which commonly occurs after injury, hospitalization, bed rest, surgery, or spaceflight. Crucially, we identified an age-dependent molecular memory: a *protective* transcriptional attenuation in young muscle, where repeated disuse elicited blunted transcriptional responses, and a *detrimental* memory in aged muscle, where repeated atrophy exaggerated suppression of NAD^+, aerobic metabolism, and mitochondrial gene pathways.

4.3 | Attenuated Transcriptional Memory in Young Adult Humans and a Detrimental Exaggerated Transcriptional Memory in Aged Animal Muscle

In young adult human muscle, the vast majority of genes suppressed during initial atrophy largely recovered and were less perturbed by repeated disuse, indicating a transcriptional protection or resilience. These responses predominantly involved oxidative metabolism and mitochondrial pathways, including TCA cycle, NAD^+/NADH, ETC and ATP synthesis genes. In contrast, aged animal muscle showed the opposite pattern, in which these same pathways were further suppressed during repeated atrophy despite transcriptional recovery after the initial disuse, accompanied by unique activation of proteasomal, ECM, and DNA damage gene pathways after repeated atrophy. These signatures are consistent ageing-associated skeletal muscle deficits in metabolic regulation, proteostasis, NMJ dysfunction (discussed below), and mitochondrial function [10, 19, 84]. Importantly, expression of these gene pathways recovered even though muscle mass continued to decline in aged rat muscle, confirming that the exaggerated transcriptional and physiological responses reflected a detrimental molecular memory rather than incomplete recovery of these molecular pathways.

4.4 | Mitochondrial Vulnerability and Loss of mtDNA With Repeated Disuse Atrophy

Repeated disuse caused significant loss of mtDNA that was not significantly evident after the initial atrophy period in either young adults or aged animals, with the most pronounced decline observed in aged muscle after repeated atrophy. These findings align with previous bed rest studies demonstrating broad downregulation of mitochondrial genes and reduced content/respiration during unloading [24, 64, 85]. Our transcriptomic data also revealed widespread suppression of electron transport chain and mitochondrial genes during atrophy and repeated atrophy, followed by recovery upon reloading/return to activity. Although aged muscle exhibited the greatest mitochondrial vulnerability, young muscle also exhibited a loss of mtDNA and citrate synthase protein abundance after repeated atrophy, despite the transcriptional protection discussed above. This suggests that repeated disuse may increase susceptibility to mitochondrial loss, raising the question as to whether further atrophic episodes of disuse atrophy could drive even young muscle more toward the detrimental molecular program observed in aged muscle.

4.5 | A Similar Epigenetic Program in Both Species Represses Aerobic Metabolism Genes

Integrative methylome and transcriptome analyses revealed differentially methylated, differentially expressed genes (DmDEGs) enriched in oxidative metabolism and mitochondrial structure/turnover in both humans and rats. These genes were hypermethylated and downregulated during atrophy and repeated atrophy, returning toward baseline on recovery. This extends prior observations of disuse-linked methylation (e.g., nNOS hypermethylation [65], *Chrna1* hypomethylation/upregulation [66]) and contrasts with the hypomethylating effects of exercise training, higher physical activity, and aerobic fitness associated with a 'younger' skeletal muscle methylome [36, 37, 39, 48, 57, 58, 59, 60, 63].

4.6 | Neuromuscular Signaling Pathways in Response to Repeated Atrophy: Epigenetic Priming of the AChR Subunit Genes

Repeated disuse increased expression of acetylcholine receptor subunits, *CHRNA1, CHRND and CHRNG* in young human muscle, alongside hypomethylation at these loci (*CHRNA1* and *CHRND*), and similarly elevated *Chrna1, Chrnd, and Chrng* expression in aged rat muscle. Although potentially compensatory, such extra-junctional expression, especially of the fetal-type gamma subunit (*Chrng*), is typically linked to NMJ dysfunction rather than stabilization [10]. In young muscle, this response emerged after repeated atrophy, coinciding with the strongest hypomethylation, suggesting an epigenetic memory within AChR genes. In aged rat muscle, upregulation of *Chrna1* (16-fold) and *Chrnd* (12.5-fold) after repeated disuse was more than double that observed after initial disuse (*Chrna1* 7-fold, *Chrnd*-5.8 fold), with significant elevation of *Chrng* occuring after repeated atrophy only. Whilst we did not detect hypomethylation of these genes in aged rat muscle using RREM, prior studies have reported *Chrna1* hypomethylation in young adult rats utilizing the same model of disuse [66]. Therefore, despite a predominance of transcriptional resilience, young muscle still exhibited exaggerated AChR gene responses to repeated atrophy. Further, the exaggerated response in aging muscle is consistent with aging studies associating poor recovery with NMJ instability and ER stress [10, 26, 86], and imply that repeated stress, even in young muscle, may epigenetically prime these genes, heightening vulnerability in response to future disuse.

4.7 | NR Supplementation Partially Restored NMRK2 Levels and Increased Myotube Size in Human MuSCs Derived Post-atrophy

NMRK2, a key NAD^+ salvage enzyme, was the most downregulated genes after both periods of atrophy in young adult humans (with inversely associated DNA methylation) and was significantly downregulated in aged rat muscle after repeated atrophy, with broader NAD^+/NADH metabolism pathway repression across species, most pronounced in aged muscle. In human MuSCs derived post-atrophy, supplementation with NMRK2 substrate, nicotinamide riboside (NR), improved myotube growth, suggesting NAD^+ salvage as a potential target. However, whilst this provides initial in vitro evidence, preclinical work shows intravenous NR elevates muscle NAD^+, while oral NR trials report mixed efficacy [83, 87]. Rigorous clinical studies in older, immobilization-prone populations are essential before considering NR as a viable therapeutic intervention.

4.8 | ECM Remodeling During Recovery and Repeated Atrophy in Aged Muscle

Upregulation of genes associated with the extracellular matrix (ECM), collagen organization, collagen binding, and sarcomere structure were unique in aged muscle during recovery from initial disuse. This suggests structural remodeling as a compensatory response, which may stabilize tissue but also increase stiffness [88, 89], a hallmark of muscle aging, and perhaps impaired functional recovery. Previous work has reported that repeated cycles of atrophy in rats can lead to structural remodeling of the extracellular matrix (ECM), which may influence muscle resilience and susceptibility to future disuse [90]. In the present study, ECM turnover, proteasomal pathways, and ubiquitin-mediated proteolysis were exclusively enriched after repeated atrophy in aged muscle, reinforcing the concept of compromised resilience to repeated disuse with age.

4.9 | The NR4A Genes Are Important Metabolic Regulators of Repeated Disuse Atrophy in Young Human Muscle

In human muscle, NR4A1, a key energy metabolism gene, was hypermethylated and remained downregulated even after full recovery of muscle mass in young muscle, while *NR4A3* showed the largest reduction of all differentially expressed genes after initial disuse. Temporal profiling confirmed that both genes retained suppression post-atrophy, indicating a transcriptional memory. NR4A genes are highly responsive to exercise and inactivity [91]; *NR4A1* is oppositely hypomethylated and upregulated after high-intensity exercise [46], and *NR4A3* overexpression in rats enhances mitochondrial content, ATP production, and type-IIA & IIX muscle fiber protein content [92–94]. Knockdown of *Nr4a3* impairs glucose metabolism and protein synthesis in skeletal muscle [95]. Collectively, these findings nominate *NR4A* genes as candidate targets to improve recovery and protect against future disuse atrophy.

4.10 | Strengths and Limitations

This study provides a comprehensive physiological and molecular analysis of repeated disuse atrophy across young adult human and aged rat skeletal muscle. However, several limitations should be acknowledged. Interpretation of molecular protection vs. atrophy outcomes: While we observed transcriptional attenuation in young human muscle following repeated disuse, this did not translate into attenuated muscle mass loss. The term "protective molecular memory" refers specifically to reduced transcriptional responsiveness in metabolic pathways, not an attenuated loss in skeletal muscle size due to repeated atrophy. Furthermore, whilst there was a predominance of transcriptional attenuation in young human muscle to repeated atrophy, there was loss of citrate synthase and mtDNA content as well as larger increases in AChR subunit gene expression (discussed above) after repeated disuse-atrophy. This raises the interesting question as to whether further atrophic episodes of disuse atrophy could drive even young muscle toward the detrimental program observed in aged muscle and requires future investigation into further serial encounters with disuse across the lifespan.

Cross-species comparisons and protocol differences: Although both models were analyzed independently before integration, differences in species, disuse protocols (immobilization vs. TTX), recovery durations, and age must be considered when interpreting cross-species comparisons. Although the human and rat models differ in species, age, and the method of disuse induction (immobilization vs. TTX), both exhibited highly conserved molecular signatures in key pathways, including aerobic metabolism, mitochondrial function, and NAD^+ metabolism; these similarities were unexpected and suggest that molecular responses to disuse-atrophy may represent a shared biological phenomenon across species. Nevertheless, these cross-species comparisons should be interpreted cautiously and considered exploratory, as biological variability between species, strains, and age groups may influence interpretation. Further, young and aged rats compared were of different strains (Wistar vs. Fischer 344), which may influence physiological and molecular responses to TTX-induced disuse independently of age. This should be considered when interpreting cross-strain comparisons. Nevertheless, transcriptomic analysis revealed substantial overlap in downregulated genes during atrophy in both young adult and aged rats (Figure 5), suggesting that the core molecular response to disuse is largely conserved across strains. The greatest divergence occurred during recovery, where young rats regained muscle mass, whereas aged rats continued to lose muscle mass despite transcriptional recovery. This indicates that age, rather than strain, is the primary determinant of impaired recovery following repeated disuse.

Sex differences and sample size: In young adult humans, only 3 females compared to 7 males were recruited, thus, it was not feasible to decipher sex-specific differences to repeated atrophy. The animal study also utilized only male aged rats. This choice was driven by practical and welfare considerations specific to the extended pre-experimental housing period, as male Fischer 344 rats form stable social groups after import whereas female rats do not reliably do so, and social housing was essential to minimize stress in very old animals. Although necessary for

welfare and housing stability, this precluded evaluation of sex specific responses and should be considered when interpreting the findings. In addition to this sex-related constraint, a relatively small group size of aged rats was used. To address this, the unilateral TTX model was employed because it offers a methodological advantage. The contralateral limb remains fully innervated and untreated, allowing each animal to serve as its own internal control. This paired design substantially increases statistical power and reduces between-animal variability, enabling robust detection of physiological and molecular changes with fewer animals and aligning with the principles of Reduction and Refinement. This was particularly important given the four experimental timepoints and the use of very old Fischer 344 rats, where availability was inherently limited. Although bilateral hindlimb unloading remains a valuable model of disuse, it affects both limbs simultaneously and therefore typically requires larger group sizes to achieve comparable statistical sensitivity. The unilateral approach used here was therefore selected to maximise statistical robustness while minimizing total animal use.

Age comparisons, recovery protocols and activity/nutritional monitoring: Although protocol differences exist between young and aged rat studies, the observation that young rats recovered muscle mass after a slightly longer TTX exposure and shorter recovery period, whereas aged rats failed to recover despite a shorter exposure and extended recovery, strongly suggests that age is the primary determinant of impaired recovery. The extreme age of the Fischer 344 rats (~23 months) likely further contributed to this phenotype. In aged rats, molecular pathways recovered during TTX cessation despite continued muscle wasting, suggesting that the transcriptional response was TTX dependent rather than a consequence of incomplete recovery. Further, we present a comparison of the aged rats with young adult rats [66] that recover half of their muscle mass following a slightly longer period of TTX-induced atrophy (and thus greater muscle wasting than aged animals herein) in a shorter recovery period. However, whilst rat activity was confirmed by the ability to perform dorsiflexion, activity levels during recovery were not directly measured. Future studies should therefore incorporate objective tracking of habitual activity (for example, EMG, respirometry or automated behavioural monitoring) together with detailed measures of nutritional intake to fully disentangle behavioural influences from molecular and physiological recovery. Furthermore, during human immobilization considering wearables (accelerometers) or bed-rest protocols may better characterize recovery dynamics. It is also worth noting that recovery dynamics after unloading have been previously characterized in young vs. old rats [96], where older rats exhibit impaired but gradual recovery. In contrast, the very old Fischer 344 rats used in our study (~23 months) continued to lose muscle mass during recovery, suggesting that advanced age may exacerbate susceptibility to repeated disuse.

Methodological constraints and data integration: The integration of multi-omics data across species and models introduces complexity. While individual analyses within species are robust, interpretation of age-related effects must consider differences. For example, due to limited fiber number in the cross-sections from human samples we also inferred fiber type proportions using gene expression data. Moreover, ETC protein data were not available for repeated atrophy in aged rats, and ETC protein changes were not statistically significant despite reductions in ETC-related genes, NAD^+ content (rat), and mtDNA (human and rat). While our integration strategy used SOM profiling to cluster DEGs and DMRs temporally, advanced computational multi-omic frameworks such as BETA [43] could provide deeper mechanistic insights. Implementing such approaches was beyond the scope of the manuscript but represents an important avenue for future work.

Translational scope and in vitro validation: NR supplementation improved myotube size in human MuSCs derived post-atrophy, suggesting a potential therapeutic avenue with translation to humans. However, these findings are limited to preliminary in vitro experiments in young adult MuSCs. Further studies are needed to validate NAD^+ salvage interventions in aged muscle and in vivo models of repeated disuse. Further, as a limitation to the cell culture experiments, these in vitro studies were performed in differentiating human cultures, as MuSC isolation from aged rat muscle was not possible because the in vitro work was initiated after omics discovery had been completed, which precluded parallel aged rat studies, and stable primary rat myotube cultures suitable for mechanistic assays are technically challenging to generate. Nevertheless, the data provide preliminary insight into NAD^+ salvage and *NMRK2* responsiveness, including partial recovery of *NMRK1/2* expression, modulation of *MYOD* and *MYOG* and improved myotube size with NR supplementation. Furthermore, the nicotinamide riboside intervention was applied after differentiation had been induced, consistent with common practice in human skeletal muscle cell studies that administer nutrient, pharmacological, or genetic interventions at approximately day six to eight of differentiation. Future studies should address targeted manipulation of *Nmrk2* in aged rat tissue in vivo under atrophic conditions to provide important mechanistic insight into the role of NR in protecting against disuse-induced atrophy and improving recovery.

Epigenetic interpretation and functional relevance: While DNA methylation changes were inversely associated with gene expression in key metabolic pathways, functional consequences of these epigenetic modifications remain to be fully elucidated. To complement the multi-omics dataset, we incorporated targeted validation of mitochondrial function, including gene expression profiling, NAD^+ content, mtDNA copy number, citrate synthase activity, and ETC protein abundance. While most measures aligned with the omics findings, some species-specific differences were evident, such as unchanged NAD^+ content in humans despite reductions in aged rats, and unchanged ETC protein abundance in humans and rats despite consistent transcriptional suppression of mitochondrial pathways and reductions in mtDNA content. Nevertheless, the strong concordance between omics and targeted analyses at the pathway level reinforces the robustness of the findings. Future work should explore whether these methylation signatures directly modulate transcriptional memory or serve as biomarkers of prior disuse and recovery. In addition, structural correlates were not assessed in detail where in the future, additional histological analyses of denervation markers (e.g., NCAM, eMyHC, central nucleation) and ECM organization in the rat repeated atrophy model, would have provided further corroboration of the omics data. These analyses were not feasible within the scope of the current study, however future studies should incorporate detailed his-

tological assessments of neuromuscular junction integrity and ECM remodeling alongside multi-omic profiling to strengthen mechanistic interpretation.

4.11 | Future Mechanistic and Clinical Directions

We propose mechanistic and translational studies that address testable hypothesis, such as: (i) Does enhancing NAD^+ salvage attenuate the maladaptive transcriptional response to repeated disuse in aged muscle? ii) Does exercise 'preconditioning' [97, 98] or training reprogram methylation signatures to prevent negative molecular memory in the nuclear [39, 57] and mitochondrial genome [63]? (iii) Does targeted activation of *NR4A* family, AChR subunit and *NMRK2* genes during atrophy or recovery prevent or offset disuse-induced atrophy and/or promote recovery from atrophy?

5 | Conclusion

Disuse atrophy can be remembered at the molecular level in skeletal muscle. It is predominantly protective in young skeletal muscle yet detrimental in aged skeletal muscle. This memory is partially epigenetically encoded at the single locus level and converges in aerobic metabolism, mitochondrial, and NAD^+ pathways, and nominates molecular targets to preserve muscle mass and function after recurrent immobilization or disuse.

Author Contributions

A.P.S. conceived the project, secured funding as principal investigator, and led the human experimental design, ethical approvals, data/finance management, dissemination, and oversaw analysis of all human and rat experiments, and supervised postdoctoral fellow D.C.T. D.C.T. conducted most of the experimental work in the labatory of A.P.S., including recruitment, human testing, biopsy processing, wet lab work, data collection, analysis, visualization, dissemination, and manuscript drafting. J.C.J. supervised and undertook the animal intervention studies with H.S. was subsequently analysed in the wet lab and all downstream analysis by D.C.T and A.P.S. J.C.J also provided vital input as a co-investigator into the funding application and expertise in experimental design, analysis, and interpretation. S.C.B., D.C.H., D.J.O., and T.R. were co-investigators in the funding application and heavily involved in study design, biopsy sampling, interpretation of results, and manuscript preparation. S.F.C. undertook experimental work for the mtDNA analysis in MuSCs. J.T.T. and E.D.K. undertook NAD^+ content experiments. E.W., C.M., and J.B. undertook RNA-seq and RRBS/RREM wet lab experiments and preprocessing of RNA-seq, RRBS/RREM, and bioinformatics. M.U. assisted in omics analysis and visualization. All authors contributed significantly to the final manuscript.

Acknowledgements

This research was funded by The Research Council of Norway (RCN) (314157) awarded to principal investigator Adam P. Sharples, post-doc fellow Daniel C. Turner and co-investigators Sue Bodine, Jonathan C. Jarvis, David C. Hughes, Daniel J. Owens, Truls Raastad and Olivier Seynnes. We thank Olivier Seynnes for his critical expertise and input into the funding application, training & supervision of post-doctoral researcher for the design, testing and analysis of the human experiments and associated physiological data acquisition and analysis (muscle size/mCSA & strength). We thank Jostein Hallèn, Siri T. Dalen, Hege N. Ødemark and Emil Løvstakken (NIH) for assistance with muscle biopsies and tissue processing; Josephine A. Eyrich (UCPH) for assisting with the measurements of NAD^+ content; Rune Enger, as the medical lead for the human biopsies; Enovis/DJO LLC for kindly donating the knee braces and; ChromaDex, Inc., a subsidiary of Niagen Bioscience for providing nicotinamide riboside for in vitro studies. Finally, sincere gratitude to all participants who volunteered to participate in this demanding study that included two periods of muscle wasting.

Conflicts of Interest

The authors declare no conflicts of interest related to this study. ChromaDex, Inc., a subsidiary of Niagen Bioscience, supplied nicotinamide riboside for the in vitro experiments. The company had no involvement in any aspect of the study, including its conception, design, data acquisition, analysis, interpretation, or manuscript preparation. No authors are affiliated with ChromaDex or Niagen Bioscience. Niagen Bioscience is the main sponsor of a scientific meeting Jonas T. Treebak is organising (i.e., "NAD for Health-Opportunities & Challenges" in Copenhagen, March 2026); this sponsorship is unrelated to the present study.

Data Availability Statement

Raw and pre-processed RNA-seq and bisulfite sequencing data are available via the Gene Expression Omnibus (GEO) repository (Human RNA-seq: GSE310344; Human RRBS: GSE310743; Rat RNA-seq: GSE310848; Rat RREM: GSE310849). Processed DEG and DMR data are provided in Supplementary Data S1–4. Any other processed data are available upon reasonable request to the corresponding authors.

Software and Code Availability

All analysis code used for preprocessing, normalization, differential expression/methylation, enrichment and visualization of the data is freely available/open source with links and references detailed in Supplementary Table S2. Any unique code is available on reasonable request to the corresponding authors.

References

1. V. A. Hughes, W. R. Frontera, M. Wood, et al., "Longitudinal Muscle Strength Changes in Older Adults: Influence of Muscle Mass, Physical Activity, and Health," *The Journals of Gerontology Series A: Biological Sciences and Medical Sciences* 56 (2001): B209–B217, https://doi.org/10.1093/gerona/56.5.B209.

2. A. J. Cruz-Jentoft, F. Landi, E. Topinkova, and J. P. Michel, "Understanding Sarcopenia as a Geriatric Syndrome," *Current Opinion in Clinical Nutrition and Metabolic Care* 13 (2010): 1–7.

3. C. Beaudart, M. Zaaria, F. Pasleau, J.-Y. Reginster, and O. Bruyère, "Health Outcomes of Sarcopenia: A Systematic Review and Meta-Analysis," *PLoS ONE* 12 (2017): 0169548, https://doi.org/10.1371/journal.pone.0169548.

4. L. P. Fried, C. M. Tangen, J. Walston, et al., "Frailty in Older Adults: Evidence for a Phenotype," *The Journals of Gerontology: Series A* 56 (2001): M146–M157.

5. E. Rejc, M. Floreani, P. Taboga, et al., "Loss of Maximal Explosive Power of Lower Limbs after 2 Weeks of Disuse and Incomplete Recovery after Retraining in Older Adults," *The Journal of Physiology* 596 (2018): 647–665, https://doi.org/10.1113/JP274772.

6. R. Pisot, U. Marusic, G. Biolo, et al., "Greater Loss in Muscle Mass and Function but Smaller Metabolic Alterations in Older Compared with Younger Men Following 2 Wk of Bed Rest and Recovery," *Journal of Applied Physiology* 120 (1985): 922–929, https://doi.org/10.1152/japplphysiol.00858.2015.

7. I. F. Kramer, T. Snijders, J. S. J. Smeets, et al., "Extensive Type II Muscle Fiber Atrophy in Elderly Female Hip Fracture Patients," *The Journals of Gerontology: Series A* 72 (2017): 1369–1375, https://doi.org/10.1093/gerona/glw253.

8. C. Suetta, L. G. Hvid, L. Justesen, et al., "Effects of Aging on Human Skeletal Muscle after Immobilization and Retraining," *Journal of Applied Physiology* 107 (2009): 1172–1180, https://doi.org/10.1152/japplphysiol.00290.2009.

9. L. M. Baehr, D. W. D. West, A. G. Marshall, G. R. Marcotte, K. Baar, and S. C. Bodine, "Muscle-Specific and Age-Related Changes in Protein Synthesis and Protein Degradation in Response to Hindlimb Unloading in Rats," *Journal of Applied Physiology* 122 (2017): 1336–1350, https://doi.org/10.1152/japplphysiol.00703.2016.

10. L. M. Baehr, D. W. D. West, G. Marcotte, et al., "Age-Related Deficits in Skeletal Muscle Recovery Following Disuse Are Associated with Neuromuscular Junction Instability and ER Stress, Not Impaired Protein Synthesis," *Aging* 8 (2016): 127–146, https://doi.org/10.18632/aging.100879.

11. L. Hvid, P. Aagaard, L. Justesen, et al., "Effects of Aging on Muscle Mechanical Function and Muscle Fiber Morphology During Short-Term Immobilization and Subsequent Retraining," *Journal of Applied Physiology* 109 (2010): 1628–1634, https://doi.org/10.1152/japplphysiol.00637.2010.

12. P. T. Reidy, A. I. McKenzie, Z. S. Mahmassani, et al., "Aging Impairs Mouse Skeletal Muscle Macrophage Polarization and Muscle-Specific Abundance During Recovery from Disuse," *American Journal of Physiology-Endocrinology and Metabolism* 317 (2019): E85–E98, https://doi.org/10.1152/ajpendo.00422.2018.

13. S. C. Bodine, E. Latres, S. Baumhueter, et al., "Identification of Ubiquitin Ligases Required for Skeletal Muscle Atrophy," *Science* 294 (2001): 1704–1708, https://doi.org/10.1126/science.1065874.

14. M. L. Dirks, B. T. Wall, T. Snijders, C. L. Ottenbros, L. B. Verdijk, and L. J. van Loon, "Neuromuscular Electrical Stimulation Prevents Muscle Disuse Atrophy During Leg Immobilization in Humans," *Acta Physiologica* 210 (2014): 628–641, https://doi.org/10.1111/apha.12200.

15. S. P. Kilroe, J. Fulford, S. R. Jackman, L. J. C. VANL, and B. T. Wall, "Temporal Muscle-Specific Disuse Atrophy During One Week of Leg Immobilization," *Medicine & Science in Sports & Exercise* 52 (2020): 944–954, https://doi.org/10.1249/MSS.0000000000002200.

16. T. S. O. Jameson, S. P. Kilroe, J. Fulford, et al., "Muscle Damaging Eccentric Exercise Attenuates Disuse-Induced Declines in Daily Myofibrillar Protein Synthesis and Transiently Prevents Muscle Atrophy in Healthy Men," *American Journal of Physiology-Endocrinology and Metabolism* 321 (2021): E674–E688, https://doi.org/10.1152/ajpendo.00294.2021.

17. B. T. Wall, M. L. Dirks, T. Snijders, J. M. G. Senden, J. Dolmans, and L. J. C. van Loon, "Substantial Skeletal Muscle Loss Occurs During Only 5 Days of Disuse," *Acta Physiologica* 210 (2014): 600–611, https://doi.org/10.1111/apha.12190.

18. B. T. Wall, M. L. Dirks, T. Snijders, et al., "Short-Term Muscle Disuse Lowers Myofibrillar Protein Synthesis Rates and Induces Anabolic Resistance to Protein Ingestion," *American Journal of Physiology-Endocrinology and Metabolism* 310 (2016): E137–E147, https://doi.org/10.1152/ajpendo.00227.2015.

19. M. V. Franchi, J. Candia, F. Sarto, et al., "Previous Short-Term Disuse Dictates Muscle Gene Expression and Physiological Adaptations to Subsequent Resistance Exercise," *The Journal of Physiology* 603 (2025): 3725–3753, https://doi.org/10.1113/JP287003.

20. L. Brocca, E. Longa, J. Cannavino, et al., "Human Skeletal Muscle Fibre Contractile Properties and Proteomic Profile: Adaptations to 3 Weeks of Unilateral Lower Limb Suspension and Active Recovery," *The Journal of Physiology* 593 (2015): 5361–5385, https://doi.org/10.1113/JP271188.

21. E. L. Campbell, O. R. Seynnes, R. Bottinelli, et al., "Skeletal Muscle Adaptations to Physical Inactivity and Subsequent Retraining in Young Men," *Biogerontology* 14 (2013): 247–259, https://doi.org/10.1007/s10522-013-9427-6.

22. M. L. Dirks, B. T. Wall, B. van de Valk, et al., "One Week of Bed Rest Leads to Substantial Muscle Atrophy and Induces Whole-Body Insulin Resistance in the Absence of Skeletal Muscle Lipid Accumulation," *Diabetes* 65 (2016): 2862–2875, https://doi.org/10.2337/db15-1661.

23. M. M. Bamman, M. S. F. Clarke, D. L. Feeback, et al., "Impact of Resistance Exercise During Bed Rest on Skeletal Muscle Sarcopenia and Myosin Isoform Distribution," *Journal of Applied Physiology* 84 (1998): 157–163, https://doi.org/10.1152/jappl.1998.84.1.157.

24. J. Noone, A. Damiot, H. Kenny, et al., "The Impact of 60 Days of −6° Head Down Tilt Bed Rest on Mitochondrial Content, Respiration and Regulators of Mitochondrial Dynamics," *The Journal of Physiology* 603 (2025): 3777–3794, https://doi.org/10.1113/JP284734.

25. S. Ringholm, R. S. Biensø, K. Kiilerich, et al., "Bed Rest Reduces Metabolic Protein Content and Abolishes Exercise-Induced mRNA Responses in Human Skeletal Muscle," *American Journal of Physiology-Endocrinology and Metabolism* 301 (2011): E649–E658, https://doi.org/10.1152/ajpendo.00230.2011.

26. E. Motanova, F. Sarto, S. Negro, et al., "Neuromuscular Junction Instability with Inactivity: Morphological and Functional Changes after 10 Days of Bed Rest in Older Adults," *The Journal of Physiology* 604 (2025): 868–885.

27. V. R. Edgerton, M. Y. Zhou, Y. Ohira, et al., "Human Fiber Size and Enzymatic Properties after 5 and 11 Days of Spaceflight," *Journal of Applied Physiology* 78 (1995): 1733–1739, https://doi.org/10.1152/jappl.1995.78.5.1733.

28. M. Murgia, J. Rittweger, C. Reggiani, et al., "Spaceflight on the ISS Changed the Skeletal Muscle Proteome of Two Astronauts," *NPJ Microgravity* 10 (2024): 60, https://doi.org/10.1038/s41526-024-00406-3.

29. M. Murgia, S. Ciciliot, N. Nagaraj, et al., "Signatures of Muscle Disuse in Spaceflight and Bed Rest Revealed by Single Muscle Fiber Proteomics," *PNAS Nexus* 1 (2022): pgac086, https://doi.org/10.1093/pnasnexus/pgac086.

30. A. P. Sharples, C. E. Stewart, and R. A. Seaborne, "Does Skeletal Muscle Have an 'Epi'-Memory? The Role of Epigenetics in Nutritional Programming, Metabolic Disease, Aging and Exercise," *Aging Cell* 15 (2016): 603–616, https://doi.org/10.1111/acel.12486.

31. A. P. Sharples and D. C. Turner, "Skeletal Muscle Memory," *American Journal of Physiology-Cell Physiology* 324 (2023): C1274–C1294, https://doi.org/10.1152/ajpcell.00099.2023.

32. J. C. Bruusgaard, I. B. Johansen, I. M. Egner, Z. A. Rana, and K. Gundersen, "Myonuclei Acquired by Overload Exercise Precede Hypertrophy and Are Not Lost on Detraining," *Proceedings of the National Academy of Sciences USA* 107 (2010): 15111–15116, https://doi.org/10.1073/pnas.0913935107.

33. Y. Wen, C. M. Dungan, C. B. Mobley, T. Valentino, F. von Walden, and K. A. Murach, "Nucleus Type-Specific DNA Methylomics Reveals Epigenetic "Memory" of Prior Adaptation in Skeletal Muscle," *Function* 2 (2021): zqab038.

34. C. J. Weidenhamer, Y. H. Huang, S. Natua, A. Kalsotra, and D. Hernández-Saavedra, "Muscle Memory of Exercise Optimizes Mitochondrial Metabolism to Support Skeletal Muscle Growth," *American Journal of Physiology-Cell Physiology* 329 (2025): C1239–C1255, https://doi.org/10.1152/ajpcell.00451.2025.

35. I. M. Egner, J. C. Bruusgaard, E. Eftestøl, and K. Gundersen, "A Cellular Memory Mechanism Aids Overload Hypertrophy in Muscle Long after an Episodic Exposure to Anabolic Steroids," *The Journal of Physiology* 591 (2013): 6221–6230, https://doi.org/10.1113/jphysiol.2013.264457.

36. R. A. Seaborne, J. Strauss, M. Cocks, et al., "Human Skeletal Muscle Possesses an Epigenetic Memory of Hypertrophy," *Scientific Reports* 8 (2018): 1898, https://doi.org/10.1038/s41598-018-20287-3.

37. D. C. Turner, R. A. Seaborne, and A. P. Sharples, "Comparative Transcriptome and Methylome Analysis in Human Skeletal Muscle Anabolism, Hypertrophy and Epigenetic Memory," *Scientific Reports* 9 (2019): 4251, https://doi.org/10.1038/s41598-019-40787-0.

38. J. J. Hulmi, E. J. Halonen, A. P. Sharples, et al., "Human Skeletal Muscle Possesses both Reversible Proteomic Signatures and a Retained Proteomic Memory after Repeated Resistance Training," *The Journal of Physiology* 603 (2025): 2655–2673, https://doi.org/10.1113/JP288104.

39. S. Blocquiaux, M. Ramaekers, R. Van Thienen, et al., "Recurrent Training Rejuvenates and Enhances Transcriptome and Methylome Responses in Young and Older Human Muscle," *JCSM Rapid Communications* 5 (2022): 10–32, https://doi.org/10.1002/rco2.52.

40. A. M. Pilotto, D. C. Turner, R. Mazzolari, et al., "Human Skeletal Muscle Possesses an Epigenetic Memory of High-Intensity Interval Training," *American Journal of Physiology-Cell Physiology* 328 (2025): C258–C272, https://doi.org/10.1152/ajpcell.00423.2024.

41. C. L. Sexton, J. S. Godwin, M. C. McIntosh, et al., "Skeletal Muscle DNA Methylation and mRNA Responses to a Bout of Higher versus Lower Load Resistance Exercise in Previously Trained Men," *Cells* 12 (2023): 263, https://doi.org/10.3390/cells12020263.

42. D. S. Rowlands, R. A. Page, W. R. Sukala, et al., "Multi-Omic Integrated Networks Connect DNA Methylation and miRNA with Skeletal Muscle Plasticity to Chronic Exercise in Type 2 Diabetic Obesity," *Physiological Genomics* 46 (2014): 747–765, https://doi.org/10.1152/physiolgenomics.00024.2014.

43. S. Edman, R. G. Jones III, P. R. Jannig, et al., "The 24-Hour Molecular Landscape after Exercise in Humans Reveals *MYC*is Sufficient for Muscle Growth," *EMBO reports* 25 (2024): 5810–5837, https://doi.org/10.1038/s44319-024-00299-z.

44. F. Von Walden, M. Rea, C. B. Mobley, et al., "The Myonuclear DNA Methylome in Response to an Acute Hypertrophic Stimulus," *Epigenetics* 15 (2020): 1151–1162, https://doi.org/10.1080/15592294.2020.1755581.

45. T. L. Chambers, A. Dimet-Wiley, A. R. Keeble, et al., "Methylome–proteome Integration after Late-Life Voluntary Exercise Training Reveals Regulation and Target Information for Improved Skeletal Muscle Health," *The Journal of Physiology* 603 (2025): 211–237, https://doi.org/10.1113/JP286681.

46. M.-F. Maasar, D. C. Turner, P. P. Gorski, et al., "The Comparative Methylome and Transcriptome after Change of Direction Compared to Straight Line Running Exercise in Human Skeletal Muscle," *Frontiers in Physiology* 12 (2021): 619447, https://doi.org/10.3389/fphys.2021.619447.

47. M. Jacques, S. Landen, J. A. Romero, et al., "Methylome and Proteome Integration in Human Skeletal Muscle Uncover Group and Individual Responses to High-Intensity Interval Training," *The FASEB Journal* 37 (2023): 23184.

48. P. P. Gorski, T. Raastad, M. Ullrich, et al., "Aerobic Exercise Training Resets the Human Skeletal Muscle Methylome 10 Years after Breast Cancer Treatment and Survival," *The FASEB Journal* 37 (2023): 22720, https://doi.org/10.1096/fj.202201510rr.

49. P. P. Gorski, D. C. Turner, J. Iraki, J. P. Morton, A. P. Sharples, and J. L. Areta, "Human Skeletal Muscle Methylome after Low-Carbohydrate Energy-Balanced Exercise," *American Journal of Physiology-Endocrinology and Metabolism* 324 (2023): E437–E448, https://doi.org/10.1152/ajpendo.00029.2023.

50. R. Barrès, J. Yan, B. Egan, et al., "Acute Exercise Remodels Promoter Methylation in Human Skeletal Muscle," *Cell Metabolism* 15 (2012): 405–411.

51. M. D. Nitert, T. Dayeh, P. Volkov, et al., "Impact of an Exercise Intervention on DNA Methylation in Skeletal Muscle from First-Degree Relatives of Patients with Type 2 Diabetes," *Diabetes* 61 (2012): 3322–3332, https://doi.org/10.2337/db11-1653.

52. C. Geiger, M. Needhamsen, E. B. Emanuelsson, et al., "DNA Methylation of Exercise-Responsive Genes Differs between Trained and Untrained Men," *BMC Biology* 22 (2024): 147, https://doi.org/10.1186/s12915-024-01938-6.

53. R. Furrer, B. Heim, S. Schmid, et al., "Molecular Control of Endurance Training Adaptation in Male Mouse Skeletal Muscle," *Nature Metabolism* 5 (2023): 2020–2035, https://doi.org/10.1038/s42255-023-00891-y.

54. M. E. Lindholm, F. Marabita, D. Gomez-Cabrero, et al., "An Integrative Analysis Reveals Coordinated Reprogramming of the Epigenome and the Transcriptome in Human Skeletal Muscle after Training," *Epigenetics* 9 (2014): 1557–1569, https://doi.org/10.4161/15592294.2014.982445.

55. M. Jacques, S. Landen, A. P. Sharples, et al., "Molecular Landscape of Sex- and Modality-Specific Exercise Adaptation in Human Skeletal Muscle through Large-Scale Multi-Omics Integration," *Cell Reports* 44 (2025): 115750, https://doi.org/10.1016/j.celrep.2025.115750.

56. B. Egan and A. P. Sharples, "Molecular Responses to Acute Exercise and Their Relevance for Adaptations in Skeletal Muscle to Exercise Training," *Physiological Reviews* 103 (2023): 2057–2170, https://doi.org/10.1152/physrev.00054.2021.

57. S. Voisin, K. Seale, M. Jacques, et al., "Exercise Is Associated with Younger Methylome and Transcriptome Profiles in Human Skeletal Muscle," *Aging Cell* 23 (2023): 13859, https://doi.org/10.1111/acel.13859.

58. M. R. Sailani, J. F. Halling, H. D. Møller, et al., "Lifelong Physical Activity Is Associated with Promoter Hypomethylation of Genes Involved in Metabolism, Myogenesis, Contractile Properties and Oxidative Stress Resistance in Aged Human Skeletal Muscle," *Scientific Reports* 9 (2019): 3272, https://doi.org/10.1038/s41598-018-37895-8.

59. D. C. Turner, P. P. Gorski, M. F. Maasar, et al., "DNA Methylation across the Genome in Aged Human Skeletal Muscle Tissue and Muscle-Derived Cells: the Role of HOX Genes and Physical Activity," *Scientific Reports* 10 (2020): 15360, https://doi.org/10.1038/s41598-020-72730-z.

60. S. Voisin, M. Jacques, S. Landen, et al., "Meta-Analysis of Genome-Wide DNA Methylation and Integrative Omics of Age in Human Skeletal Muscle," *Journal of Cachexia, Sarcopenia and Muscle* 12 (2021): 1064–1078, https://doi.org/10.1002/jcsm.12741.

61. A. Zykovich, A. Hubbard, J. M. Flynn, et al., "Genome-Wide DNA Methylation Changes with Age in Disease-Free Human Skeletal Muscle," *Aging Cell* 13 (2014): 360–366, https://doi.org/10.1111/acel.12180.

62. R. Barrès, M. E. Osler, J. Yan, et al., "Non-CpG Methylation of the PGC-1alpha Promoter through DNMT3B Controls Mitochondrial Density," *Cell Metabolism* 10 (2009): 189–198.

63. B. A. Ruple, J. S. Godwin, P. H. C. Mesquita, et al., "Resistance Training Rejuvenates the Mitochondrial Methylome in Aged Human Skeletal Muscle," *The FASEB Journal* 35 (2021): 21864, https://doi.org/10.1096/fj.202100873rr.

64. A. C. Alibegovic, M. P. Sonne, L. Højbjerre, et al., "Insulin Resistance Induced by Physical Inactivity Is Associated with Multiple Transcriptional Changes in Skeletal Muscle in Young Men," *American Journal of Physiology-Endocrinology and Metabolism* 299 (2010): E752–E763, https://doi.org/10.1152/ajpendo.00590.2009.

65. Y. Tomiga, A. Ito, M. Sudo, et al., "One Week, but Not 12 Hours, of Cast Immobilization Alters Promotor DNA Methylation Patterns in the nNOS Gene in Mouse Skeletal Muscle," *The Journal of Physiology* 597 (2019): 5145–5159, https://doi.org/10.1113/JP277019.

66. A. G. Fisher, R. A. Seaborne, T. M. Hughes, et al., "Transcriptomic and Epigenetic Regulation of Disuse Atrophy and the Return to Activity in Skeletal Muscle," *The FASEB Journal* 31 (2017): 5268–5282, https://doi.org/10.1096/fj.201700089RR.

67. T. Falick Michaeli, O. Sabag, R. Fok, B. Azria, J. Monin, and Y. Nevo, "Muscle Injury Causes Long-Term Changes in Stem-Cell DNA Methylation," *Proceedings of the National Academy of Sciences USA* 119 (2022): 2212306119, https://doi.org/10.1073/pnas.2212306119.

68. P. H. Lee, D. J. Macfarlane, T. H. Lam, and S. M. Stewart, "Validity of the International Physical Activity Questionnaire Short Form (IPAQ-SF): A Systematic Review," *International Journal of Behavioral Nutrition and Physical Activity* 8 (2011): 115, https://doi.org/10.1186/1479-5868-8-115.

69. Y. Li, X.-H. Guan, R. Wang, et al., "Active Ankle Movements Prevent Formation of Lower-Extremity Deep Venous Thrombosis after Orthopedic Surgery," *Medical Science Monitor* 22 (2016): 3169–3176, https://doi.org/10.12659/MSM.896911.

70. F. Sarto, D. W. Stashuk, M. V. Franchi, et al., "Effects of Short-Term Unloading and Active Recovery on Human Motor Unit Properties, Neuromuscular Junction Transmission and Transcriptomic Profile," *The Journal of Physiology* 600 (2022): 4731–4751, https://doi.org/10.1113/JP283381.

71. Ø. Skattebo, D. Peci, M. Clauss, E. I. Johansen, and J. Jensen, "Increased Mass-Specific Maximal Fat Oxidation Rate with Small versus Large Muscle Mass Exercise," *Medicine & Science in Sports & Exercise* 54 (2022): 974–983, https://doi.org/10.1249/MSS.0000000000002864.

72. R. A. Seaborne, D. C. Hughes, D. C. Turner, et al., "UBR5 is a Novel E3 Ubiquitin Ligase Involved in Skeletal Muscle Hypertrophy and Recovery from Atrophy," *The Journal of Physiology* 597 (2019): 3727–3749, https://doi.org/10.1113/JP278073.

73. Y. S. Elhassan, A. Kabli, T. Nielsen, et al., "OR03-06 NAD+ Availability Modulates 11β-HSD1-Mediated Glucocorticoid Regeneration in Mouse Skeletal Muscle," *Journal of the Endocrine Society* 4 (2020): OR03–06, https://doi.org/10.1210/jendso/bvaa046.1657.

74. M. Alsharidah, N. R. Lazarus, T. E. George, C. C. Agley, C. P. Velloso, and S. D. Harridge, "Primary Human Muscle Precursor Cells Obtained from Young and Old Donors Produce Similar Proliferative, Differentiation and Senescent Profiles in Culture," *Aging Cell* 12 (2013): 333–344, https://doi.org/10.1111/acel.12051.

75. T. D. Schmittgen and K. J. Livak, "Analyzing Real-Time PCR Data by the Comparative CT Method," *Nature Protocols* 3 (2008): 1101–1108, https://doi.org/10.1038/nprot.2008.73.

76. J. P. Rooney, I. T. Ryde, L. H. Sanders, et al., "PCR Based Determination of Mitochondrial DNA Copy Number in Multiple Species," *Methods in Molecular Biology* 1241 (2015): 23–38.

77. H. A. K. Lapatto, M. Kuusela, A. Heikkinen, et al., "Nicotinamide Riboside Improves Muscle Mitochondrial Biogenesis, Satellite Cell Differentiation, and Gut Microbiota in a Twin Study," *Science Advances* 9 (2023): add5163, https://doi.org/10.1126/sciadv.add5163.

78. M. F. Kemper, C. Stirone, D. N. Krause, S. P. Duckles, and V. Procaccio, "Genomic and Non-Genomic Regulation of PGC1 Isoforms by Estrogen to Increase Cerebral Vascular Mitochondrial Biogenesis and Reactive Oxygen Species Protection," *European Journal of Pharmacology* 723 (2014): 322–329, https://doi.org/10.1016/j.ejphar.2013.11.009.

79. A. Arduini, G. Serviddio, J. Escobar, et al., "Mitochondrial Biogenesis Fails in Secondary Biliary Cirrhosis in Rats Leading to Mitochondrial DNA Depletion and Deletions," *American Journal of Physiology-Gastrointestinal and Liver Physiology* 301 (2011): G119–G127, https://doi.org/10.1152/ajpgi.00253.2010.

80. J. Stevanović-Silva, J. Beleza, P. Coxito, P. J. Oliveira, A. Ascensão, and J. Magalhães, "Gestational Exercise Antagonises the Impact of Maternal High-Fat High-Sucrose Diet on Liver Mitochondrial Alterations and Quality Control Signalling in Male Offspring," *International Journal of Environmental Research and Public Health* 20 (2023): 1388.

81. M. Dall, M. Penke, K. Sulek, et al., "Hepatic NAD+ Levels and NAMPT Abundance Are Unaffected During Prolonged High-Fat Diet Consumption in C57BL/6JBomTac Mice," *Molecular and Cellular Endocrinology* 473 (2018): 245–256, https://doi.org/10.1016/j.mce.2018.01.025.

82. T. Van der Stede, R. Moreno-Justicia, F. Van de Casteele, et al., "Deconvoluting Fiber Type Proportions from Human Skeletal Muscle Transcriptomics and Proteomics Data Using FibeRtypeR," BioRxiv (2025): 2025.2009.2017.676778.

83. M. V. Damgaard and J. T. Treebak, "What Is Really Known about the Effects of Nicotinamide Riboside Supplementation in Humans," *Science Advances* 9 (2023): adi4862, https://doi.org/10.1126/sciadv.adi4862.

84. S. C. Bodine, I. Sinha, and H. L. Sweeney, "Mechanisms of Skeletal Muscle Atrophy and Molecular Circuitry of Stem Cell Fate in Skeletal Muscle Regeneration and Aging," *The Journals of Gerontology: Series A* 78 (2023): 14–18.

85. L. Zuccarelli, M. De Martino, A. Filippi, et al., "Mitochondrial Sensitivity to Submaximal [ADP] Following Bed Rest: a Novel Two-Phase Approach Associated with Fibre Types," *Journal of Cachexia, Sarcopenia and Muscle* 16 (2025): 13775, https://doi.org/10.1002/jcsm.13775.

86. F. Sarto, M. Kalc, E. S. Motanova, et al., "Twenty-One Days of Bed Rest Alter Motor Unit Properties and Neuromuscular Junction Transmission in Young Adults," *Journal of Applied Physiology* 138 (2025): 1411–1424, https://doi.org/10.1152/japplphysiol.00178.2025.

87. M. V. Damgaard, T. S. Nielsen, A. L. Basse, S. Chubanava, K. Trost, and T. Moritz, "Intravenous Nicotinamide Riboside Elevates Mouse Skeletal Muscle NAD(+) Without Impacting Respiratory Capacity or Insulin Sensitivity," *iScience* 25 (2022): 103863.

88. K. M. Stearns-Reider, A. D'Amore, K. Beezhold, et al., "Aging of the Skeletal Muscle Extracellular Matrix Drives a Stem Cell Fibrogenic Conversion," *Aging Cell* 16 (2017): 518–528, https://doi.org/10.1111/acel.12578.

89. P. Pavan, E. Monti, M. Bondí, et al., "Alterations of Extracellular Matrix Mechanical Properties Contribute to Age-Related Functional Impairment of Human Skeletal Muscles," *International Journal of Molecular Sciences* 21 (2020): 3992, https://doi.org/10.3390/ijms21113992.

90. K. L. Shimkus, Y. Shirazi-Fard, M. P. Wiggs, et al., "Responses of Skeletal Muscle Size and Anabolism Are Reproducible with Multiple Periods of Unloading/Reloading," *Journal of Applied Physiology* 125 (2018): 1456–1467, https://doi.org/10.1152/japplphysiol.00736.2017.

91. N. J. Pillon, B. M. Gabriel, L. Dollet, et al., "Transcriptomic Profiling of Skeletal Muscle Adaptations to Exercise and Inactivity," *Nature Communications* 11 (2020): 470, https://doi.org/10.1038/s41467-019-13869-w.

92. J. R. White, A. L. Confides, S. Moore-Reed, J. M. Hoch, and E. E. Dupont-Versteegden, "Regrowth after Skeletal Muscle Atrophy Is Impaired in Aged Rats, Despite Similar Responses in Signaling Pathways," *Experimental Gerontology* 64 (2015): 17–32, https://doi.org/10.1016/j.exger.2015.02.007.

93. M. A. Pearen, N. A. Eriksson, R. L. Fitzsimmons, et al., "The Nuclear Receptor, nor-1, Markedly Increases Type II Oxidative Muscle Fibers and Resistance to Fatigue," *Molecular Endocrinology* 26 (2012): 372–384, https://doi.org/10.1210/me.2011-1274.

94. J. M. Goode, M. A. Pearen, Z. K. Tuong, et al., "The Nuclear Receptor, nor-1, Induces the Physiological Responses Associated with Exercise," *Molecular Endocrinology* 30 (2016): 660–676, https://doi.org/10.1210/me.2015-1300.

95. J. A. B. Smith, B. M. Gabriel, A. J. Brady, et al., "Inactivity-Induced NR4A3 Downregulation in Human Skeletal Muscle Affects Glucose Metabolism and Translation: Insights from in Vitro Analysis," *Molecular Metabolism* 99 (2025): 102200, https://doi.org/10.1016/j.molmet.2025.102200.

96. J. D. Fuqua, M. M. Lawrence, Z. R. Hettinger, et al., "Impaired Proteostatic Mechanisms Other than Decreased Protein Synthesis Limit Old Skeletal Muscle Recovery after Disuse Atrophy," *Journal of Cachexia, Sarcopenia and Muscle* 14 (2023): 2076–2089.

97. L. Brocca, M. Rossi, M. Canepari, R. Bottinelli, and M. A. Pellegrino, "Exercise Preconditioning Blunts Early Atrogenes Expression and Atrophy in Gastrocnemius Muscle of Hindlimb Unloaded Mice," *International Journal of Molecular Sciences* 23 (2022): 148, https://doi.org/10.3390/ijms23010148.

98. J. M. Michel, J. S. Godwin, D. L. Plotkin, et al., "Effects of Leg Immobilization and Recovery Resistance Training on Skeletal Muscle-Molecular Markers in Previously Resistance-Trained versus Untrained Adults," *Journal of Applied Physiology* 138 (2025): 450–467, https://doi.org/10.1152/japplphysiol.00837.2024.

Supporting Information

Additional supporting information can be found online in the Supporting Information section.

Supporting File 1: advs74388-sup-0001-Figure S1.pdf.
Supporting File 2: advs74388-sup-0002-Figure S2.pdf.
Supporting File 3: advs74388-sup-0003-Figure S3.pdf.
Supporting File 4: advs74388-sup-0004-Figure S4.pdf.
Supporting File 5: advs74388-sup-0005-Figure S5.pdf.
Supporting File 6: advs74388-sup-0006-Figure S6.pdf.
Supporting File 7: advs74388-sup-0007-Table S1.pdf.
Supporting File 8: advs74388-sup-0008-Table S2.pdf.
Supporting File 9: advs74388-sup-0009-DataS1.xlsx.
Supporting File 10: advs74388-sup-0010-DataS2.xlsx.
Supporting File 11: advs74388-sup-0011-DataS3.xlsx.
Supporting File 12: advs74388-sup-0012-DataS4.xlsx.